2009

Therapeutic Drugs in Cancer

Teneille Walker
Virginia Commonwealth University

Virginia Commonwealth University
School of Medicine

This is to certify that the dissertation prepared by Teneille Denise Walker entitled "THERAPEUTIC DRUGS IN CANCER" has been approved by the student advisory committee as satisfactory for completion of the dissertation requirement for the degree of Doctor of Philosophy.

Paul Dent, Ph.D., Director of Dissertation, School of Medicine, Department of Biochemistry and Molecular Biology

David A.Gewirtz, Ph.D., School of Medicine, Department of Pharmacology and Toxicology

Adly Yacoub, Ph.D., School of Medicine, Department of Radiation Oncology and Biochemistry

Suzanne E. Barbour, Ph.D., School of Medicine, Department of Biochemistry and Molecular Biology

Joseph Ritter, Ph.D., School of Medicine, Department of Pharmacology and Toxicology

Stephen T. Sawyer, Ph.D., School of Medicine, Department of Pharmacology and Toxicology

William Dewey, Ph.D., Chair, Department of Pharmacology and Toxicology

Jerome F. Strauss, III, M.D., Ph.D., Dean, School of Medicine

F. Douglas Boudinot, Ph.D., Dean, Graduate School

Date

THERAPEUTIC DRUGS IN CANCER

A Dissertation submitted in partial fulfillment of the requirements for the degree of Doctor of Philosophy at Virginia Commonwealth University.

by

TENEILLE DENISE WALKER
Master of Science, Virginia State University, 2004
Bachelor of Science, Virginia Commonwealth University, 2001

Director: PAUL DENT, PH.D.
VICE CHAIR, DEPARTMENT OF BIOCHEMISTRY

Virginia Commonwealth University
Richmond, Virginia
May 2009

Acknowledgement

First and foremost I would like to thank the Lord above for giving me the will to succeed. Next, I would like to thank my family, especially my mother Ms. Kaye Walker and grandparents, Mr. Harold Walker and Mrs. Thelma Walker, for their love and support throughout my college years. You all helped me to never give up and to strive forward in life. I could not have made it without you, so this dissertation is dedicated to you all.

I would also like to thank the many other family members who have prayed for me and supported me throughout this long process. If I could name all of you I would. My friends have also played a significant role in my success (especially Shannon Diggs, Tangela Jennings, Kim Johnson, and Annitra Williams). I want to thank you for listening to my praises and complaints and for bearing with me throughout my graduate experience. To the 2004 VCU crew who came in with me (Kia Jackson, Lynn Hull, Dena Kota, and Scott Lawrence), I really have enjoyed the laughs we shared and all of the support we have for each other. I could not have met a better group of peers.

This degree could not have been obtained if it wasn't for Dr. David Gewirtz, who gave me the opportunity to join his research team when I was earning my master's degree. Thank you for taking a genuine interest in me. I appreciate the knowledge I have obtained under your guidance. I have also enjoyed working with Xu Di (Michael), Molly Hilliker, and Sheena Aris in the lab. Thanks for all your support. Dr. Suzanne Barbour,

I would have never known about the Bridges program if it was not for you. Thank you for giving me the opportunity to pursue a career in science. I truly appreciate your wisdom throughout my experiences here at VCU. Dr. Jan Chlebowski, thank you for believing in me. I appreciate your help throughout my graduate experience. I also want to thank Dr. Steve Sawyer, who has also guided me throughout my Ph.D. experience and who also believed in me. I would also like to recognize Dr. Joseph Ritter, who agreed to be a member of my graduate committee. Thank you for your kind words you have given me over the years. Dr. Adly Yacoub, thank you for the educational meetings we would have about my research data. I really appreciate your help. Lastly but certainly not least, I want to thank Dr. Paul Dent who gave me the opportunity to complete my degree. Thank you for your positive criticism. Your wisdom, knowledge, and commitment to the highest standards inspired and motivated me.

To the Dent lab, I have enjoyed all of you. Dr. Margaret Park, thank you for helping me with experiments, even when you were really busy. Thank you also for your knowledge, advice, and even our girl talks. I have really appreciated all your help. You are going to make a great Principal Investigator (PI)! Hossien Hamed, thanks for spicing up the lab with your humorous demeanor. Thanks also for ordering all of the laboratory supplies even when I asked you at the last minute. Dr. Clint Mitchell, thank you for your knowledge and advice as well. Thanks for all the colony assays too. Aditi Martin,

thanks for all the talks. It was nice to have a lab mate who was also finishing graduate school.

I am truly blessed to me surrounded by so many professors, family, friends, and co-workers who always knew I would make it, even when I didn't believe in myself. Now you all can stop asking me when I will be done!

Table of Contents

Page

List of Tables

Page

List of Figures

Page

List of Abbreviations

Full Name	Abbreviation
17-allylamino-17-demethoxygeldanamycin	17AAG
Activating Transcription Factor 4	ATF4
Apoptotic Protease-activating Factor 1	Apaf-1
c-Jun NH_2-terminal kinase	JNK
Cytokine response modifier A	CrmA
Death Domain	DD
Death Effector Domain	DED
Death-inducing Signaling Complex	DISC
Epidermal Growth Factor Receptor	EGFR
Eukaryotic translation initiation factor 2 alpha	eif2α
FADD-like interlukin-1 β-converting enzyme-like protease	FLIP
Fas-asscoaited Protein with Death Domain	FADD
Fas Ligand	FasL
G-protein coupled receptors	GPCR
Guanosine Diphosphate	GDP
Guanosine Triphosphate	GTP

Heat Shock Protein	Hsp
Hepatocellular Carcinoma	HCC
Histone deacetylase inhibitor	HDACI
Inhibitor of apoptosis	IAPS
Mammalian Target of Rapamycin	mTor
Microliter	µl
Microtubule-associated Protein 1 Light Chain 3	LC3
Milliliter	ml
Mitogen Acitvated Protein Kinase	MAPK
Preautophagosome	PAS
Phosphatidylinositol 3'-kinase	PI3K
Protein kinase-like ER kinase	PERK
Receptor Tyrosine Kinase	RTK
Suberoylanilide Hydroxamic Acid	SAHA
Sphingomyelinase	SMase
Sphingosine-1-Phosphapate	S1P
Unfolded Protein Response	UPR

Abstract

Therapeutic Drugs in Cancer

By Teneille Denise Walker, M.S., MT (ASCP)

A Dissertation submitted in partial fulfillment of the requirements for the degree of Doctor of Philosophy at Virginia Commonwealth University.

Virginia Commonwealth University, 2009

Major Director: Paul Dent, Ph.D.
Vice Chair, Department of Biochemistry

The first study examined the interaction between low doses of the multi-kinase inhibitor sorafenib and the histone deacetylase inhibitor vorinostat in colon cancer cells. Sorafenib and vorinostat synergized to kill HCT116 and SW480 cells. In SW480 cells, sorafenib+vorinostat toxicity correlated with CD95 activation and CD95-stimulated autophagy. Drug lethality in SW480 cells was blocked by knock down of CD95. In SW620 cells that are patient matched to SW480 cells, sorafenib+vorinostat toxicity was significantly reduced that correlated with a lack of CD95 activation and lower expression of ceramide synthase 6 (LASS6). Overexpression of LASS6 in SW620 cells enhanced

drug-induced CD95 activation and tumor cell killing, whereas knock down of LASS6 in SW480 cells suppressed CD95 activation. In HCT116 cells, sorafenib+vorinostat did not increase CD95 plasma membrane levels, weakly induced caspase 8 association with CD95, and knock down of CD95 *enhanced* drug lethality. In HCT116 cells sorafenib+vorinostat treatment caused CD95-dependent autophagy that was a protective signal. Thus, treatment of tumor cells with sorafenib+vorinostat activates CD95 that promotes viability via autophagy or degrades survival via extrinsic or intrinsic pathways. Drug-induced activation of the de novo ceramide synthesis pathway plays a key role in CD95 activation. The second project explores the mechanism by which the combination of 17AAG, an hsp90 inhibitor, and PD184352, a MEK1/2 inhibitor alters survival in colon cancer cells. 17AAG and PD184352 synergized to kill HCT116 and SW480 cells. In HCT116 cells drug-exposure increased CD95 plasma membrane levels In SW620 cells, 17AAG and PD184352 toxicity was significantly reduced that correlated with a lack of CD95 activation and lower expression LASS6. Overexpression of LASS6 in SW620 cells enhanced drug-induced CD95 activation and tumor cell killing. In Mia Paca2 cells, a pancreatic cell line, inhibition of caspase 8 or overexpression of c-FLIP-s suppressed cell killing by PD184352 and 17AAG exposure. Drug lethality in Mia Paca2 cells was blocked by knock down of CD95. Additionally, overexpression of Bcl-xL or knockdown of caspase 9 decreased cell killing in 17AAG and PD184352 combination treatment. Thus, 17AAG+PD184352 exposure activates the extrinsic and intrinsic apoptotic pathways to kill Mia Paca2 cells. This document was created in Microsoft Word 2000.

CHAPTER 1 INTRODUCTION: GENERAL

1.1 Cancer

Cancer is a group of diseases in which cells grow and divide without respect to normal limits. In other words cancer cells are aggressive, they invade and destroy adjacent tissues, and they can metastasize, spreading to other locations in the body eventually leading to death. Benign tumors are not cancerous however. They are limited in their growth, and do not invade or metastasize. Cancer is caused by external and internal factors that may act together to promote or initiate carcinogenesis. External factors include tobacco, radiation, chemicals, or infectious agents. Internal factors include genetic mutations, hormones, or immune conditions [1].

Cancer accounts for nearly one-quarter of deaths in the United States, exceeded only by heart disease. Lung cancer is the most common fatal cancer in men (31%), followed by prostate (10%), and colon and rectal (8%). In women, lung (26%), breast (15%), and colon & rectum (9%) are the leading sites of cancer death [2].

There are various treatments for cancer, each dependent on the type and/or stage of the cancer. Treatment options include: (1) surgery (removal of the tumor), but this is not always possible if the cancer has metastasized (2) Radiation therapy (also called irradiation) in which ionizing radiation is used to kill cancer cells and shrink tumors. The effects of radiation therapy are localized and confined to the region of the tumor. Radiation damages the genetic material of a cell. Therefore it also damages healthy cells, which is the reason why radiation is given in fractions to allow normal cells to recover and

function properly. (3) Chemotherapy, the treatment of cancer with drugs that can destroy cancer cells. This term refers to cytotoxic drugs which affect rapidly dividing cells and are not specific for cancer cells. Therefore, chemotherapy can harm healthy tissue. (4) Combination Therapy, combining drugs that have different modes of action and different toxicities. An advantage of combination therapy is that it may delay or prevent drug resistance [1]. Even with these current treatments however, more novel therapeutics are needed to improve patient outcomes.

1.2 Raf/MEK/ERK Mitogen-activated protein kinase (MAP) pathway

Targeted-based therapies are considered to be the future of cancer treatment and much attention has been focused on the development of inhibitors of the Raf/MEK/ERK MAP kinase pathway. The Raf/MEK/ERK MAP kinase pathway is commonly dysregulated in cancer cells [3-5]. There are four well characterized MAPKs. Each cascade consists of three proteins that act as a relay mainly by phosphorylation signaling. There is a MAPK kinase kinase (MAPKKK), a MAPK kinase (MAPKK), and a MAPK. The terminal serine/threonine kinases (MAPKS) comprises, ERK1/2, c-Jun NH_2-terminal kinase (JNK1/2), p38, and ERK5 (Figure 1.1). Activation of the ERK1/2 pathway is often associated with cell survival, whereas JNK, p38, and ERK5 are activated by stress and growth factors [6, 7]. Although the mechanisms by which ERK1/2 activation promote survival are not fully characterized, a number of anti-apoptotic effector proteins have been identified, including increased expression of anti-apoptotic proteins such as c-FLIP, Bcl-xL, XIAP, and Mcl-1 [4, 8-12].

In the ERK MAPK module, Ras is a small GTP-binding protein which acts as the molecular switch that controls this signaling pathway. There are four Ras proteins, namely H-Ras, N-Ras, Ki-Ras 4A and Ki-Ras4B. Ras is mutationally active in a variety of cancers and this leads to persistent activation of downstream effectors [13]. In normal quiescent cells, Ras is inactivated (GDP-bound). Extracellular stimuli (i.e. EGF), induce the exchange of guanosine diphosphate (GDP) for guanosine triphosphate (GTP) which converts Ras into its active conformation. This process relies on the recruitment of GDP/GTP exchange factors to the cell membrane. Guanonine nucleotide exchange factors (GEFs; i.e. Sons of Sevenless, SOS) promote formation of active Ras-GTP whereas; GTP activating proteins (GAPS) stimulate GTP hydrolysis and formation of inactive Ras-GDP [6]. Ras activation leads to the recruitment and activation of the MAPKKK (MAP3K), Raf serine/threonine kinases (c-Raf-1, B-Raf, and A-Raf). Activation of Raf kinases is a multistep process that involves dephosphorylation of inhibitor sites by protein phosphatases 2A (PP2A) as well as phosphorylation of activating sites by PAK (p21 activated kinase). The regulatory mechanisms of various isoforms differ in that A-Raf and C-Raf-1 require additional phosphorylation reactions for activity whereas B-Raf has a much higher level of basal kinase activity. B-Raf is mutated in over 60% of cancers making it constitutively active in some types of tumors [6]. Raf kinases phosphorylate and activate MAPKKs, MEK1/2. MEK1/2 then phosphorylates and activates ERK1/2 MAPKs [14, 15]. Active ERKs phosphorylate numerous cytoplasmic and nuclear targets regulating processes such as proliferation, differentiation, and survival [6](Figure 1.2).

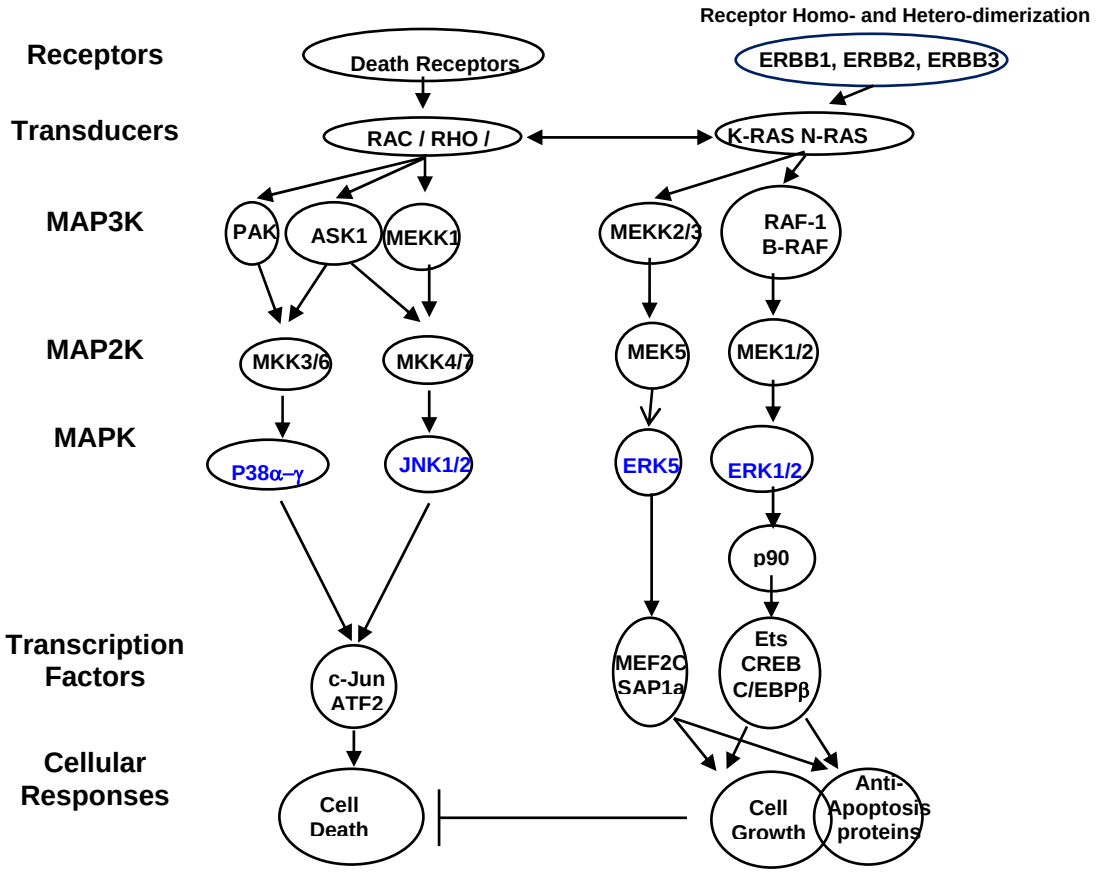

Figure 1.1. Mammalian MAPK cascades. There are four major mammalian protein kinase cascades; each consists of a MAPKKK, MAPKK, and MAPK. The ERK1/2 pathway is the activated by growth factors, whereas the JNK and p38 pathways are activated by environmental stressors such as ionizing radiation [6].

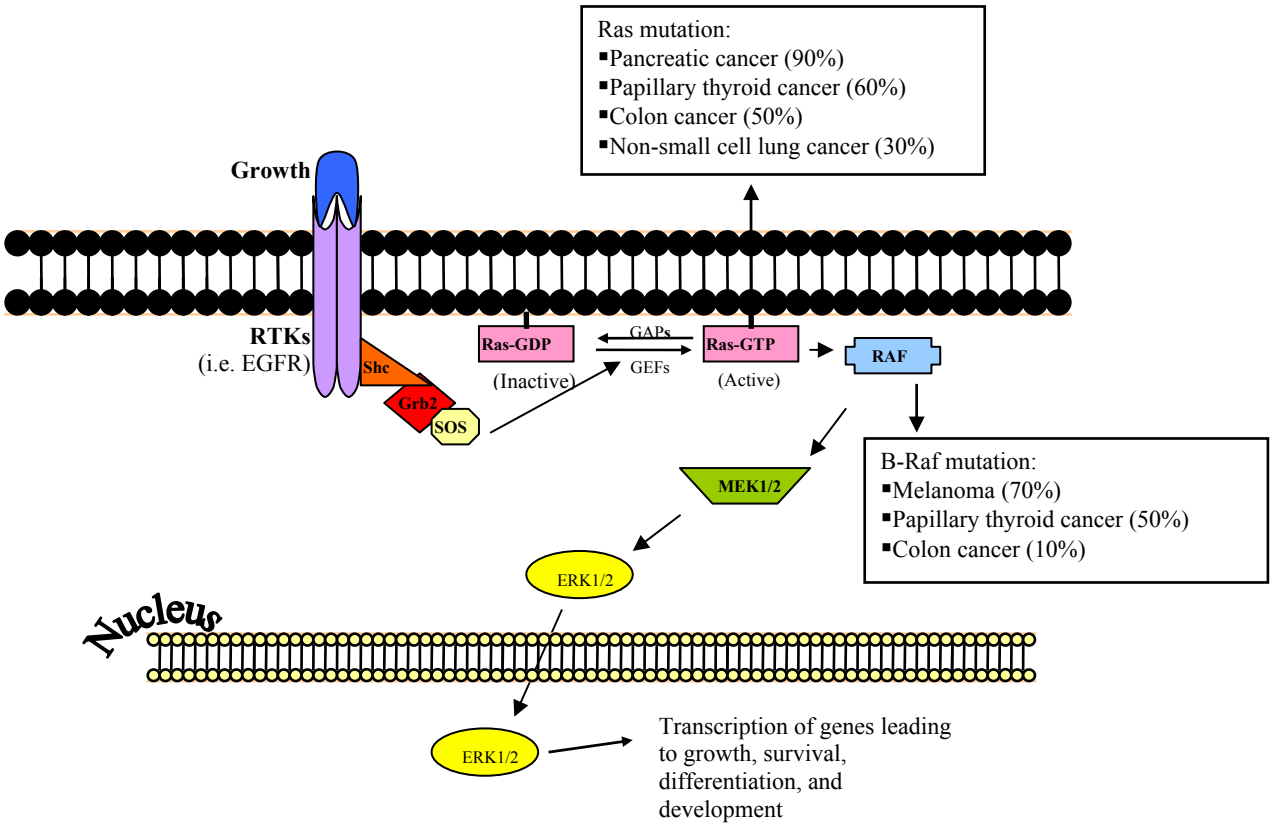

Figure 1.2. **Activation of the Raf/MEK/ERK Mitogen-activated protein kinase (MAP) pathway**. The binding of a growth factor to a growth factor receptor induces receptor dimerization and autophosphorylation on tyrosine residues. These phosphotyrosines are docking sites for signaling molecules which include Grb2-SOS complex. This complex activates the small G-protein Ras by stimulating the exchange of guanosine diphsophate (GDP) for guanosine triphosphate (GTP). Ras undergoes a conformational change which enables it to recruit Raf-1 from the cytosol to the cell membrane and bind to it where Raf-1 becomes active. Activated Raf-1 phosphorylates and activates MEK1/2 which in turn phosphorylate and activate ERK1/2. Activated ERK may translocate to the nucleus to control gene expression of transcription factors promoting growth, differentiation, and development [6, 14, 16].

1.3 JNK1/2 MAPK Pathway

JNK1/2 pathway signaling often causes apoptosis. JNK activation is much more complex than that of the ERK1/2 pathway owing to inputs by a greater number of MAPKKKs (at least 13, including MEKK1 (MAP/ERK Kinase-Kinase-1)-MEKK4 (MAP/ERK Kinase-Kinase-4), ASK (Apoptosis Signal-regulating Kinase), and MLKs (Mixed-Lineage Kinases), which are activated by upstream Rho-family GTPases. These phosphorylate and activate MAPKKs MEK4 (MAPK/ERK Kinase-4) and MEK7 (MAPK/ERK Kinase-7),which further phosphorylate and activate JNKs. JNK activation requires dual phosphorylation of tyrosine and threonine residues. The JNK family consists of JNK 1, 2, and 3 (also known as SAPKγ, SAPKα, and SAPKβ, respectively). JNK 1 and 2 are ubiquitously expressed, whereas JNK 3 is restricted to the brain, heart, and testis [17].

JNKs (MAPKs) are primarily activated in response to cytokines, UV irradiation, DNA-damaging agents, growth factor deprivation, and to a lesser extent, serum, and G-protein coupled receptors. The JNKs are able to translocate to the nucleus following stimulation. JNKs are generally thought to be involved in inflammation, proliferation and apoptosis. Accordingly, its substrates are transcription factors and anti-apoptotic proteins. One well known substrate of JNK is the transcription factor c-Jun. Others include Elk1, p53, ATF2 (Activating Transcription Factor-2), NFAT4 (Nuclear Factor of Activated T-Cell-4), and NFAT1 (Nuclear Factor of Activated T-Cell-1) . JNK mediates apoptosis not only through its effects on gene transcription, but also through a transcriptional-independent mechanism. For example, JNK1 directly phosphorylates Bcl-2 (B-Cell

CLL/Lymphoma-2) in vitro, co-localizes and collaborates with Bcl-2 to mediate prolonged cell survival. JNK can also phosphorylate the pro-apoptotic protein Bim and Bmf to promote their pro-apoptotic effects [18]. JNK cascade can also phosphorylate and activate HSF1 (Heat Shock Factor-1) and JNK-mediated phosphorylation of HSF1 selectively stabilizes the HSF1 protein and confers protection to cells under conditions of severe stress [6]. Thus, JNKs have opposing roles in promoting proliferation and transformation and inducing apoptosis.

1.4 p38 MAPK Pathway

In a similar manner to that of the JNK1/2 pathway**,** the p38 MAPK pathway is activated by numerous cellular stresses. The p38 module consists of several MAPKKKs, to include TAK1, ASK1/2, DLK, MEKK1-4, MLK2 and -3, and Tpl-2. The MAPKKKS phosphorylate and activate MAPKKs, MEK3 and MEK6. These MAPKKs show a high degree of specificity toward p38 as they do not activate JNK or ERK1/2. MEK4 however, activates both JNK and p38 and can thus be seen as a site of integration for the p38 and JNK pathways [6]. The MAPKKs phosphorylate and activate the MAPK, p38. There are four isoforms of p38, α, β, γ, and δ. p38 α and p38β are ubiquitously expressed while p38γ and p38δ are differentially expressed in certain tissues. All p38 kinases have a dual phosphorylation sites. MEK6 activates all p38 isoforms, but MEK3 selectively phosphorylates the p38 α and p38β isoforms [19].

The p38 MAPK pathway has a diverse role in the signaling of cellular responses that varies with cell type and stimulus. p38 phosphorylates and activates transcription factors that regulate inflammatory gene expression. A protein kinase termed MAP kinase-

activated protein kinase 2 (MAPKAP2) is phosphorylated by p38 and is also involved in many cellular processes including stress and inflammatory responses, nuclear export, gene expression regulation and cell proliferation. Heat shock protein HSP27 (a chaperone) was shown to be one of the substrates of this kinase in vivo. Other substrates of p38 include p53 involved in tumor suppression, and cell cycle regulators such as CDC25A, B, and C. p38 has also been implicated in other cellular responses such as cell death, development, and cell differentiation [20].

1.5 PI3-Kinase/Akt Pathway

The phosphatidylinositol 3'-kinase (PI3-K)/ Akt signaling is regarded as a pro-survival pathway in cells. PI3Ks are a family of intracellular lipid kinases that phosphorylate the 3'-hydroxyl group of phosphatidylinositols and phosphoinositides. PI3Ks are heterodimeric kinases that are composed of a regulatory and catalytic subunit that are encoded by different genes. PI3Ks are classified into three groups, class I, II, and III based on structure and function [21].

Class I PI3Ks phosphorylate the lipid phosphatidylinositol 4, 5, bisphosphate (PIP_2) to generate the second messenger phosphatidylinositol 3, 4, 5, trisphosphate (PIP_3). The class I PI3Ks are further subdivided according to the signaling receptors that activate them. Class IA PI3Ks are activated by growth factor receptor tyrosine kinases (RTKs), and class IIB PI3Ks are activated by G-protein coupled receptors (GPCRs). The regulatory subunit of class IA is p85 (with three isoforms: p85α, p85β, p55γ). The catalytic subunit of class IA is p110 (also with three isoforms: α, β, γ). Class IB members consist of a p101 regulatory subunit and a p110γ catalytic subunit [21]. Class II and class III PI3Ks

phosphorylate phosphatidylinositol (PI) to generate PI3P. Class II PI3Ks bind clathrin coated pits and may function in membrane trafficking or receptor internalization [22]. VPS34 is the only mammalian class III PI3K and acts as a sensor signaling to mammalian target of rapamycin (mTOR) to regulate cell growth and autophagy in response to low nutrient pools [23]. Class IA however, is the only PI3K class that has been demonstrated to be clearly involved in oncogenesis [21].

Upon ligand binding to RTKs, RTKs dimerize and autophosphorylate at tyrosine residues. This allows them to interact with Src homology 2 (SH2) domain containing molecules. PI3K can be activated by three independent pathways. In one activation pathway, PI3K p85 regulatory subunit binds directly to tyrosine motifs within the RTK triggering activation of PI3Ks catalytic subunit. Another pathway consists of the adapter protein GRB2 which binds preferentially to phosphotyrosine motifs in the RTK. GRB2 can bind to the scaffolding protein GAB (GRB2-asssociated binding protein), which can bind to p85. GRB2 can also bind to SOS and activate RAS. RAS can activate p110 independently of p85 [24]. When PI3K is activated it results in the generation of PIP_3. 3'-phosphoinositide dependent kinase 1 (PDK1) and Akt preferentially bind to PIP_3 (by recruitment to the membrane) which lead to Akt activation depending on its phosphorylation at Ser473 or Thr308 sites by PDK1. Phosphatase tensin homolog (PTEN) is a negative regulator of PI3-K pathway that converts PIP_3 back to PIP_2 [21]. Akt (also known as protein kinase B, PKB) phosphorylates Bad at Ser136 preventing cytochrome c release. Akt also phosphorylates caspase 9 at Ser196, causing a conformational change

that results in the inhibition of its proteolytic activity (Figure 1.3). The overall result is protection from apoptosis and increased proliferation, events that favor tumorgenesis [25].

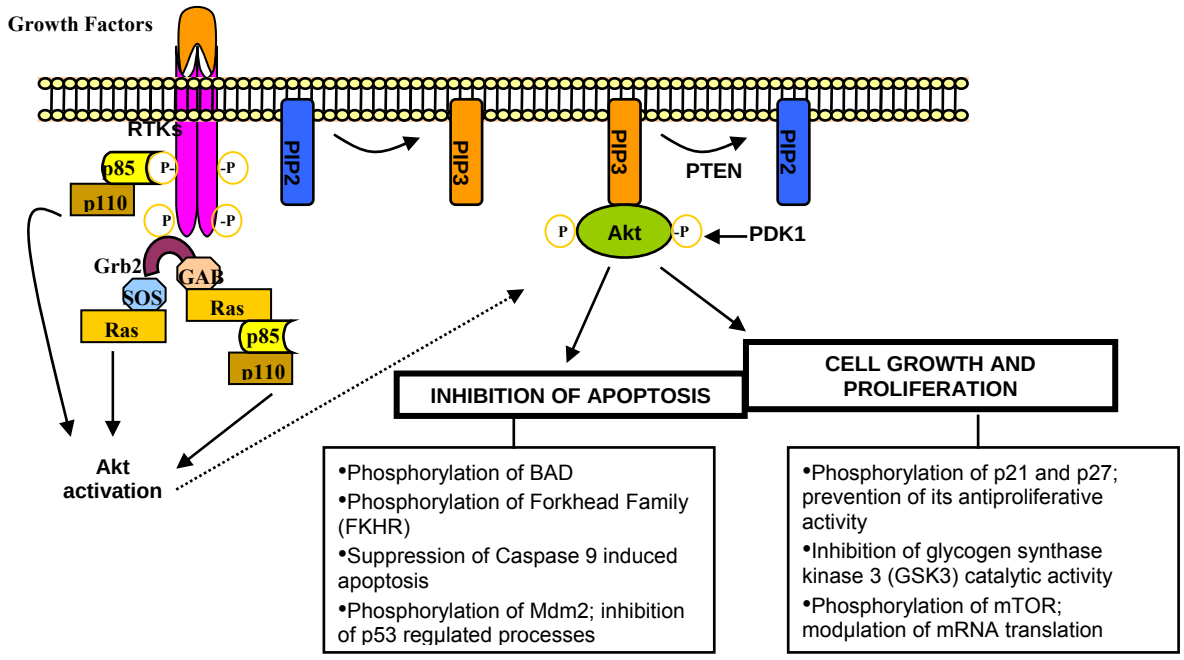

Figure 1.3. Model of PI3K/Akt Pathway Activation. In response to extracellular stimuli (i.e. growth factors), the catalytic subunit of PI3K (p110) is recruited to receptor tyrosine kinases (RTKS) at the membrane through its regulator subunit (p85). PI3K phosphorylates phosphatidylinositol 4, 5, bisphosphate (PIP_2) to generate the second messenger phosphatidylinositol 3, 4, 5, trisphosphate (PIP_3). PIP_3 recruits serine/threonine Akt and 3-phosphoinositide dependent kinase (PDK1) to the membrane. Membrane bound Akt is rendered fully active through its phosphorylation by PDK1. Activated Akt may phosphorylate a variety of substrates thereby activating or inhibiting targets important for cellular growth, survival, and proliferation [24, 25].

1.6 Apoptosis: Extrinsic and Intrinsic Pathways

There are two well described pathways to initiate apoptosis. One is referred to as the extrinsic pathway mediated by death receptors on the cell surface, and the other is identified as the intrinsic pathway, mediated by cytochrome c release from the mitochondria. Both extrinsic and intrinsic pathways have in common a group of cystine dependent aspartate specific proteases called procaspases, which require activation to become full caspases and carry out the cleaving of cellular substrates that result in biochemical and morphological changes. Biochemical processes include the externalization of phosphatidylserine on the cell surface. The morphological changes during apoptosis include chromatin condensation, cytoplasmic shrinkage, membrane blebbing, and phagocytosis of the cell or the cell breaks apart forming apoptotic bodies [26].

The extrinsic pathway involves engagement of death receptors that belong to the tumor necrosis factor receptor (TNF-R) family. Death receptors are activated by their natural ligands, TNF family. Members of the TNF receptor family share similar cysteine–rich extracellular domains and have a cytoplasmic domain called the "death domain". Death receptors include CD95 (Fas), TRAIL-R1 (APO-2, DR4), TRAIL-R2 (DR5, KILLER, TRICK2), TNF-R1 (CD120a), and DR3 (APO-3, LARD, TRAMP, WSL1). Among these receptors, CD95 is the best well characterized death receptor.

Fas is a 45-kDa Type I transmembrane protein, which, like many members of the TNF/NGF superfamily, contains a number (three in the case of Fas) of cysteine-rich repeats in its extracellular domain. Such cysteine repeats serve as recognition sites with respective ligands, and disruption of these repeats leads to the loss of ligand binding and

effector signaling. The Fas receptor is ubiquitously expressed on a variety of normal cells, including activated T- and B-cells, hepatocytes, and ovarian epithelial cells, although regulated expression has been reported in various systems. High levels of Fas expression have also been detected on solid tumors of the breast, ovary, colon, prostate, and liver. In contrast, FasL is a Type II cell surface glycoprotein of 40 kDa, which has a cytosolic N-terminus and an extracellular C-terminus. FasL expression is limited, but has been detected on activated T-cells, natural killer cells, Sertoli cells of the testis, and the corneal epithelium and the retina of the eye. Some tumors also express FasL, which may be a mechanism to escape immune surveillance. Metalloproteinase-mediated shedding of membrane-bound FasL as a soluble form from effector cells is believed to serve as a mechanism of turning off apoptosis in bystander cells [27].

Ligation of Fas with FasL (expression of which can be on the same or different cells) triggers the combination of Fas monomers into trimeric Fas-complexes. Trimer formation is critical for effector function. The intracellular domain of Fas contains a stretch of 80 amino acids known as the death domain (DD). DD enables the recruitment and construction of a multi-protein death-inducing signaling complex (DISC) following Fas trimerization. DISC formation appears to be required for Fas-mediated apoptosis, as it both serves as a central relay station to downstream signaling proteins and, more importantly, provides docking sites for critical effectors in the Fas-death pathway. Immediately following Fas/FasL ligation, there is recruitment of the serine-phosphorylated adapter Fas-associated DD (FADD)/MORT1. Fas/FADD interaction is coordinated through the highly conserved DD motifs found in both proteins. The presence of a functional FADD is

critical for Fas-mediated apoptosis, whereby the expression of a dominant-negative FADD completely abrogates Fas-induced cell death. Moreover, in vivo studies revealed a substantial attenuation of lymphocyte death in mice lacking FADD. FADD serves as a bridge between Fas and downstream molecules, such as Fas-like interleukin (IL)-1β converting enzyme (FLICE)/procaspase-8α/β. FADD is a true adapter protein in that it harbors an N-terminal DD along with a C-terminal death effector domain (DED). Its unique structure enables FADD to proximally bind Fas on one end, while being able to distally recruit FLICE on the other [28]. The caspases that are recruited to this death-inducing signaling complex (DISC) are caspase 8 and caspase 10 which are the initiator caspases. Once these are activated, caspase 8 can cleave Bid and the intrinsic pathway is initiated or caspase 8 can directly lead to the activation of executioner caspases (caspase 3, 6, and 7). The active executioner caspases cleave death substrates leading to apoptosis [26].

The intrinsic apoptotic pathway involves non-receptor mediated stimuli that produce mitochondrial initiated events. Examples include radiation, hypoxia, free radicals, and hyperthermia. All of these stimuli cause changes in the inner mitochondrial membrane that result in mitochondria permeability [26]. The members of the Bcl-2 family regulate the intrinsic pathway. Bcl-2 family members are divided into three subfamilies based on their function and structure: (1) anti-apoptotic proteins (Bcl-2, Bcl-xL, Bcl-w, Mcl-1, A1/Bfl1, Boo/Diva, NR-13) that have four BCL-2 homology domains, (2) pro-apoptotic members of the Bax subfamily that have three BH domains (Bax, Bak, Bok/Mtd) and (3) the BH-3 only pro-apoptotic proteins (Bik, Bad, Bid, Blk, Hrk, MimL, BNIP3, NOXA, PUMA). The BH-3 domain is present in all members and is essential for heterodimerization among

members and is the minimum domain required for the apoptotic function [29]. Activation of the mitochondria is by the Bcl-2 family member, Bid. Bid is cleaved by active caspase 8 and translocates to the mitochondria. Bid inserts into the membrane and activates Bax and Bak leading to mitochondrial events that make the membrane permeable for the release of cytochrome c from the mitochondria. Cytochrome c binds the apoptotic protease activating factor 1 (Apaf-1) to form the apoptosome. At the apoptosome, the initiator caspase 9 is activated. Once the initiator caspase is activated, it cleaves and activates executioner caspases converging to the final common pathway leading to cell death [30](Figure 1.4).

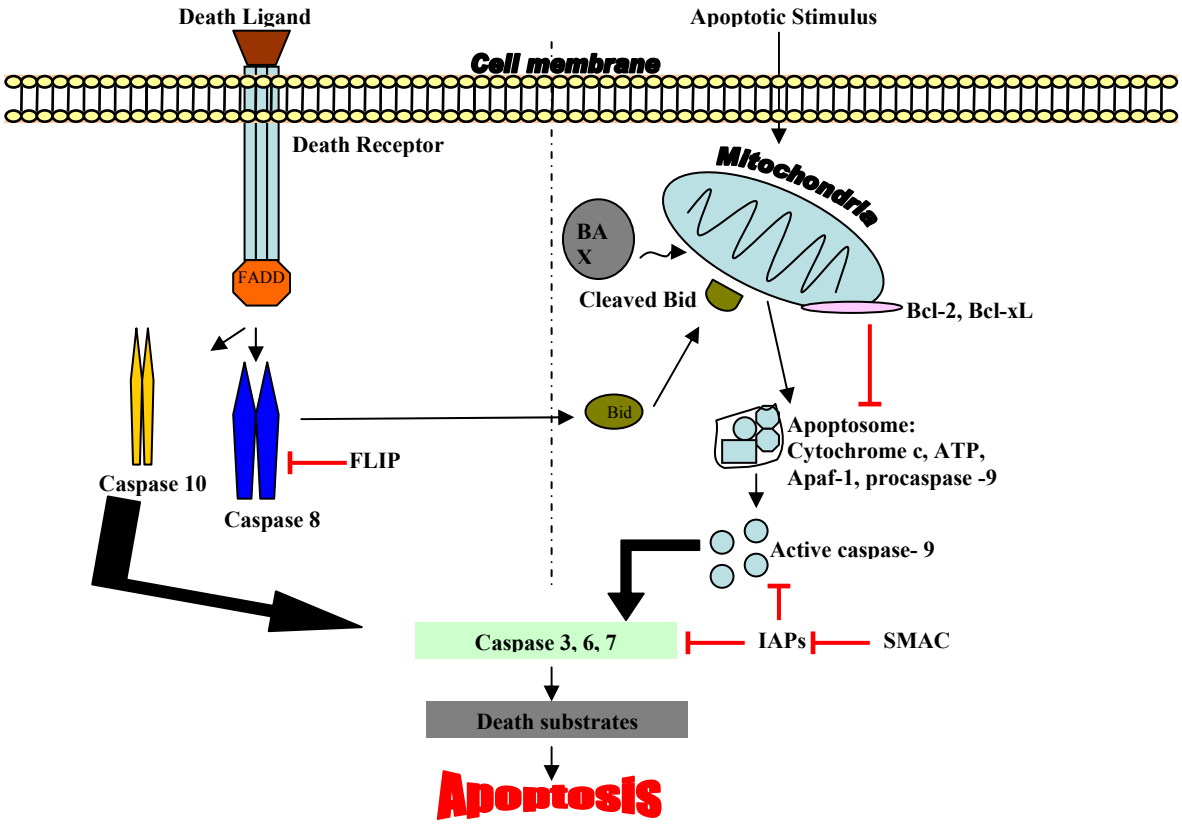

Figure 1.4. The Apoptosis Signaling Pathway. Apoptosis can be initiated by two pathways, the extrinsic pathway through death receptors or the intrinsic pathway through the mitochondria. In both pathways, induction of apoptosis leads to the activation of an initiator caspase (caspase 8 or 10 for the extrinsic pathway, and caspase 9 for the intrinsic pathway), and activation of executioner caspases, leading to the common pathway of cell death.

1.7 Regulation of Apoptosis Signaling

Death receptor mediated apoptosis can be inhibited by a protein named c-FLIP (FADD-like interlukin-1 β-converting enzyme-like protease). Three splice variants have been identified in humans. One termed v-FLIP is found only at the mRNA level, whereas the long form ($FLIP_L$) and a short form ($FLIP_S$) are at the protein level and share structural homology with procaspase-8, but lack catalytic activity. This structural homology can allow FLIP to bind to FADD and caspase 8, rendering them ineffective [28].

Anti-apoptotic member, Bcl-2 suppresses cytochrome c release, thereby enhancing cell survival. Bcl-xL interacts with Apaf-1 to prevent the activation of executioner caspases and subsequent apoptosis. Bak is maintained in an inactive state on the surface of the mitochondria to Mcl-1 or Bcl-xL until an apoptotic stimulus occurs. The depletion of Mcl-1 in some cells permits Bak oligomerization, activation, and apoptotic cell death [31].

Inhibitor of apoptosis (IAP) proteins directly binds and inhibits caspases 3, 7, and 9. There are eight mammalian members of the IAP family which include, XIAP, c-IAP1, c-IAP2, NAIP, ILP-2, survivin, bruce, and ML-IAP. There are three proteins that are negative regulators of IAP proteins, which include, XIAP-associated factor (XAF1), Second mitochondrial activator of caspases/direct IAP binding protein with low pI (Smac/DIABLO), and Omi/HtrA2. These proteins can bind to IAPs and abolish their anti-apoptotic function. XAF1 accumulates in the nucleus and can sequester XIAP from the cytosol. Smac/Diablo and Omi/HtrA2 are located in the mitochondria and are released into the cytosol upon apoptotic stress [32].

1.8 Autophagy: Function and Process

Autophagy is a process of lysosomal protein degradation in which the cell "eats" itself. Autophagy serves as an evolutionary conserved survival mechanism in virtually all cells by providing a way of cells to dispose of damaged organelles and proteins and recycle molecules for energy. However, it can become deleterious to cells when upregulated and hence causes cell death, commonly referred to as type II programmed cell death [33]. Autophagy can be separated into three types, macroautophagy, microautophagy, and chaperone-mediated autophagy. The focus will be on macroautophagy (hereafter termed autophagy) because this is the most characterized and well understood form of autophagy [34].

The first stage of autophagy is vesicle nucleation and begins with a crescent shaped double membrane vesicle forming that appears in the cytoplasm. This membrane continues to elongate, entering the elongation stage, while gathering cytoplasmic cargo until it closes forming an autophagosome. The formation of the autophagosome constitutes the completion stage. The docking and fusion stage occurs when the autophagosome targets the lysosome and fuses with it allowing the captured material and the inner membrane to be degraded (Figure 1.5). The molecular mechanism of autophagy involves yeast genes termed ATG and its products, Atg. The Atg proteins function at distinct stages in the autophagy process, of which most have been identified in mammalian cells as well [33].

The assembly of the preautophagosome (PAS) is referred to as nucleation (Figure 1.6). This step begins with Atg17. Atg17 recruits Atg13 and Atg9, which together

activate the phosphoinositide 3-kinase (PI3K) class III complex to include Atg14, Atg15, and vacuolar protein sorting-associated (VPS) 34, or its mammalian counterpart p150. Atg6, Beclin 1 in mammalians, and UV-irradiation resistance-associated tumor suppressor gene (UVRAG) also associate with the PI3K complex. Under conditions of nutrient starvation, Atg13 interacts with Atg1 and the PI3K complex to recruit Atg18 and Atg2. Atg18 and Atg2 are involved in retrograde transport of Atg9 to the periphery to aid in membrane recycling [35].

Elongation of the autophagosome is generated by two ubiquitin-like conjugation systems, Atg12-Atg5 and Atg8-phosphatidylethanolamine (PE). The PI3K complex is required for the localization of both systems. In addition, both systems are similar to the ubiquination system, consisting of three enzymes: a ubiquitin-activating enzyme (E1), a ubiquitin-conjugating enzyme (E2) and a ubiquitin-protein ligase (E3) [36]. Atg12 is activated by Atg7 functioning as an E1 enzyme. Atg10 acts as an E2 enzyme, forming a new thioester bond and Atg7 is released. The last step is the covalent linkage of Atg12 to a lysine residue of Atg5 and the release of Atg10. This Atg12-Atg5 complex interacts with Atg16L in mammalians (where Atg16L only binds to Atg5), forming an 800 kDa structure on the outer membrane necessary for the elongation of the PAS. Once the autophagosome is complete, this conjugate system dissociates and thus is not a part of the mature autophagosome [37]. The second ubiquitination system is Atg8-PE. Atg8 is a soluble cytoplasmic protein that conjugates with PE and becomes attached to the preautophagosome, as well as the mature autophagosome, and the autophagic bodies. The mammalian orthologue of Atg8, is microtubule-associated protein 1 light chain 3 (LC3)

and this protein is one of two credible markers to detect autophagy in mammalian cells. LC3 is detected in two forms, LC3 I (18 kDa) and LC3 II (16 kDa). LC3 I becomes active when it is cleaved by Atg4 also known as autophagin. Next, with the catalysis of Atg7 and Atg3, LC3 I undergo ubiquitination-like reactions and is modified to LC3 II. LC3 II is tightly bound to the PAS as well as the autophagosome whereas LC3 I is located in the cytoplasm. Thus, the relative amount of LC3 II reflects the abundance of autophagosomes present in cells [38]. Another marker, p62, also named sequestosome 1 (SQSTM1) is a more recent protein that may be used to detect autophagy. This protein is a common component of polyubiquitinated protein aggregates that are degraded by autophagy. The C-terminal part of p62 contains an ubiquitin-associated (UBA) domain, which binds to ubiquitin noncovalently. The p62 protein also recognizes LC3 on the autophagosome. Positive p62 structures are degraded via autophagy and this protein can be recognized along with LC3 [39].

After the completion of the mature autophagosome, the next step is the fusion of the autophagosome with the lysosome. This degrading structure is commonly referred to as the autolysosome or autophagolysosome [40]. There are several factors that are involved in autophagosome fusion to include the SNARE proteins (i.e. SEC17, SEC18, and YPT7). Degradation of the autophagosome once fused requires a low pH, proteinase B (PRB1), and the lipase Atg15. PRB1 is a hydrolase involved in the activation of vacuolar zymogens which indirectly affects the vesicle breakdown whereas, Atg15 functions directly in vesicle breakdown [36].

1.9 Autophagy: Regulation

There are a number of pathways involved in the regulation of autophagy. A critical player in autophagy regulation is the mammalian target of rapamycin kinase (mTOR). mTOR is a serine/threonine kinase that is involved in the control of multiple cellular processes in response to changes in nutrient conditions [33]. It exerts an inhibitory signal on autophagy, remaining active when the supply of amino acids and other nutrients are ample. When mTOR is active, it can phosphorylate proteins that are important for cell growth. mTOR is inactivated when a cell is deprived of nutrients, allowing proteins that are required for cell survival to be translated. Autophagy is therefore the attempt to provide an alternate source of nutrients to a cell. Treatment of cells with rapamycin, an inhibitor of mTOR, blocks cell cycle progression and triggers autophagy. mTOR also appears to affect Atg proteins, resulting in interference with autophagosome formation. Under nutrient-rich conditions, activated mTOR causes hyperphosphorylation of Atg13, thereby preventing the association of Atg13 with Atg1 (Figure 1.6). This step is necessary in the biogenesis of the PAS.

Another signaling pathway involved in the regulation of autophagy is the PI3K classes. Evidence that PI3K was involved in autophagy steers from the use of 3-methyladenie (3MA), a PI3K inhibitor, that inhibits the autophagy process. Other PI3K inhibitors (i.e. wortmannin and LY294002) have also been shown to inhibit autophagy [41]. There are three classes of PI3Ks in mammalian cells. Activation of class I PI3K inhibits autophagy in HT29 colon cancer cells [42]. Class II PI3K does not appear to have an effect on autophagy, however class III PI3K plays a significant role in the early steps of

autophagy induction as stated previously [35]. In addition, the class III PI3K product, phosphatidylinositol 3-phosphate (PI3P), stimulates autophagy [42].

1.10 Autophagy and Cancer

Autophagy may play dual roles in cancer progression, providing a mechanism for cell survival in some tumor cells and cell death in others. One of the players in autophagy, beclin 1 displays tumor suppressor activity. Consequently, beclin 1 is monoallelically deleted in 40-75% of human breast, ovarian, and prostate cancers. Mice with heterogeneous disruption of beclin 1 are more prone to developing spontaneous tumors and show a decrease in autophagy [43]. Beclin 1 was originally isolated as a Bcl-2 interacting protein. Furthermore, Bcl-2 downregulation stimulates autophagy. Consequently, beclin 1 mutations that abolish the interaction with Bcl-2 or Bcl-xL confer a gain-of-function phenotype with respect to autophagy. Similarly, mutations in Bcl-xL that prevent its binding to beclin 1 also eliminate its capacity to antagonize autophagy induction. The autophagy inducing activity of beclin 1 is also inhibited by Mc1-1 [44]. PTEN, a tumor suppressor which dephosphorylates class I PI3K products, prevents autophagy [43]. UVRAG another protein discussed previously as a part of the class III PI3K complex suppresses the proliferation of human colon cancer cells. However, UVRAG, like beclin 1, is also monoallelically deleted at a high frequency in human colon cancer cells [45]. Thus, autophagy signaling is tightly linked to oncogenic signaling. Currently, the variability of autophagy signaling in cancer cells is the forefront of discussion.

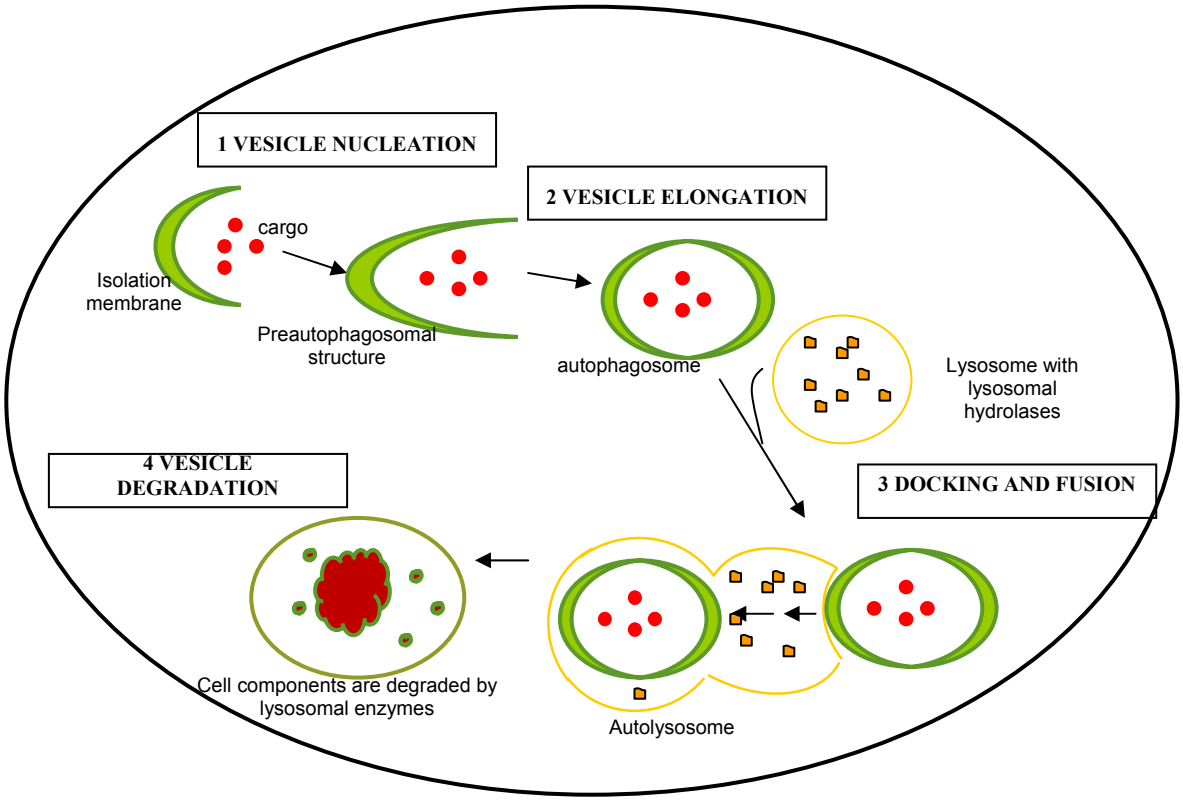

Figure 1.5. The Cellular Aspect of Autophagy. The cellular process of autophagy follows distinct stages: vesicle nucleation (formation of the isolation membrane), vesicle elongation (growth of the membrane from the preautophagosomal structure to the mature autophagosome), docking and fusion of the autophagosome with the lysosome to form an autolysosome, and lastly breakdown of the autolysome and the degradation of its contents.

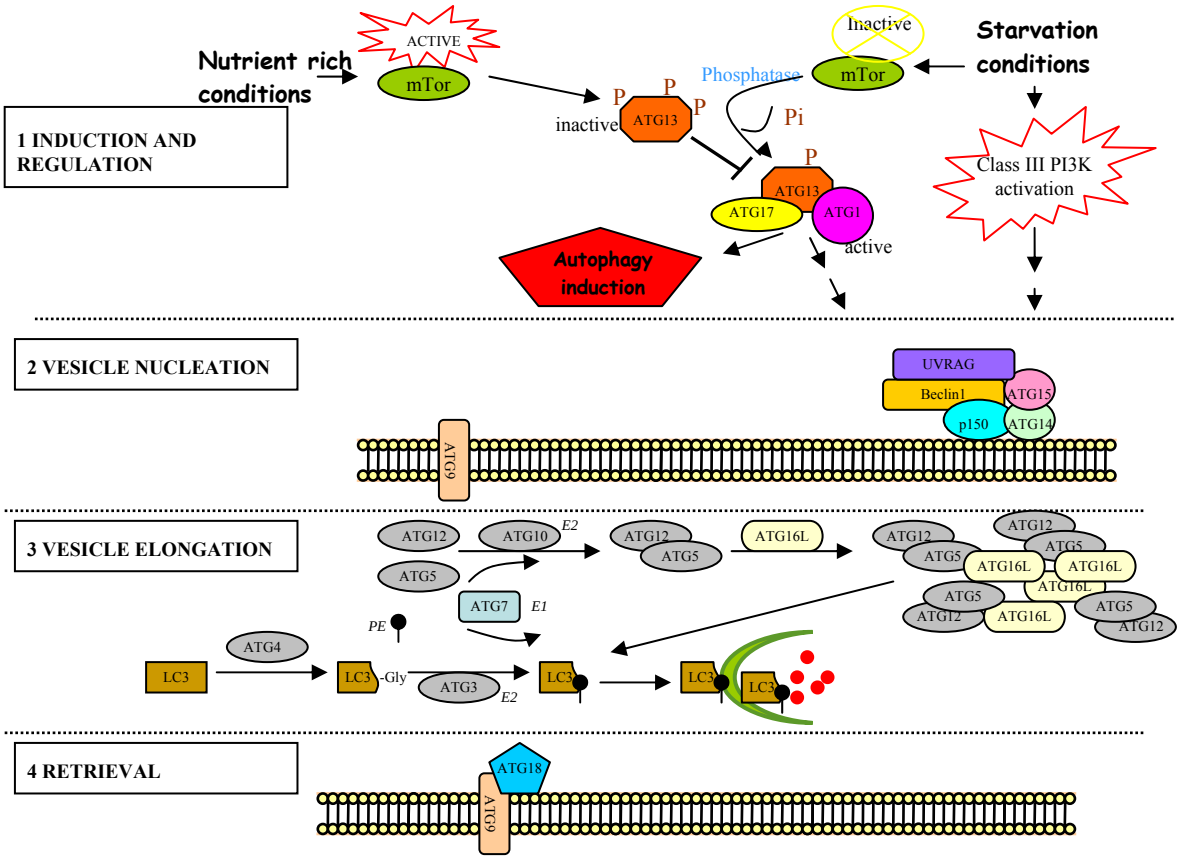

Figure 1.6. The Molecular Aspect of Mammalian Autophagy. The first regulatory process involves the mTor kinase which inhibits autophagy by phosphorylating Atg13. When mTor is inhibited as in starvation conditions, hypophosphorylated Atg13 forms a complex with Atg1 and Atg17, inducing autophagy. Starvation conditions also activate class III phophatidylinositol 3-kinase (PI3K) which activates the PI3K complex leading to vesicle nucleation. The PI3K complex consists of Atg14, Atg15, and a myristylated kinase named p150. The formation and activity of this complex also depends on its binding to Beclin 1 and UV irradiation resistance-associated tumor suppressor gene (UVRAG). Vesicle elongation begins with two ubiquitin-like conjugation systems. One system involves the conjugation of Atg12 and Atg5 by the E1 like enzyme Atg7 and the E2 like enzyme Atg10. The second pathway involves the conjugation of LC3 and phosphatidylethanolamine (PE) by the protease Atg4 and the E1 enzyme Atg7 and the E2 enzyme Atg3. This conjugation leads to the conversion of the soluble form LC3 I to the autophagic vesicle form LC3 II. The retrieval of essential amino acids is through the association of Atg18 with Atg9, however this mechanism is poorly understood. Shown above are the complexes that have been identified in mammalian cells, with the exception of Atg13 and Atg17 that have only been identified in yeast.

1.11 ER Stress: The Unfolded Protein Response

The endoplasmic reticulum (ER) is the site of biosynthesis of proteins targeted for membranes or secreted from the cell. The ER is a membranous network throughout the cytoplasm of eukaryotic cells that folds, assembles, and glycosylates these proteins. Homeostasis within the ER is important for proper protein folding, thus to prevent the accumulation of unfolded proteins, the ER activates the unfolded protein response (UPR)[46]. UPR allows for an increase in the degradation of misfolded proteins, the reduction in newly translated proteins entering the ER, and an increase in the capacity of protein folding. If the stress on the cells is too much, the UPR signals for the cells to undergo cell death in order to preserve the surrounding cells.

There are three primary UPR sensors, protein kinase-like ER kinase (PERK), activating transcription factor 6 (ATF6), and IRE1 (Figure 1.7). There are several chaperones which aid in proper proteins folding including binding lg protein (BiP). BiP, is also known as glucose regulated protein 78 (GRP78), and is a member of the heat shock protein 70 family [46]. Bip is bound to the luminal domains of the three UPR sensors under normal conditions. When there is an increase in unfolded proteins within the ER, Bip will preferentially bind to the misfolded proteins, and dissociates from PERK, ATF6, or IRE1 leaving these proteins free to perform their functions. One sense stressor, IRE1, is an ER transmembrane protein kinase endoribonuclease that dimerizes (alpha and beta subunits) upon dissociation from Bip activating its cytosolic RNase domain. Its RNase activity cleaves an X box DNA binding sequence. The resulting XBP1 migrates to the nucleus and binds the upstream DNA UPR element, and thus is a potent activator of UPR genes

that are essential for protein folding, migration, and degradation. ATF6, upon release form Bip, travels to the Golgi where it is cleaved by site 1 and site 2 proteases (S1P and S2P). This now active form of ATF6 migrates to the nucleus and binds to the ER stress response elements (ERSE) to promote the transcription of ER-resident chaperones and other assistant folding enzymes. When the third UPR sensor, PERK, is dissociated from Bip, it homodimerizes, autophosphorylates, and phosphorylates the alpha subunit of eukaryotic translation initiation factor 2 (eif2α) at serine 51 [46]. Eif2α is required to bring the initiator methionyl-transfer RNA (Met-tRNAi) to the 40S ribosome. Thus, when eif2α is phosphorylated, it can no longer exchange GDP for GTP and this prevents the 40S ribosome and the 60S ribosomal unit from forming the 80S initiation complex necessary for translation. However, activating transcription factor 4 (ATF4) is translated after eif2α is phosphorylated and activates genes involved in amino acid metabolism, transport, oxidative-reduction reactions, and ER stress-induced apoptosis. One of these proteins, C/EBP homologous transcription factor (CHOP) is implicated in both growth arrest and cellular apoptosis. Thus with prolonged UPR activation, ATF4 can induce expression of CHOP leading to caspase 3 activation and apoptosis [47].

Before a cell commits itself to apoptosis due to prolonged UPR activation, a cell coordinates itself with the ER associated degradation (ERAD) system. This system allows the misfolded proteins to be degraded. XBP1 is responsible for increasing expression of genes encoding proteins required for ERAD. Alternatively, under prolonged UPR, ER calcium homeostasis is significantly disrupted, leading to activation of caspase 12 (in mice only). The human caspase-12 gene however, contains several missense mutations and

clearly cannot have a role in UPR-induced apoptosis. Recent data indicates that caspase 4 in humans is homologous to murine caspase12 [48]. Caspase 12/4 activation leads to the activation of caspase 9 and 3, leading to apoptosis.

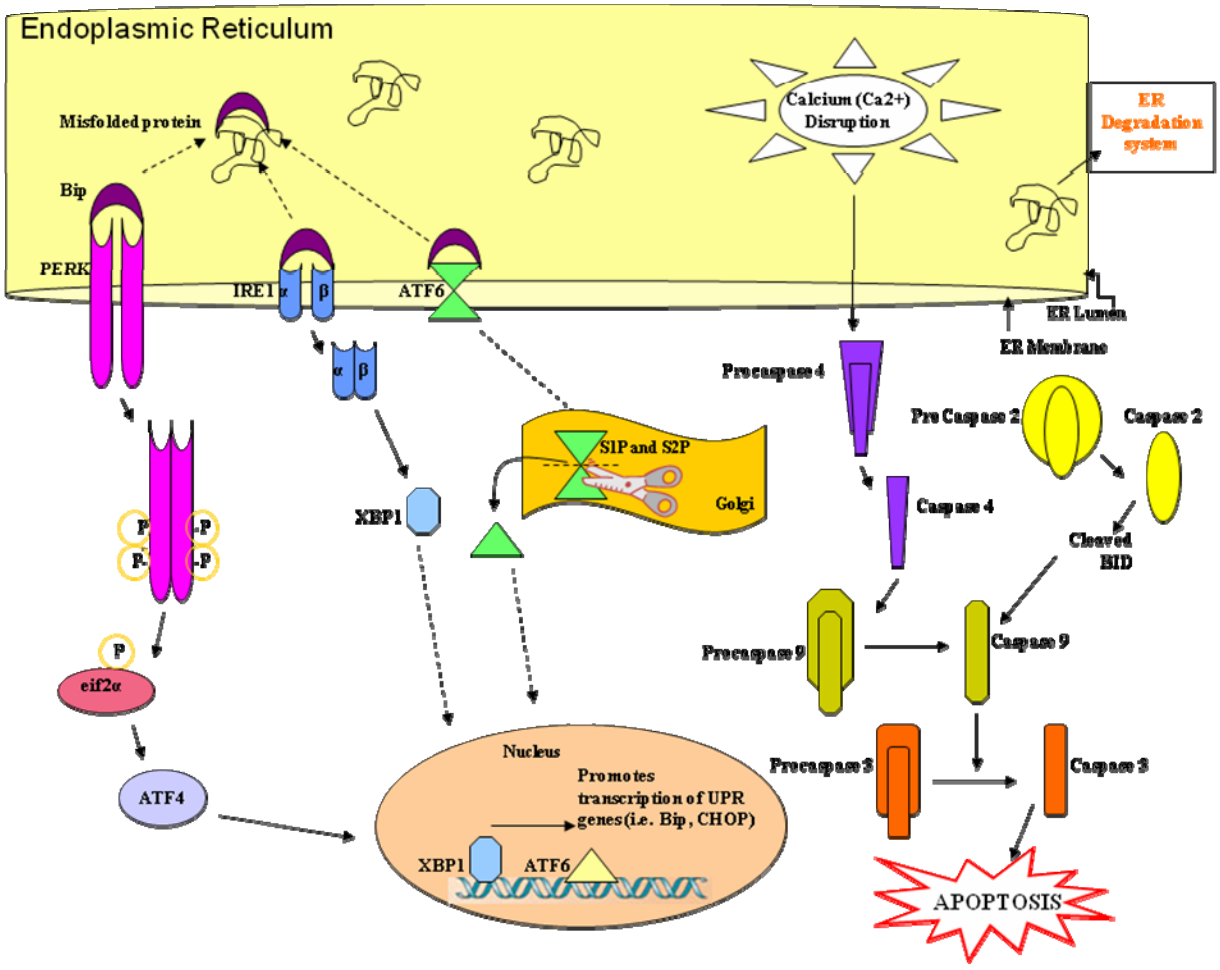

Figure 1.7. The Unfolded Protein Response. Upon accumulation of misfolded or unfolded proteins in the ER lumen, Bip/Grp78 dissociates from UPR sensors PERK, IRE1 and ATF6. Bip/Grp78 release from PERK results in PERK's dimerization and autophosphorylation. Activated PERK phosphorylates eif2α, inhibiting translation and resulting in cell cycle arrest. However, selective mRNAs such as ATF4 can be preferentially translated by the phosphorylated eif2α. Bip/Grp78 release from IRE1 permits its dimerization and activates its kinase and RNase activities to cleave an X box DNA binding sequence, to form the transcription factor XBP1. XBP1 translocates to the nucleus and binds to the upstream DNA UPR element. Paradoxically, Bip/Grp78 release from ATF6, activates ATF6 and allows it to translocate to the Golgi where it is cleaved by site 1 and site 2 (S1 and S2) proteases to form an active 50kDa fragment (ATF6 p50). This fragment migrates to the nucleus and binds to the ER stress response elements (ERSE) to activate transcription of UPR responsive genes. Additionally, calcium homeostasis is disrupted leading to the activation of caspase 4 (or caspase 12 in rodents), thus signaling an ER dependent apoptotic response. Caspase 2 cleaves Bid in response to ER stress, leading to caspase 9 activation and apoptosis.

1.12 Ceramide

Long chain sphingoid bases are the defining feature of sphingolipids. Ceramide is a spingosine-based lipid signaling molecule that regulates differentiation, proliferation, and apoptosis. Ceramide has attracted great attention due to its emerging role as an intracellular effector molecule in apoptosis. Several environmental stresses shown to initiate apoptosis, such as ionizing radiation, induce rapid ceramide generation [49]. Ceramide is one of the most hydrophobic molecules in mammalian cells. It can be synthesized de novo (anabolism) or by sphingomyelinase (SMase)-dependent catabolism of sphingomyelin (SM) (Figure 1.8).

De novo synthesis begins by condensation of serine and palmitoyl-CoA to form ketosphinganine, which is then reduced to dihydrosphingosine. The acylation of dihydrosphingosine to dihydroceramide is catalyzed by ceramide synthase (sphinganine N-acyl transferase) [50]. It is now known that there are six mammalian genes that encode dihydroceramide synthase and they are termed longevity-assurance homologues (LASS1-LASS6). These ceramide synthases show distinct preferences for the different fatty acyl-CoA substrates and therefore generate distinct ceramides with different acyl-chain lengths [51]. Dihydroceramide reductase catalyzes the oxidation of dihydroceramide to form the trans-4,5, double bond of ceramide. Dihydroceramide is generated in the endoplasmic reticulum as well as the mitochondria [50].

The catabolic pathway for ceramide involves the action of sphingomyelinases and sphingomyelin-specific forms of phospholipase C, which hydrolyzes the phosphodiester bond of sphingomyelin (N-acylsphingosin-1-phosphorylcholine; SM). Sphingomyelin is a

phospholipid preferentially found in the plasma membrane of mammalian cells that yields ceramide and phosphorylcholine [50]. There are various isoforms of sphingomyelinases which are distinguished by their pH. A-SMase is the acidic sphingomyelinases located in acidic compartments such as lysosomes or endosomes. N-SMase (neutral) operates at the plasma membrane [52]. Ceramide can also be generated by breakdown of complex glycosphingolipids through acid hydrolases referred to as the salvage pathway [51]. Most of the ceramide required for the production of complex lipids is synthesized in the endoplasmic reticulum (ER), with subsequent metabolism occurring in the Golgi apparatus. A cytoplasmic ceramide transporter or 'CERT', mediates the transport of ceramide between the ER and the Golgi in a non-vesicular manner. It has a phosphatidylinositol-4-monophosphate-binding domain, which targets the Golgi apparatus, and a short peptide motif that recognizes a specific protein in the endoplasmic reticulum. The CERT protein extracts ceramides only from membrane bilayers with some specificity for those containing C_{14} to C_{20} fatty acids, and delivers it for the synthesis of sphingomyelin but not for glycosylceramide. The pool of ceramide utilized for synthesis of the glycosylceramide is delivered to the Golgi by a vesicular transport mechanism [51]

The physical properties of ceramides ensure that they are concentrated preferentially into lateral microdomains (rafts) with other sphingolipids, especially sphingomyelin. Ceramides may be generated within these rafts by the action of sphingomyelinases, causing small rafts to merge into larger units and modifying the membrane structure in a manner that is believed to permit oligomerization of specific proteins (i.e. integrins). Through the medium of rafts, they are then able to function in

signal transduction. Specific receptor molecules and signaling proteins cluster within such domains [53].

Once generated, ceramide can accumulate in the cell or be converted into a variety of metabolites. Ceramide can be converted to ceramide-1-phosphate by ceramide kinase and to SM by transfer of phosphorylcholine from phosphatidylcholine to ceramide by the enzyme SM synthase. Additionally, ceramide can be glycosylated by glucosylceramide synthase in the Golgi apparatus. Ceramide can also be deacylated by either neutral or acid ceramidases to yield sphingosine, which then may be further phosphorylated to sphingosine-1-phosphapate (S1P) by sphingosine kinase. Thus, ceramide generated under multiple metabolic pathways may act differently in response to different stimuli. [49].

There is the existence of a "SIP Rheostat" that may explain how ceramide can have a variety of diverse functions. This proposal is based on the fact that ceramide and its metabolite S1P can have opposing effects. Ceramide is usually considered pro-death and anit-proliferative while S1P promotes survival and cellular proliferation [54]. Ceramide plays a leading role in apoptotic signaling, including death receptor mediated TNF-α and CD95 cell death. After stimulation through these death receptors, the intracellular adapter FADD is required to activate A-SMase which then causes ceramide production and activation of caspases as well as p38 and JNK MAPKs [49]. S1P has also been implicated in protection against ceramide-induced cell death [55] Thus, the cell is destined for cell death when the balance leans towards ceramide and sphingosine, and towards cell survival and proliferation when S1P levels are increased [54].

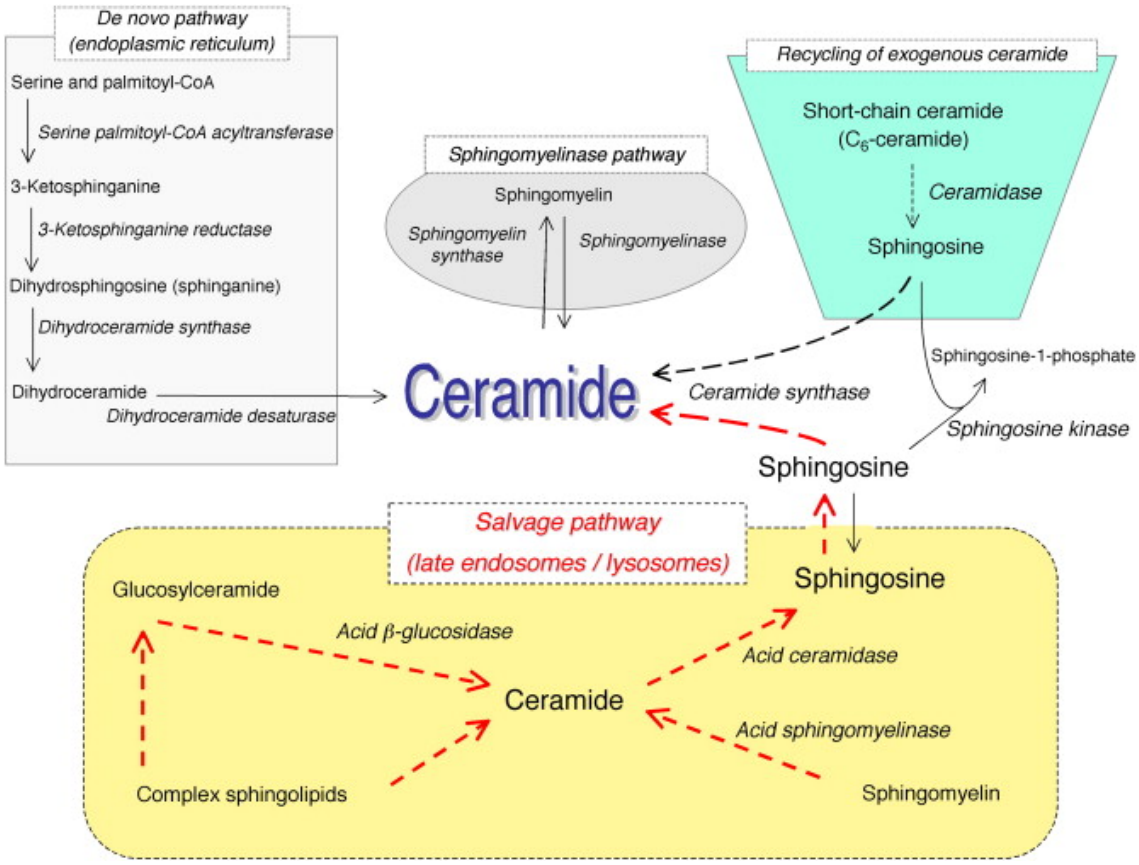

Figure 1.8. Ceramide Synthesis [51]. The main pathways to ceramide generation include the *de novo* pathway, the sphingomyelinase pathway, and the salvage pathway.

1.13 Molecular Chaperones in Protein Folding

Protein folding is the physical process by which a polypeptide folds into its characteristic three-dimensional structure. Protein structure can be described at four levels. The primary structure consists of the amino acid sequence and this determines the three-dimensional structure. The secondary structure refers to the polypeptide chain folding into a regular structure (i.e. alpha helix, beta sheet, and turns and loops). The tertiary structure is the compact, asymmetric structure in which all proteins have the common features of interior amino acids with a hydrophobic side chain and hydrophilic amino acids that can interact with the aqueous environment. The quaternary structure refers to the assembly of multisubunit structures. The correct structure of the protein is essential for its function. Thus, incorrect folding usually produces inactive proteins. The process of folding in vivo beings co-translationally so that the protein's N-terminus begins to fold while the C-terminus is still being synthesized on the ribosome [56].

Molecular chaperones also known as heat shock proteins (hsps) are ubiquitous in nature and act to maintain proper protein folding within the cell or proteasome-mediated degradation in the case of damaged proteins [56]. These proteins facilitate the correct folding in vivo but they do not contain steric information regarding the correct folding. Instead, they prevent incorrect interactions within non-native polypeptides increasing the yield but not the rate of folding reactions [56]. The demand of these heat shock proteins increases after environmental stress (i.e. drugs, toxic chemicals, and extreme temperatures), non-stress conditions, and disease states (i.e. Alzheimer's disease and cystic fibrosis) [57].

Hsps are classified by molecular weight into six major hsp families to include the small hsps (20-25 kda), hsp40, hsp60, hsp70, hsp90, and hsp100 [58]. The small hsps bind to partially denatured proteins and are responsible for protecting proteins from irreversible aggregation via an energy-independent process. Once suitable conditions are obtained for renewed cellular function, protein release and refolding are mediated by ATP-dependent chaperones like hsp70 [59]. The small hsps also function to maintain the integrity of membranes via specific lipid interactions under physiological conditions [60]. Hsp40, hsp60, and hsp70 are all involved in nascent protein folding [56]. Additionally, hsp40 is considered a co-chaperone for hsp70, playing a vital role in the stimulation of conformational changes in the ATPase domain of hsp70 [61]. Hsp70 is also important in the degradation of misfolded proteins as well as stabilization processes [56]. The hsp100 family of chaperones, function to disaggregate proteins and some members of this family target specific classes of proteins for degradation [62]. Hsp90 however, seems to be more important in cancer progression, stabilizing a number of signaling proteins involved in cancer progression and is it not required for de novo protein synthesis [63].

1.14 Hsp90 Structure and Function

Hsp90 is a heat shock protein that conserves the folding of newly translated protein [64]. It is distinctly different from other chaperones in that most of its substrates are signaling proteins. Classic examples include steroid hormone receptors and signaling kinases [65, 66]. Thus, disruption of Hsp90 in tumor cells has been shown to induce improper folding of many proteins, including Raf-1, B-Raf, Akt, and ERBB family receptors culminating in their proteosomal degradation [67]. Hsp90 is a constitutive homodimer and

has 3 domains, a 25 kda N-terminal domain, a charged linker domain, and a 55 kda C-terminal domain. The N-terminal domain binds ATP and other purine analogues [68], while the C-terminal domain is responsible for dimerization and is required for biologic activity [69, 70]. Hsp90 consists of two isoforms, alpha and beta. Hsp90α is elevated under stress conditions whereas hsp90β is constitutively expressed. The proteins are encoded on two separate genes, chromosome 14 for Hsp90α and chromosome 6 for hsp90β [71]. Although there are some functional differences between the two the isoforms [72] they are usually not distinguished from each other [73]. However, a knockout mouse strain for hsp90β is embryonic lethal [74].

The activity of hsp90 depends on an organized series of conformational changes and interactions with co-chaperones and client proteins operating in an ATP dependent cycle. There are over one hundred client proteins many being signal transduction proteins [75]. The interaction between hsp90 and many of its co-chaperones occur within the C-terminal domain of hsp90 [76]. The extreme C- terminus contains the amino acid sequence MEEVD, which is the binding site for co-chaperones that contain the tetratricopeptide repeat (TPR) region [77]. The biochemical mechanism of hsp90 binding to its client proteins involve ADP-bound hsp90 binding to hsp70 through accessory proteins like Hip and Hop. Hop has a TPR domain and binds to the C-terminus of hsp90. Hop also binds the N-terminal region of hsp70 thus linking hsp90 to hsp70 [76]. The binding of Hop induces a conformational change in the ATPase domain of hsp90 that inhibits the ATPase activity [68]. Dissociation of Hop and hsp70 results in another conformational change in the ATPase domain that enables ATP to bind. Upon this ATP binding, the N-terminal regions

transiently dimerize while the C-terminal domains remain dimerized and a molecular clamp is formed around the client protein [78]. Mature complexes of hsp90 with bound substrate (client proteins) are also characterized by binding of the co-chaperone p23. p23 stimulates the ATP hydrolysis and opening of the molecular clamp formed which causes dissociation of the hsp90-substrate complex. Thus the hsp90substrate binding and release cycle is regulated by Hop and p23 [78]. Hsp90-bound proteins can also be targeted for degradation by the co-chaperone CHIP. This protein has a TPR domain that recognizes both hsp90 and hsp70. CHIP contains a U-box domain similar to the E4 ubiquination proteins and may function to present misfolded proteins for ubiquination [79].

1.15 Hsp90 Regulation: Heat Shock Factors

Hsp90 genes are regulated by a family of transcription factors known as heat shock factors (HSFs). Hsp90 genes contain heat shock-responsive elements in their promoters, which are bound by the HSFs to initiate transcription. There are 4 HSF proteins to include HSF1, 2, and 4 which are ubiquitous in nature, and HSF3 which has been characterized in avain species [57]. Of the HSFs, HSF1 is the principal stress-induced transcription factor [80]. Mice lacking HSF1 can develop normally and reach adulthood. However, fibroblasts from these deficient mice are incapable of stress-induced transcription of heat shock genes [81].

HSFs consist of four conserved structural domains. The DNA binding domain is characterized by a helix-turn-helix motif. There is also a hydrophobic repeat domain essential for trimer formation and a carboxy-terminal transactivation domain [82]. Under unstressed conditions, HSF1 exists as a cytosolic monomer in complexes containing hsp70 and hsp90. Upon exposure to stress, HSF1 is activated and binds to the heat shock

promoter element (HSE) in hsp promoters. HSF1 forms a phosphorylated homotrimer in the nucleus that activates a program of transcription, including the upregulation of HSP production [83].

The transcriptional regulation of HSF1 is controlled in part by heat shock proteins. It has been shown that the binding of hsp70 to HSF1 at the hydrophobic carboxy-terminus suppresses the function of HSF1. When there is accumulation of non-native proteins during a stressful event, these may compete with HSF1 for binding to chaperone hsp70. Unbound HSF1 could then homotrimerize and be available for transcription [84]. Similarly, hsp90 can form a complex with HSF1 and repress its function as well. Additionally, geldanamycin, an inhibitor of hsp90, activates HSF1 in vitro [85].

CHAPTER 2 INTRODUCTION: SORAFENIB AND VORINOSTAT

2.1 Colon Cancer

Colorectal cancer is cancer of the colon or the rectum. The colon and the rectum are part of the digestive system, normally referred to as the gastrointestinal or GI system. Before colon cancer develops, benign polyps (abnormal masses of tissue) begin growing on the inner lining of the colon or rectum. These growths spread very slowly, taking from 10 - 20 years to become cancerous. Colonic polyps are divided into 3 groups, hyperplastic polyps, adenomas, and polyposis syndromes. Hyperplastic polyps comprise about 90% of all polyps and are benign protrusions. This type of polyp is usually insignificant. Adenomas comprise approximately 10% of polyps and pose a risk of becoming invasive. The risk of progression to carcinoma though, is related to both the size and the histology of the adenoma. Polyposis syndromes are hereditary conditions which may lead to an increased risk of developing colon cancer. Once colorectal cancer is diagnosed, the prognosis depends on how far the cancer has spread [86].

Colon cancer is the third most commonly diagnosed cancer among men and women in the United States. Each year more than 50,000 patients die from colorectal cancer with a 5 year survival rate of ~60%. However, for patients with non-localized tumor at diagnosis, the 5 year survival is ~10% [2]. These statistics indicate the need to develop new therapies to combat this type of cancer.

2.2 Colon Cancer Resistance

There are two main inherited predisposition syndromes for colorectal cancer: hereditary non-polyposis colorectal cancer (HNPCC) and familial adenomatous polyposis

(FAP). One reason for resistance may be related to genetics, for example chromosomal instability since colon cancer has a predisposition. A significant obstacle for successful management of patients with colorectal cancer is intrinsic drug resistance or, in patients who initially responded to chemotherapy, acquired drug resistance. Failures in normal apoptotic pathways contribute to resistance against anti-cancer drugs or radiotherapy. Also resistance generally is observed from cancers that arise from tissues that have detoxifying functions (i.e. colon, stomach, and kidney). It is thought that tissue-specific detoxification mechanisms are operative in the cancer cells and protect them from chemotherapy. Most improvements in the advancement of colon cancer stems from the use of drug combinations [87].

2.3 Sorafenib

In view of the importance of the RAF-MEK1/2-ERK1/2 pathway in neoplastic cell survival, inhibitors have been developed that have entered clinical trials, including sorafenib (Bay 43-9006, Nexavar®; a Raf kinase inhibitor). Sorafenib is an orally available bi-aryl urea compound (Figure 2.1). Sorafenib is marketed as Nexavar by Bayer and it is approved for the treatment of advanced renal cell carcinoma. It was originally developed as a small molecular inhibitor of Raf kinase (to include C-Raf, B-Raf, and mutant B-Raf or V599E), a member of the MAP kinase pathway. However, it is shown to also inhibit proteins involved in tumor angiogenesis. Sorafenib inhibits class III tyrosine kinase receptors such as platelet-derived growth factor (PDGFR-β), vascular endothelial growth factor receptors 2 and 3 (VEGFR-2, VEGFR-3), c-kit, and Flt-3 tyrosine kinases [88].

Thus, sorafenib has the potential to prevent tumor growth by combining two anticancer activities: inhibition of both tumor cell proliferation and tumor angiogenesis (Table 2.1).

Sorafenib has undergone numerous Phase 1 evaluation trials in refractory solid tumors. In 2000, Phase 1 trials showed the optimum regimen to be 400 mg b.i.d. orally. All four trials identified a hand-foot skin reaction as the most prominent dose-limiting toxicity [89]. Sorafenib is metabolized by oxidative metabolism mediated by cytochrome P450 (CYP) 3A4 and glucoronidation mediated by UGT1A9. The main metabolite of sorafenib is pyridine N-oxide. The intake of food does not impact sorafenib metabolism but a high fat meal does reduce bioavailability by 29%, although the label recommendation is that sorafenib be taken with food [90]. Anti-tumor effects of sorafenib in renal cell carcinoma and in hepatoma have been ascribed to anti-angiogenic actions of this agent through inhibition of the growth factor receptors [90-92]. Several groups, including ours, have shown *in vitro* that sorafenib kills human leukemia cells at concentrations below the maximum achievable dose (C_{max}) of 15-20 μM, through a mechanism involving down-regulation of the anti-apoptotic Bcl-2 family member Mcl-1 [93, 94]. In these studies sorafenib-mediated Mcl-1 down-regulation occurred through a translational rather than a transcriptional or post-translational process that was mediated by endoplasmic reticulum (ER) stress signaling [95, 96]. This suggests that the previously observed anti-tumor effects of sorafenib are mediated by a combination of inhibition of *Raf* family kinases and the ERK1/2 pathway; receptor tyrosine kinases that signal angiogenesis; and the induction of ER stress signaling.

2.4 Vorinsotat

Vorinostat or suberoylanilide hydroxamic acid (SAHA), marketed as Zolinza, is a histone deactylase inhibitor (Figure 2.2). Histone deacetylase inhibitors (HDACI) represent a class of agents that act by blocking histone de-acetylation, thereby modifying chromatin structure and gene transcription. HDACs, along with histone acetyl-transferases, reciprocally regulate the acetylation status of the positively charged NH_2-terminal histone tails of nucleosomes. HDACIs promote histone acetylation and neutralization of positively charged lysine residues on histone tails, allowing chromatin to assume a more open conformation, which favors transcription [97]. However, HDACIs also induce acetylation of other non-histone targets (Figure 2.3), actions that may have plieotropic biological consequences, including inhibition of HSP90 function, induction of oxidative injury and up-regulation of death receptor expression [98-100]. Vorinostat inhibits the enzymatic activity of HDAC1, HDAC2 and HDAC3 (Class I) and HDAC6 (Class II) at nanomolar concentrations. Vorinostat inhibits HDACs by binding to a zinc ion in the catalytic domain of the enzyme [101]. Vorinostat has shown preliminary pre-clinical evidence of activity in hepatoma and other malignancies with a C_{max} of ~9 μM [102-104].

Vorinostat is the first new HDACI to be approved for clinical use by the food and drug administration [105]. It is used for the treatment of cutaneuous T cell lymphoma (CTCL). The recommended dose for vorinostat is 400 mg orally once daily with food. The major dose-limiting toxicities associated with oral vorinostat were observed in phase 1 and 2 clinical trials and included anorexia, dehydration, diarrhea, and fatigue. The major pathways of vorinostat metabolism involve glucoronidation and hydrolysis followed by β-

oxidation. There are two pharmacologically inactive metabolites, O-glucoronide of vorinostat and 4-anilino-4oxobutanoic acid that are formed [106].

2.5 Basis for Sorafenib and Vorinostat Project

With respect to combinatorial drug studies with a multi-kinase inhibitor such as sorafenib, HDACIs are of interest in that they have potential to down-regulate multiple oncogenic kinases by interfering with HSP90 function, leading to proteasomal degradation of these proteins. Thus, if we combine sorafenib and vorinostat, this combination may prove to be more effective than individual drug alone. Additionally, lower does of these agents could be given to achieve the same toxic effects individually. We recently published that sorafenib and vorinostat to interact to kill in renal, hepatocellular and pancreatic carcinoma cells via activation of the CD95 extrinsic apoptotic pathway, concomitant with drug-induced reduced expression of c-FLIP-s via PKR like endoplasmic reticulum kinase (PERK) signaling to eIF2α [107, 108]. Subsequent work mechanistically advanced our understanding to reveal that sorafenib and vorinostat interact by activating acidic sphingomyelinase and the de novo ceramide pathway to promote CD95 activation which regulates both apoptosis and autophagy [108]. The present studies determined whether the same killing mechanisms apply after sorafenib and vorinostat treatment in colon cancer cells.

Sorafenib (BAY 43-9006)

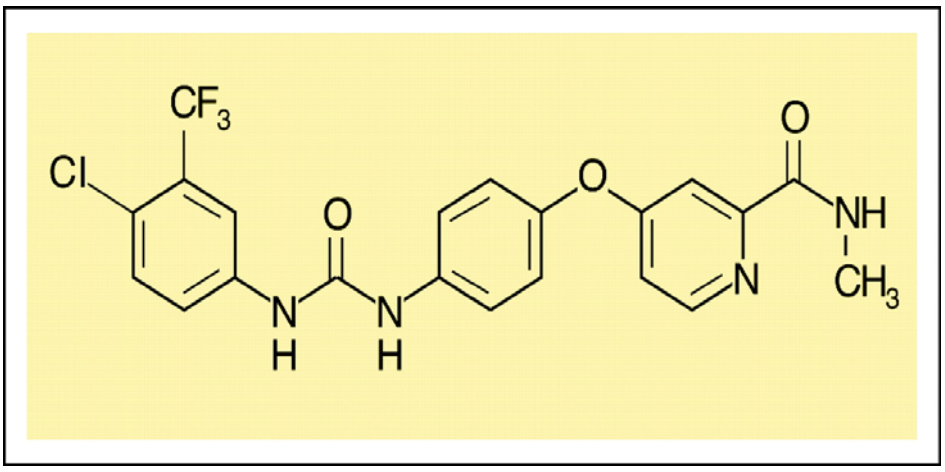

Figure 2.1. Chemical Structure of Sorafenib [109].

Biochemical Assay *	IC_{50} (nM) ± SD
Raf-1 **	6 ± 3
BRAF wild-type	22 ± 6
V599E BRAF mutant	38 ± 9
VEGFR-2	90 ± 15
mVEGFR-2 (flk-ss1)	15 ± 6
mVEGR-3	20 ± 6
mPDGFR-β	57 ± 20
Flt-3	58 ± 20
c-KIT	68 ± 21
FGFR-1	580 ± 100
ERK-1, MEK-1, EGFR, HER-2, IGFR-1, c-met, PKB, PKA, cdk1/cyclinB, PKC, PKC, pim-1	>10,000

Table 2.1. Sorafenib inhibition of the MAP Kinase pathway and receptor tyrosine kinases involved in tumor angiogenesis. ***** Kinase assays were carried out at ATP concentrations at or below Km (1-10 μM)** Lck-activated NH2-terminal-truncated Raf-1. (Adapted from [110].)

Figure 2.2. Chemical Structure of Vorinostat [111].

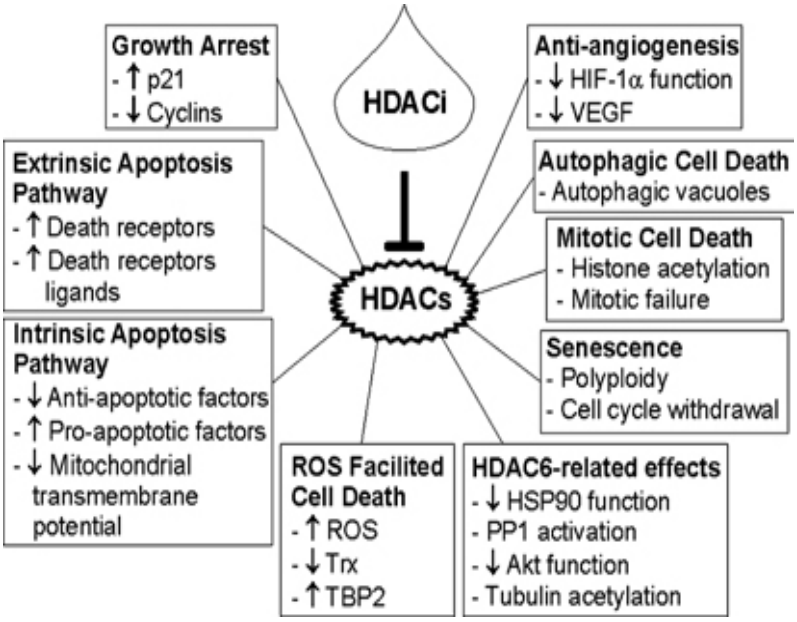

Figure 2.3. HDACI complex mechanism of action [112].

CHAPTER 3 MATERIALS AND METHODS: SORAFENIB AND VORINOSTAT

3.1 Materials

Dulbecco's Modified Eagle's Medium (DMEM), RPMI 1640 medium, trypsin-EDTA, and penicillin-streptomycin were purchased from GIBCOBRL (GIBCOBRL Life Technologies, Grand Island, NY). Trypan blue solution, formaldehyde, 6-Diamidino-2-Phenylidole (DAPI), and dimethyl sulfoxide (DMSO) were all obtained from Sigma Chemical (St. Louis, MO).

Sorafenib (BAY-439006; Bayer) and vorinostat (Merck) were provided by the Cancer Treatment and Evaluation Program, National Cancer Institute/NIH (Bethesda, MD). Obatoclax was generously provided Gemin X Biotechnologies. JNK inhibitor peptide was supplied by Calbiochem (San Diego, CA) as a powder, dissolved in sterile DMSO, and stored frozen under light-protected conditions at -80˚C.

Anti-caspase 3 (1719//35 kDa cleaved/full, 1:1000, rabbit monoclonal), Anti-caspase 8 (18/43/57 kDa cleaved/full, 1:1000, mouse monoclonal), Anti-FLIP (30/60 kDa short/long, 1:1000, rabbit polyclonal), anti-Beclin-1 (60 kDa, 1:1000, rabbit polyclonal), anti-Mcl-1 (40 kDa, 1:1000, rabbit polyclonal), phospho-eIF2α (38 kDa, 1:1000, rabbit polyclonal), phospho-/total-p38α/β (38 kDa, 1:1000, rabbit polyclonal), phospho-/total-JNK1/2 (46, 54 kDa, 1:1000, rabbit polyclonal), anti-Bcl-2 (26 kDa, 1:500, mouse monoclonal), anti-Bcl-xL (30 kDa, 1:1000, rabbit polyclonal), anti-BID (15/22 kDa cleaved/full, 1:1000, rabbit polyclonal), anti-Bip (78 kDa, 1:1000, rabbit polyclonal), anti-

FAS receptor (48 kDa, 1:1000, rabbit polyclonal), anti-FAS ligand (40 kDa, 1:1000, rabbit polyclonal), anti-Bak (25 kDa, 1:1000, rabbit polyclonal) and anti-Bax (20 kDa, 1:1000, rabbit polyclonal) were obtained from Cell Signaling Technology (Worcester, MA). Anti-GAPDH (37 kDa, 1:1000, mouse monoclonal), phospho-PERK (125 kDa, 1:500, rabbit polyclonal), phospho-/total ERK1/2 (42, 44 kDa, 1:1000, mouse monoclonal), phospho-/total-Akt (60 kDa, 1:1000, rabbit polyclonal), phospho-MEK and all of the secondary antibodies (anti-rabbit-HRP, anti-mouse-HRP, and anti-goat-HRP) were obtained from Santa Cruz Biotechnology (Santa Cruz, CA). Anti-Atg5 (49 kDa, 1:1000, rabbit polyclonal) was purchased from Abcam (Cambridge, MA). Anti-LC3 (17/19 kDa, LC3II/LC3I, rabbit polyclonal) was obtained from Novus Biologicals (Littleton, CO).

Commercially available siRNA duplexes to knockdown RNA/protein levels were from Qiagen (Valencia, Ca): CD95 (SI02654463; SI03118255); ATG5 (SI02655310); Beclin 1 (SI00055573, SI00055587). The plasmids to express green fluorescent protein (GFP)- tagged human LC3; wild type and dominant negative PERK (Myc-tagged PERKΔC); were kindly provided by Dr. S. Spiegel, VCU, Dr. J.A. Diehl University of Pennsylvania, Philadelphia, PA.

3.2 Cell Culture

HCT116 (p53 wild type) cells are a colon cancer cell line from American Type Culture Collection (ATCC). These cells express an active K-RAS D13 mutation. HCT116 stably transfected cell lines were previously generated. The empty vector HCT116 cell line is genetically deleted for K-RAS D13. These cells were then transfected to express a mutant active H-Ras (H-Ras V12) where the plasmid was kindly provided by Dr. M.

Wigler (Cold Spring Harbor, NY). HCT116 H-RAS V12 cells were then transfected with either an active mutant of PI3K, Ral, or Raf. These cells were maintained in Geneticin (GIBCOBRL Life Technologies, Grand Island, NY) for selection. All the above cells were cultured in DMEM medium with L-glutamine and supplemented with 5% (v/v) fetal bovine serum and 2% (v/v) penicillin/streptomycin according to supplier instructions. HD6 cells (p53 mutant) were subcloned from HT29 cells and recloned as HD6-4 cell line. The cells are from the lab of Eileen Friedman [113]. The HD6-4 cell line has wildtype ras genes. These cells were transfected with either overexpression of K-Ras (G3), an active K-Ras mutant (V1), or an active H-Ras mutant (H18). Both active mutants are mutated at codon 12 from Gly to Val. These transfectants as well as the parental HD6-4 cell line were maintained in DMEM medium with L-glutamine and supplemented with 10% (v/v) fetal bovine serum and 2% (v/v) penicillin/streptomycin according to supplier instructions. SW480 cells are from ATCC. These cells were maintained in RPMI medium with L-glutamine and supplemented with 10% (v/v) fetal bovine serum and 2% (v/v) penicillin/streptomycin according to supplier instructions. SW620 cells (ATCC), patient matched to SW480 cells were maintained in DMEM with L-glutamine and supplemented with 10% (v/v) fetal bovine serum and 2% (v/v) penicillin/streptomycin according to supplier instructions. SW620 cells expressing LASS6 were provided by Dr. Voelkel-Johnson. All cells were routinely subcultured and maintained in a 10 % CO_2/90 % air/37^{o}C humidified incubator. In addition, all cells were examined frequently for contamination with bacteria or fungus by visual inspection. Also, cells were routinely tested for mycoplasma contamination. Cells were not cultured in reduced serum media

during any study in this manuscript. Table 3.1 outlines the various cell lines that were used.

3.3 Assessment of Cell Viability

A method used for evaluating cell viability involves the trypan blue inclusion/exclusion of isolated cells under light microscopy and scoring the percentage of cells exhibiting blue staining indicative of cell death. Cells were washed once with PBS and trypsinized to detach cells from 12 well plates. Cells were centrifuged for 4 minutes at 1400 rpm at 25ºC (room temperature). The media was then aspirated off and trypan blue was added to the tube depending on pellet size. The trypan blue inclusion/exclusion represents the integrity of the cellular membrane in that healthy, viable cells contain intact cell membranes and thus reject the trypan blue stain, while damaged cells exhibit a blue color due to a compromised cellular membrane that allows the trypan blue stain to be incorporated into the cell. Viable cells and trypan blue stained cells were counted in a hemacytometer viewed under a microscope. Calculations of cell death were made using the number of trypan blue positive cells divided by alive cell number multiplied by 100 to get the percentage of cell death.

3.4 Western Blot Analysis for Protein Expression

a.) Protein Isolation

Cells were plated at an appropriate density and treated with drug. At the indicated times after drug exposure, cells were washed in PBS and then scraped from the using whole-cell lysis buffer (0.5 M Tris-HCl, pH 6.8, 2% (w/v) SDS, 10% (v/v) glycerol, 1% (v/v) β-mercaptoethanol, 0.02% (w/v) bromophenol blue). A 1:20 dilution of protease inhibitor

cocktail (Roche) and a 1:100 dilution of phosphatase inhibitor cocktail (Roche) was also added to the lysis buffer. The samples were then vortexed to dislodge the pellet, heated at 95-100ºC for 5 minutes and placed immediately on ice.

b.) Electrophoresis

50-100 µg aliquots of cell protein (depending on the protein analyzed) was loaded onto a polyacrylamide gel (10-15%, depending on the size of the protein analyzed). Samples were run in a SDS-PAGE running buffer (3.02g Tris-base, 14.40g glycine, 1.0g SDS, QS to 1 L deionized water) for approximately 6 hours with a constant current of 60 mA. Proteins were transferred onto a nitrocellulose membrane electrophoretically for 4 hours on ice at 450 mA in transfer buffer (5.8g Tris-base, 2.9g glycine, milli-Q water to 800 ml, 1.8 ml 20% (w/v) SDS, 200 ml methanol.)

c.) Immunoblotting

The membrane was blocked in TBS-tween buffer containing 5% (w/v) non-fat dry milk for 30 minutes. After removal of the blocking solution, the primary antibody was added at a certain dilution to fresh block solution. After an overnight exposure with the primary antibody at 4ºC with orbital shaking, the antibody/wash solution was removed and the membrane was washed with blotto wash (5 x 5 minutes). The membrane was then incubated with the corresponding goat anti-mouse or rabbit secondary antibody for 2 hours at room temperature with orbital shaking. The secondary antibody was then removed and the membrane washed in blotto wash again, 5 x 5 minutes. All immunoblots were visualized by ECL. For presentation, immunoblots were digitally scanned at 600 dpi using

Adobe PhotoShop CS2, and their color removed and figures generated in Microsoft PowerPoint.

3.5 Co-Immunoprecipitation: DISC Formation

Cells were plated at an appropriate density and treated with drug. At the indicated times after drug exposure, cells were washed in PBS and then scraped from the flask in 200 µl NP40 Buffer (50 mM Tris-HCL pH 7.5, 150 mM NaCl, 1 mM EDTA, 0.75% NP40). The cells are then harvested and placed in a 1.5 ml eppendorf tube and pipetted up and down 10 times using a 25-gauge needle. The cells are placed on iced for 5 minutes and then spun down at 6000 rpm for 3 minutes. The supernatant is collected and anti-CD95 is added to the samples (8 µl/sample). The cells are left at 4ºC overnight rocking. The next day, 25 µl/sample of protein Sepharose beads are added, shaking or rocking at 4ºC for an hour. The samples are then spun at 8000 rpm for 3 minutes. The supernatant is collected for immunoblot analysis of the GAPDH for loading control. The pellet is saved, washed with NP40 buffer, and spun down again two more times at 8000 rpm for 3 minutes. Approximately 60 µl of lysis buffer (0.5 M Tris-HCl, pH 6.8, 2% (w/v) SDS, 10% (v/v) glycerol, 1% (v/v) β-mercaptoethanol, 0.02% (w/v) bromophenol blue) is added per sample, placed on ice for 10 minutes, and boiled for 5 minutes. The samples are stored at 80º C until immnoblot analysis.

3.6 Colony Formation Assay for Cell Survival

Cells were plated as single cells (100– 125 cells/well) in a 6 well plate. Twenty four hours after plating, cells were treated with three different drug concentrations of each

drug as well as the combination of both drugs for 48 h. After 48 h, the drug-containing media was carefully removed, the cells were washed once, and fresh media lacking drugs were added. Colony formation assays were cultured for an additional 10 to 14 days. Upon colony formation, the medium was removed and the cells washed in 1X PBS. The cells were then fixed on the dish by adding 100% methanol for 10 minutes. The methanol was then removed and the cells were placed in a 0.1% (v/v) crystal violet (Sigma-Aldrich) staining solution for 1 h. Colonies containing more than 50 cells were then counted and normalized to the control cell survival sample. The survival data shown includes individual assays performed at multiple dilutions with a total of six plates per data point, repeated for a total of three experiments.

3.7 Flow Cytometric Assay

Cells were plated in 12-well plates at a concentration of approximately 5 x 10^4 cells per well and 24 h later treated with drug. The medium was removed 48 h after treatment, from the cells and placed in 15 ml conical tubes (Fisher Scientific, Pittsburgh, PA). The cells were then washed in 1X PBS, trypsinized, and harvested with appropriate medium and also placed in the 15 ml conical tubes. The samples were then centrifuged at 1400 RPM for 5 minutes at 25º C in an Eppendorf 5804 R centrifuge. The supernatant was then aspirated and the cells re-suspended in ice cold PBS. The samples were centrifuged again at the same specifications. The supernatant was again aspirated. A 1:10 dilution of Annexin buffer (Annexin V-FITC kit, PD PharMingen). was prepared and 100 µl of this diluted buffer was added to each tube. Next, 1 µl of Annexin V/FITC solution and 5 µl of

dissolved propidium iodide were added to the cell suspensions. Tubes were kept on ice in the dark for fifteen minutes. After this time period, 400 µl of ice-cold 1X binding buffer was added to the suspensions and mixed gently. Flow cytometry was performed using a Becton Dickinson FACScan flow cytometer (Mansfield, MA).

3.8 Recombinant Adenoviral Vectors: Infection in Vitro

We purchased recombinant adenoviruses to express (CRM-A, c-FLIPs, Bcl-xL, XIAP) or to express dominant negative (Akt, MEK, caspase 9, or activated MEK1 or caAkt) as well as a negative control using CMV (Vector Biolabs, Philadelphia, PA). rAAV vectors mediate long-term gene transfer without any known toxicity and can be used to transfer exogenous genes. *In vitro* adenoviral infections were performed 24 hours after plating cells. Monolayer cultures were washed in PBS prior to infection and specific virus was added to the monolayer cultures in serum-free growth medium at an m.o.i. (multiplicity of infection) of 25 (m.o.i. = # of virus per cell). The dishes were then placed on a rocker for 4 hours in a humidified atmosphere of 5% (v/v) CO_2 at 37º C. The serum free growth medium was removed after 4 hours and the appropriate medium was added back to the cells and allowed to incubate overnight in the same humidified atmosphere. The expression of the recombinant viral transgene was allowed to occur for 24 h to ensure adequate expression of transduced gene products before drug exposures.

3.9 Transfection using Small Interfering RNA Molecules (siRNA) or plasmids

RNA interference or gene silencing for down-regulating the expression of specific siRNA was performed using validated target sequences designed by Ambion (Austin, TX). Plasmids were used at a concentration of 1 µg/µl or appropriate vector control plasmid

DNA. For siRNA, 10 nM concentration of the annealed siRNA or the negative control (a "scrambled" sequence with no significant homology to any known gene sequences from mouse, rat, or human cell lines) were used. The siRNA molecules were transfected into cells according to the manufacturer's instructions.

Briefly, cells were plated and allowed to sit overnight until about 80% confluent. For each well 2 µl of siRNA (or 1µl/µg plasmid) was diluted in 100 µl pen-strep-and-FBS-free medium (100 µl for chamber slides), in a 96 well plate. For each well, 2 µl of lipofectamine 2000 reagent (Invitrogen, Carlsbad, CA) was diluted into 100 µl pen-strep-and-FBS-free medium in a separate tube. The two solutions were incubated separately for approximately 5 minutes, then combined and incubated at room temperature for 30 minutes. After incubation, the total mix (400 µl) was added to each well. Cells were incubated for 4 hours at 37º C with gentle rocking. After 4 hours, the media was then replaced with 1 ml of its regular media with antibiotics and FBS.

3.10 Immunohistochemistry: CD95 surface localization

Cells were plated on chamber slides, collected from the culture the next day, and washed once with DPBS (Dulbecco's PBS without calcium and magnesium, Mediatech, Inc, Herndon, VA). The cells were then fixed in a solution of 4% paraformaldehyde in PBS for twenty minutes. Cells were washed again in DPBS and nonspecific binding was blocked with a 1% (v/v) BSA and 2% (v/v) rat serum DPBS solution for 1 hour. Slides were then incubated with a 1:100 dilution of the primary anti-Fas in block solution overnight in a humidified chamber. The next day, slides were washed once in DPBS and

incubated for 1 hour with secondary goat anti-mouse Alexa 488/647 at a dilution of 1:500 in block solution. Slides were washed after an hour, and coverglasses were mounted onto the glass slides using Vectashield with Dapi (Calbiochem, Madrid, Spain). Preparations were observed in a Zeiss LCM 510 meta-confocal microscope and analyzed using the Axio 2.0 software. No labeling was observed when using the secondary antibodies alone.

3.11 GFP-LC3 Assay

The green fluorescent protein (GFP)-tagged microtubule-associated protein 1 light chain 3 (LC3) expression vector was kindly provided by Dr. S. Spiegel, (VCU) and Dr. J.A. Diehl, (University of Pennsylvania, Philadelphia, PA). LC3 is recruited to the autophagosomal membrane during autophagy. Therefore, GFP-tagged LC3-expressing cells have been used to demonstrate the induction of autophagy. GFP-LC3 cells present a diffuse distribution under control conditions, whereas a punctate pattern of GFP-LC3 expression) is induced by autophagy. Cells were transiently transfected with the GFP-LC3 vector using lipofectamine 2000 transfection reagent (Invitrogen, Carlsbad, CA). After overnight culture, cells were treated with the appropriate drug or drugs for 6 hours and 24 hours and examined under a fluorescence microscope. To quantify autophagic cells after drug treatment, the number of GFP-LC3 vacuoles among 50X GFP-positive cells were counted.

3.12 Statistical Analyses

The effects of various treatments were analyzed using one-way ANOVA and a two-tailed t test. Differences containing a p-value less than 0.05 were considered statistically significant. The experiments shown are the means of multiple individual points (+/-SEM).

Cell Line	Media	Antibiotic in Culture	Transfection	p53 status	Other Mutations
HCT116 wt	5% DMEM	\	\	Wt	K-RAS
HCT116 V12	5% DMEM	Geneticin (0.05mg/ml)	\	Wt	Harvey-RAS V12 mutation
HCT116 V12 - vector	5% DMEM	Geneticin (0.05mg/ml)	empty vector, K-RAS deleted	Wt	
HCT116 V12 -40	5% DMEM	Geneticin (0.05mg/ml)	PI3K	Wt	
HCT116 V12- 37	5% DMEM	Geneticin (0.05mg/ml)	RAL	Wt	
HCT116 V12- 35	5% DMEM	Geneticin (0.05mg/ml)	Raf	Wt	
DLD1	5% DMEM	\	\	Mutant	
SW480	10% RPMI	\	\	Mutant	
HT29	10% DMEM	\	\	Mutant	
HD6-4	10% DMEM	Geneticin (0.05mg/ml)	Empty Vector	mutant (inactive)	wt RAS (no mutant RAS)
HD6-4 G3	10% DMEM	Geneticin (0.05mg/ml)	overexpress wt K-RAS	mutant (inactive)	
HD6-4 V1	10% DMEM	Geneticin (0.05mg/ml)	K-RASG12V (active)	mutant (inactive)	
HD6-4 H18	10% DMEM	Geneticin (0.05mg/ml)	H-RASG12V (active)	mutant (inactive)	

Table 3.1. Cell Line Information. This table consists of cell lines used during the sorafenib and vorinostat project.

CHAPTER 4 RESULTS: Sorafenib and Vorinostat

4.1 Sorafenib and Vorinostat decrease cell viability in colon cancer cells

Colon cancer cells were plated at a density of 1.2 $x10^4$ cells per well in a 12 well plate. Cells were treated with vehicle (DMSO), 6 μM sorafenib (3 μM sorafenib for HCT116 wt cells), 500 nM vorinostat, or the combination of both drugs. After 96 hours, trypan blue exclusion assays were performed as described in materials and methods. Treatment of HCT116 wt, DLD1, SW480, and SW620 cells resulted in a greater than additive induction of cell killing than either individual agent alone. However, the percentage of cell death was much lower in SW620 cells than compared to any other cell line (Figure 4.1).

4.2 Sorafenib and Vorinostat synergize to kill HCT116 wt cells in colony formation assays

We next used colony formation assays to determine long term effects on cell survival. Colon cancer cells were plated as single cells (100-125 cells/well) in a 6 well plate. There was one treatment condition per plate. Twenty four hours after plating, cells were treated with either Sorafenib (3, 4.5 or 6 μM) or Vorinostat (0.25, 0.375, or 0.5 μM), and the combination of both drugs as indicated at a fixed concentration ratio to perform median dose effect analysis for the determination of synergy. Forty eight hours after drug exposure, the media was changed and the cells were cultured in drug free media for an additional 10-14 days. Cells were fixed, stained with crystal violet, and colonies >50 cells/colony counted as described in materials and methods under colony formation assay.

Colony formation data was entered into the Calcusyn program and combination index (CI) values determined. CI values less than 1 indicates synergy, equal to 1 indicates additive interactions, and CI values > 1 indicates antagonism (Figure 4.2). Similar results are obtained with SW480 (Figure 4.3) but not with DLD1 colon cancer cells (Figure 4.4).

4.3 Sorafenib and sodium valproate synergize in colony formation assays to kill colon cancer cells

We used an unrelated clinically used HDACI, sodium valproate instead of vorinostat to determine if similar results could be obtained. Colon cancer cells were plated as single cells (100-125 cells/well) in a 6 well plate. There was one treatment condition per plate. Twenty four hours after plating, cells were treated with either Sorafenib (3, 4.5, or 6 μM) or sodium valproate (Val. 0.5, 0.75, 1.0, 1.25, or 1.5 mM), and the combination of both drugs as indicated at a fixed concentration ratio to perform median dose effect analysis for the determination of synergy. Forty eight hours after drug exposure, the media was changed and the cells were cultured in drug free media for an additional 10-14 days. Cells were fixed, stained with crystal violet, and colonies >50 cells/colony counted as described in materials and methods under colony formation assay. Colony formation data was entered into the Calcusyn program and combination index (CI) values determined. CI values less than 1 indicates synergy, equal to 1 indicates additive interactions, and CI values > 1 indicates antagonism (Figure 4.5). Similar results are obtained with SW480 (Figure 4.6).

4.4 Sorafenib and Vorinostat induce Apoptosis by Flow Cytometry

We used flow cytometry as a better measure to detect apoptosis than trypan blue exclusion assays. The trypan blue exclusion assay measures late apoptotic events, while flow cytometry can detect early and late apoptotic events. HCT116 wt cells were plated at a density of $2.5x10^4$ cells per well in a 12 well plate. Cells were treated vehicle (DMSO), 3 μM sorafenib, 500 nM vorinostat, or the combination of both drugs. After 48 hours, flow cytometry was performed using Annexin V/propidium iodide staining as described in materials and methods. Treatment of the HCT116 wt cells resulted in a greater than additive induction of cell killing than either individual agent alone (Figure 4.7A). Similar results are shown in the SW480 cell line (Figure 4.7B). Based upon these interesting findings, the mechanism of this drug combination was investigated.

4.5 Basal activation of ERK1/2 predicts for a Sorafenib and Vorinostat response

Ras effector mutants were used to decipher the mechanism of action of the combination of sorafenib and vorinostat. Many colon cancer patients have RAS mutations, and exploring the sensitivity of this drug combination on active mutants of the MAP kinase pathways would further aid in the mechanism of action. HCT116 wt, HCT116 V12, as well as the HCT116 V12 transfectants were plated at a density of $2.5x10^4$ cells per well in a 12 well plate. Cells were treated vehicle (DMSO), 3 μM sorafenib, 500 nM vorinostat, or the combination of both drugs. After 48 hours, flow cytometry was performed using Annexin V/propidium iodide staining as described in materials and methods. HCT116 cells genetically deleted for expression of mutant K-RAS D13 (vector) are less sensitive to treatment by sorafenib and vorinostat, than in the parental wild type cells. Lethality was

restored in cells transfected to express H-RAS V12 or H-RAS V12 RAF, but not in cells expressing H-RAS V12 RAL or H-RAS V12 PI3K (Figure 4.8). This indicates that activation of the Raf/MEK/ERK MAP kinase pathway predicts for drug toxicities, and that Ras mutations can be used as a predictor tool for the sensitivity to this combination drug treatment. This also indicates that activation of ERK1/2 in the absence of PI3K or RAL GDS activation promotes HDACI toxicity.

HT29 colon cancer cells express a mutated active B-Raf protein, but do not express mutated K-RAS. In a similar manner to HCT116 cells, expression of mutated active K-RAS protein in HT29 (HD6-4) cells enhanced the lethality of the drug combination (Figure 4.9). However the toxic effect was not as profound as that observed in other colon cancer cell types.

4.6 Sorafenib and Vorinostat decrease activation of ERK1/2 but not Akt in HCT116 wt cells

We explored the MAP kinase pathways further by reviewing the expression of other members of the RAF/MEK/ERK MAP kinase pathway such as the phosphorylation of ERK and reviewing the PI3K pathway and the role of AKT. HCT116 cells were plated at a density of 1 $x10^6$ cells per 10 cm dish. Cells were exposed to vehicle (DMSO) or the combination of sorafenib and vorinostat. Cells were isolated 24 to 96 hours after drug exposure and subjected to SDS-PAGE and immunoblotting as described in materials and methods. The phoshorylation of ERK1/2, and Akt was determined (Figure 4.10). Phosphorylation of Akt (S473) was not altered over the course of 96 hours in HCT116wt cells. In a similar manner to findings in hepatoma cells, sorafenib and vorinostat exposure

transiently inactivated ERK1/2 by 48 hours in combined drug-exposed cells. This is another indication that the PI3K pathway is not involved in the mechanism of action of this combination treatment.

4.7 Activated MEK1 suppresses the toxicity of Sorafenib and Vorinostat

Based on the findings in Figure 4.10, we determined whether expression of constitutively activated MEK1 and/or Akt protected cells from vorinostat and sorafenib exposure. HCT116 wt cells were plated at a density of $2.5x10^4$ cells per well in a 12 well plate. Cells were infected 24 hours after plating with empty vector control virus (CMV) or viruses to express constitutively active MEKEE (ca-MEKEE), constitutively active Akt (caAKT1), or the combination of the active Akt and active MEKEE viruses as described in materials and methods. The next day, cells were treated vehicle (DMSO), 3 μM sorafenib, 500 nM vorinostat, or the combination of both drugs. After 48 hours, flow cytometry was performed using Annexin V/propidium iodide staining as described in materials and methods. Activated MEK1 protected the cells from the increase in cell death seen in the CMV control. However, active Akt did not cause as significant a decrease in cell death (agreeing with our data in figure 4.10), indicating that one mechanism of drug toxicity is via inhibiting the Raf/MEK/ERK MAP kinase pathway and not the PI3K pathway. The combination of active MEK1 and active Akt did not suppress cell death to a greater extent than active MEK1 alone (Figure 4.11). Expression of activated MEK1 maintained ERK1/2 phosphorylation and active Akt expressed Akt phosphorylation in non-treated cells (Figure 4.11, inset).

4.8 DNMEK1 increased sorafenib and vorinostat toxicity in HCT116 wt cells

In view of the observation that activated MEK protected cells from sorafenib and vorinostat toxicity, studies were performed to determine the effects silencing MEK and/or AKT. HCT116 wt cells were plated at a density of $2.5x10^4$ cells per well in a 12 well plate. Cells were infected 24 hours after plating with empty vector control virus (CMV) or viruses to knockdown MEKEE (DNMEK1), Akt (DNAKT1), or the combination of the DNAKT and active DNMEK1 viruses as described in materials and methods. The next day, cells were treated vehicle (DMSO), 3 μM sorafenib, 500 nM vorinostat, or the combination of both drugs. After 48 hours, flow cytometry was performed using Annexin V/propidium iodide staining as described in materials and methods. Expression of dominant negative MEK1, but not dominant negative Akt, enhanced the toxicity of sorafenib, vorinostat, and the drug combination (Figure 4.12). The effects we saw with DNAKT could be due to an increase in JNK activity which would promote a protective form of autophagy in these cells.

4.9 Sorafenib and Vorinostat increase the phosphorylation of p38 and JNK in HCT116 wt cells

We next explored the JNK and p38 MAP kinase pathways to understand their involvement in sorafenib and vorinostat lethality. HCT116 cells were plated at a density of $1 x10^6$ cells per 10 cm dish. Cells were exposed to vehicle (DMSO), 3 μM sorafenib, 500 nM vorinostat, or the combination of both drugs. Cells were isolated 6 and 24 hours after drug exposure and subjected to SDS-PAGE and immunoblotting as described in materials

and methods. The phoshorylation of p38 and JNK was determined. Phospho-p38 and phospho-JNK expression levels transiently increased after 6 hours with the drug combination (Figure 4.13). This is different from data seen in hepatoma cells (where no activation was observed). Consequently, JNK activation could again lead to a protective form of autophagy.

4.10 DNp38 or JNK IP did not suppress sorafenib and vorinostat lethality in HCT116 wt cells

Based on the fact that p38 and JNK was transiently activated, we used molecular approaches to define the role of the p38 and JNK pathways. HCT116 wt cells were plated at a density of $2.5x10^4$ cells per well in a 12 well plate. Cells were infected 24 hours after plating with empty vector control virus (CMV) or virus to knockdown p38 (DNp38). Thirty minutes prior to drug exposure cells were treated as indicated with vehicle (DMSO) or the JNK inhibitory peptide (JNK-IP, 10 μM). The next day, cells were treated vehicle (DMSO), 3 μM sorafenib, 500 nM vorinostat, or the combination of both drugs. After 48 hours, flow cytometry was performed using Annexin V/propidium iodide staining as described in materials and methods. Expression of dominant negative p38 MAPK modestly suppressed vorinostat lethality but did not alter the lethality of sorafenib and vorinostat exposure. Inhibition of JNK1/2 using the cell permeant JNK inhibitory peptide blunted sorafenib toxicity and enhanced the lethality of sorafenib and vorinostat exposure (Figure 4.14).

4.11 Overexpression of c-FLIP or ectopic expression of CrmA did not reduce sorafenib and vorinostat lethality in HCT116 wt cells, but c-FLIP did significantly reduce lethality in SW480 cells

Previous studies in our laboratory have shown that the downregulation of anti-apoptotic proteins or the overexpression of pro-apoptotic proteins mediate the toxic effects of sorafenib and vorinostat combination drug therapy. We explored the extrinsic apoptotic pathway first and investigated the role of caspase 8, by using inhibitors. Cells were plated at a density of 2.5 x 10^4 in 12 well plates. Cells were allowed to attach overnight and the next day cells were infected with adenovirus FLIP, cytokine response modifier A (CrmA), as well a CMV control adenovirus. FLIP is a caspase 8 inhibitor. CrmA is cowpox virus-encoded anti-apoptotic protein that is a member of the serpin family which specifically inactivates the cellular proteins caspase 1, caspase 8 and granzyme B [114]. Cells were infected as described in materials and methods. The next day, cells were treated with vehicle (DMSO), 3 μM sorafenib (6 μM in SW480 cells), 500 nM vorinostat, or the combination of both drugs. After 48 hours, flow cytometry was performed using Annexin V/propidium iodide staining as described in materials and methods. Overexpression of FLIP-s weakly blunted drug –induced cell killing HCT116 wt cells (Figure 4.15). CrmA alone had toxic effects in vehicle DMSO treated HCT116 wt cells and the addition of the individual drugs or the combination did not suppress cell death. FLIP-s, however, did reduce the toxic effects of sorafenib and vorinostat in SW480 cells, similar to previous studies in our laboratory (Figure 4.16). Total cell lysates were analyzed by immunoblotting

with anti-FLIP to assess the levels of expression of infected FLIP in both cell lines (Figure 4.15 and 4.16, inset).

4.12 Overexpression of XIAP did not reduce sorafenib and vorinostat lethality in HCT116 wt cells, but overexpresion of Bcl-xL or DNCaspase 9 did reduce the toxic effects of combination treatment

We directed our attention to the intrinsic apoptotic pathway to urther investigate its role in sorafenib and vorinostat combination treatment. HCT116 wt cells were plated at a density of 2.5 x 10^4 in 12 well plates. Cells were allowed to attach overnight and the next day cells were infected with adenovirus XIAP, dominant negative caspase 9 (DNcaspase 9), Bcl-xL, as well a CMV control adenovirus. Cells were infected as described in materials and methods. The next day, cells were treated with vehicle (DMSO), 3 μM sorafenib, 500 nM vorinostat, or the combination of both drugs. After 48 hours, flow cytometry was performed using Annexin V/propidium iodide staining as described in materials and methods. XIAP, a member of inhibitor of apoptosis (IAP) proteins, did not reduce drug lethality in HCT116 wt cells. Overexpression of Bcl-xL or expression of dominant negative caspase 9 suppressed sorafenib+vorinostat toxicity in HCT116 cells, arguing that the drugs were using the intrinsic pathway to kill this tumor cell type (Figure 4.17).

4.13 Antiapoptotic and Proapoptotic protein expression during Sorafenib and Vorinostat combination response

To delineate the role of specific pro-apoptotic and anti-apoptotic proteins, immunoblot analysis in vorinostat and sorafenib treated HCT116 wt cells were performed.

Cells were plated at 1.5 x 10^6 in 10 cm dishes. Twenty four hours after plating, cells were treated with vehicle (DMSO), 3 μM sorafenib, 500 nM vorinostat, or the combination of both drugs. Six and twenty four hours later, cells were isolated and western blot analysis was performed as described in materials and methods. The antiapoptotic BCL-2 family members, Bcl-2 and Bcl-xL, remained constant over a time period of 24 hours. FLIP-s also remained constant, which is very different from other cancer cell lines we have tested. Uncleaved bid even remained constant over the 24 hour period. There was modest reduction of Mcl-1 expression at 6 hours in combined treatment, however. Twenty four hours after drug exposure, the expression of procaspase-3 had declined (indicating caspase 3 cleavage) after combined, but not individual drug exposure (Figure 4.18). This indicates that the apoptotic pathway is involved.

4.14 Bcl-2 / Bcl-xL / Mcl-1 inhibitor GX15-070 (Obatoclax) increases cell death in Colon Cancer Cells

As an aside, we determined whether inhibition of protective BCL-2 family members facilitated drug-induced cell killing. Colon cancer cells were plated at a density of 1.2 x10^4 cells per well in a 12 well plate. Twenty four hours after plating, cells were treated with vehicle (DMSO), 3 μM sorafenib (6 μM in SW480s), 1 mM sodium valproate or the combination of both drugs with or without 100 nM obatoclax. Obatoclax is a pan inhibitor of the antiapoptotic members, Bcl-2, Bcl-xL, and Mcl-1. Twenty four or forty eight hours later, the trypan blue exclusion assay was performed as described in materials and methods. Treatment of cells with pharmacologically achievable concentrations of Obatoclax significantly increased HCT116 or SW480 cell mortality (Figures 4.19 and

4.20). Obatoclax did not significantly enhance the toxicity of sorafenib but in HCT116 cells this drug did promote the lethality of sodium valproate, as well as enhancing the toxicity of sorafenib and valproate exposure. This indicates that cell death can be facilitated thorugh targeting mitochondrial protective proteins.

4.15 HCT116 wt cells mount a death response to Sorafenib and Vorinostat that is Fas-independent; however, SW480 cells have a Fas-dependent mechanism

Prior studies have demonstrated in hepatoma cells that sorafenib and vorinostat toxicity was dependent on activation of CD95 [107, 108]. Since we have demonstrated that the apoptotic pathway is involved with our drug combination in colon cancer cells, we decided to test the role of CD95 in HCT116 and SW480 cells. Cells were plated at a density of 2.5 x 10^4 in 12 well plates. Cells were allowed to attach overnight and the next day cells were transfected with siScramble, or knockdown of CD95 (siCD95), a death receptor and part of the extrinsic apoptotic pathway. Cells were transfected as described in materials and method. The next day, cells were treated with vehicle (DMSO), 3 μM sorafenib (6 μM for SW480), 500 nM vorinostat, or the combination of both drugs. After 48 hours, flow cytometry was performed using Annexin V/propidium iodide staining as described in materials and methods. Interestingly, knockdown of CD95 increased cell death in HCT116 wt cells. In SW480 cells, knockdown of CD95 decreased cell death compared to Si-scramble group (Figure 4.21). Collectively, this data demonstrates that after sorafenib and vorinostat exposure SW480 cells respond in a manner similar to that observed in many other tumor cell types with CD95 / extrinsic pathway activation, but that HCT116 cells display an unexpected phenomenon wherein CD95 signaling is cyto-protective.

4.16 Knockdown of CD95 in SW480 cells did not prevent cell killing by GX15-070 (Obatoclax)

We have shown that knockdown of CD95 protects SW480 cells from sorafenib and vorinostat induced cell death. Thus, we explored whether knockdown of CD95 and the addition of a third drug, obatoclax (where we have seen a significant amount of cell death) would continue to protect cells from drug-induced cell death. SW480 cells were plated at a density of 2.5 x 10^4 in 12 well plates. Cells were allowed to attach overnight and the next day cells were transfected with siScramble, or knockdown of CD95 (siCD95). Cells were transfected as described in materials and method. Twenty four hours after transfection, cells were treated with vehicle (DMSO) or Obatoclax (100 nM) followed by, vehicle (DMSO), sorafenib (6 μM), sodium valproate (1.0 mM) or sorafenib+valproate. Forty eight hours after exposure, cells were isolated and viability determined via trypan blue exclusion assay (± SEM, n = 3 independent studies). Although knockdown of CD95 suppressed sorafenib+valproate induced cell death, the addition of obatoclax ameliorated this inhibition (Figure 4.22).

4.17 Lack of Fas/CD95 surface expression in HCT116 wt cells and SW620 cells, but not in SW480 cells

We next explored CD95 surface expression, since we have already established that CD95 protects SW480 cells from sorafenib and vorinostat cell death and does not protects HCT116 wt cells. Colon cancer cells were plated in 4 well chamber slides at a density of 15,000 cells per well. Next day, cells were treated with vehicle (DMSO) or the combination of sorafenib and vorinostat for 3, 6, and 8 hours. Immunohistochemistry was

performed as described in materials and methods. HCT116 wt cells did not increase CD95 plasma membrane levels after treatment with sorafenib and vorinostat (Figure 4.23A), despite the lethal effects with these drugs (Figure 4.23B). Sorafenib and vorinostat toxicity did correlate with CD95 plasma membrane activation in the SW480 cells (Figure 4.23A). SW620 cells, patient matched to SW480 cells, showed significantly lower toxicity with the drug combination (Figure 4.23B) that also correlated with a lack of CD95 activation on the cell surface (Figure 4.23A) and lower expression of ceramide synthase (LASS6).

4.18 DISC formation in HCT116 wt cells and SW480 cells

We further explored the extrinsic pathway by determining if there was DISC formation in the HCT116 wt and SW480 cells. DISC is crucial to CD95 receptor mediated apoptosis. Cells were plated at a density of 2.0 x 10^6 cells per 100 cm dish. The next day cells were treated with the combination of 3 μM sorafenib (6 μM in SW480s) and 500 nM vorinostat or vehicle (DMSO). Combined treatment in HCT116 wt cells with vorinostat and sorafenib promoted only a weak association of pro-caspase 8 with CD95. Grp78 (Bip), a protein involved in ER stress, strongly associated with CD95 (Figure 4.24A). In SW480 cells, combination treatment promoted the rapid association of procaspase-8 with CD95 (Figure 4.24B). This data correlates with other cancer cell lines that have been tested. Bip also associates with CD95 in SW480 cells (Figure 4.24B).

4.19 Sorafenib and Vorinostat stimulate autophagy in HCT116 cells

In our prior studies combining sorafenib and vorinostat in NSCLC, renal, liver, melanoma and pancreatic cancer cells induced autophagy. We decided to investigate what role autophagy played in sorafenib and vorinostat treatment in colon cancer cells. HCT116

wt cells were plated in 4 well chamber slides at a density of 15,000 cells per well. The next day, cells were transiently transfected with GFP-LC3, GFP-LC3 and siRNA beclin1, or GFP-LC3 and siRNA to Atg5 as described in materials and methods. The next day, cells were treated with vehicle (DMSO), 3 μM sorafenib, 500 nM vorinostat, or the combination of both drugs. Six hours after drug exposure cells were visualized at 40X using an Axiovert 200 fluorescent microscope under fluorescent light using the FITC filter. The mean number of autophagic vesicles per cell from random fields of 40 cells were counted (± SEM, n = 3). Sorafenib and vorinostat induced autophagy in the HCT116 wt cells as indicated by GFP-LC3 vesicularization and this was suppressed by knockdown of beclin-1 (Figure 4.25A and Figure 4.25B).

4.20 Knockdown of Beclin 1 expression enhanced Sorafenib and Vorinsotat toxicity

We have already shown (Figure 4.25) that knockdown of beclin 1 suppressed sorafenib and vorinostat autophagy. We next investigated the effect of knockdown beclin 1 on cell death in HCT116 cells. Cells were plated at a density of 2.5 x 10^4 in 12 well plates. Cells were allowed to attach overnight and the next day cells were transfected with siScramble or knockdown of beclin 1 (si-beclin1). Cells were transfected as described in materials and method. The next day, cells were treated with vehicle (DMSO), 3 μM sorafenib, 500 nM vorinostat, or the combination of both drugs. After 48 hours, flow cytometry was performed using Annexin V/propidium iodide staining as described in materials and methods. Knockdown of beclin 1 enhanced drug toxicity (Figure 4.26).

4.21 Sorafenib and Vorinostat induce autophagy that is CD95 dependent in HCT116 cells

Since CD95 is likely to be cytoprotective in HCT116 wt cells, we explored the effects of CD95 knockdown on autophagy. Cells were plated in 4 well chamber slides at a density of 15,000 cells per well. The next day, cells were transiently transfected with GFP-LC3 and siscramble or GFP-LC3 and siRNA CD95, as described in materials and methods. The next day, cells were treated with vehicle (DMSO), 3 μM sorafenib, 500 nM vorinostat, or the combination of both drugs. Six hours after drug exposure cells were visualized at 40X using an Axiovert 200 fluorescent microscope under fluorescent light using the FITC filter. The mean number of autophagic vesicles per cell from random fields of 40 cells were counted (± SEM, n = 3). Knockdown of CD95 suppressed drug treatment GFP-LC3 vesicularization (Figure 4.27A and 4.27B). Collectively, this data and the data in Figure 4.21 demonstrate that sorafenib and vorinostat treatment promote a form of CD95 activation in HCT116 cells that is non-productive with respect to pro-apoptotic signaling but is competent to stimulate an autophagic response that is cyto-protective.

4.22 Sorafenib and Vorinostat activated PERK but did not alter eif2a phosphorylation in HCT116 cells

We next investigated the mechanistic links between sorafenib and vorinostat lethality and ER stress signaling. We have already shown in HCT116 wt cells the strong association with CD95 and Bip in DISC formation. Cells were plated at 1.5 x 10^6 in 10 cm dishes. Twenty four hours after plating, cells were treated with vehicle (DMSO), 3 μM sorafenib, 500 nM vorinostat, or the combination of both drugs. Six and twenty four hours

later, cells were isolated and western blot analysis was performed as described in materials and methods. We examined the expression of phosphorylated PERK and phosphorylated eif2α. The phosphorylation of PERK increased within 6 hours after combination treatment, yet there was not an apparent increase in the phosphorylation of eif2α (Figure 4.28).

4.23 DnPERK suppresses Sorafenib and Vorinostat–stimulated autophagy in HCT116 wt cells

In hepatoma cells we have noted that sorafenib and vorinostat exposure promoted a protective form of autophagy in a CD95- and PERK-dependent fashion. We investigated the effects of dnPERK on autophagy. HCT116 wt cells were plated in 4 well chamber slides at a density of 15,000 cells per well. The next day, cells were transiently transfected with GFP-LC3 and pcDNA or GFP-LC3 and dnPERK, as described in materials and methods. The next day, cells were treated with vehicle (DMSO), 3 μM sorafenib, 500 nM vorinostat, or the combination of both drugs. Six hours after drug exposure cells were visualized at 40X using an Axiovert 200 fluorescent microscope under fluorescent light using the FITC filter. The mean number of autophagic vesicles per cell from random fields of 40 cells were counted (± SEM, n = 3). Inhibition of PERK suppressed drug treatment GFP-LC3 vesicularization (Figure 4.29). {Inset Panel: cells transfected with vector control plasmid (CMV) or a plasmid to express dominant negative PERK (but not LC3-GFP) were isolated 6h after drug exposure and lysates subjected to SDS PAGE and immunoblotting to determine LC3 expression and processing (a representative n = 3)}.

4.24 Activation of JNK1/2 is dependent on PERK

We next determined whether drug-induced PERK signaling was involved in the regulation of the JNK1/2 pathway and whether PERK activity was regulated by CD95. HCT116 cells 24h after plating were transfected with either: a vector control plasmid (CMV) or a plasmid to express dominant negative PERK; a scrambled siRNA (siSCR) or a siRNA to knock down CD95 expression (20 nM). Twenty four hours after infection, cells were treated with vehicle (DMSO) or with sorafenib (3 μM) and vorinostat (500 nM). Six hours after drug exposure cells were isolated and lysates subjected to SDS PAGE and immunoblotting to determine the phosphorylation status of PERK and of JNK1/2. Expression of dominant negative PERK blocked sorafenib and vorinostat –induced PERK phosphorylation (Figure 4.30A). Expression of dominant negative PERK also abolished drug-induced JNK1/2 activation (Figure 4.30B). Knock down of CD95 blocked JNK1/2 activation (Figure 4.30D) however, unlike data in hepatoma cells, knockdown of CD95 did not alter PERK activation (Figure 4.30C). Thus JNK1/2 activation requires separate drug-induced signals emanating from both CD95 and PERK.

4.25 Molecular inhibition of JNK1/2 signaling blocked Sorafenib and Vorinostat-stimulated autophagy

HCT116 cells 24h after plating in 4 well chamber slides were transfected with a plasmid to express LC3-GFP. Thirty minutes prior to drug exposure cells were treated as indicated with vehicle (DMSO) or the JNK inhibitory peptide (JNK-IP, 10 μM). Twenty four h after infection, cells were treated with vehicle (DMSO), sorafenib (3 μM), vorinostat (500 nM) or both drugs combined. Six hours after drug exposure cells were

visualized at 40X using an Axiovert 200 fluorescent microscope under fluorescent light using the FITC filter. The mean number of autophagic vesicles per cell from random fields of 40 cells were counted (± SEM, n = 3). Inhibition of JNK 1/2 blocked drug-induced vesicularization of GFP-LC3 (Figure 4.31).

4.26 Sorafenib and Vorinostat toxicity is acidic sphingomyelinase dependent

Compared to patient matched SW480 cells, SW620 cells were refractory to drug-induced toxicity that correlated with a lack of CD95 activation. Prior studies in hepatoma cells have demonstrated that inhibition of either the acidic sphingomyelinase (ASMase) or de novo ceramide synthesis pathways blocked drug-induced CD95 activation and sorafenib and vorinostat toxicity [107, 108]. It has also been shown that SW620 cells are refractory to death receptor signaling induced by tumor necrosis factor-related apoptosis-inducing ligand (TRAIL) which has been linked to low expression of ceramide synthase 6 (LASS6) in the de novo pathway and a lack of ceramide generation after TRAIL exposure [115, 116]. SW480 cells 24 hours after plating were transfected with siRNA molecules to knock down expression of acidic sphingomyelinase (ASMase), or transfected with scrambled siRNA molecules as described in materials and methods. Twenty four h after transfection cells were treated with vehicle (DMSO) or myriocin (1 μM) and after 30 min, cells then exposed to vehicle (DMSO), sorafenib (6 μM), vorinostat (500 nM) or both drugs combined. Forty eight hours after exposure, cells were isolated and stained with trypan blue dye and cell viability determined by visible light microscopy (± SEM, n = 2). Knock down of ASMase expression or treatment with the de novo pathway inhibitor myriocin significantly reduced sorafenib and vorinostat toxicity (Figure 4.32).

4.27 CD95 activation is acidic sphingomyelinase dependent

SW480 cells 24h after plating in 4 well chamber slides cells were transfected with siRNA molecules to knock down expression of acidic sphingomyelinase (ASMase), or LASS6, or transfected with scrambled siRNA molecules as described in materials and methods. Twenty four h after transfection cells were treated with vehicle (DMSO) or myriocin (1 μM) and after 30 min, cells then exposed to vehicle (DMSO), sorafenib (6 μM), vorinostat (500 nM) or both drugs combined. Cells were fixed 6h after exposure and the amount of plasma membrane associated CD95 determined by immunohistochemistry (± SEM, n = 2). Knockdown of ASMase, myriocin, or LASS6 blocked CD95 activation (Figure 4.33).

4.28 Overexpression of LASS6 enhanced Sorafenib and Vorinostat-induced CD95 activation and enhanced tumor cell killing in SW620 cells

Based on the data in Figure 4.32 and 4.33, we determined whether expression of LASS6 in SW620 cells facilitated drug-induced CD95 activation and cell death. SW620 cells were stably transfected with either vector control plasmid or a plasmid to express LASS6. Twenty four hours after plating, cells were exposed to vehicle (DMSO), sorafenib (6 μM), vorinostat (500 nM) or both drugs combined. Forty eight hours after exposure, cells were isolated and stained with trypan blue dye and cell viability determined by visible light microscopy (± SEM, n = 2). Inset Panel: SW620 cells 24h after plating in 4 well chamber slides were exposed to vehicle (DMSO), sorafenib (6 μM), vorinostat (500 nM) or both drugs combined. Cells were fixed 6h after exposure and the amount of plasma membrane associated CD95 determined by immunohistochemistry (± SEM, n = 2).

Overexpression of LASS6 in SW620 cells enhanced the toxicity of sorafenib, vorinostat and the drug combination (Figure 4.34A) which correlated with increased activation of CD95 (Figure 4.34B). Collectively, this data argues that activation of enzymes within the de novo ceramide pathway represents a key step in the toxic actions of sorafenib and vorinostat in colon cancer cells.

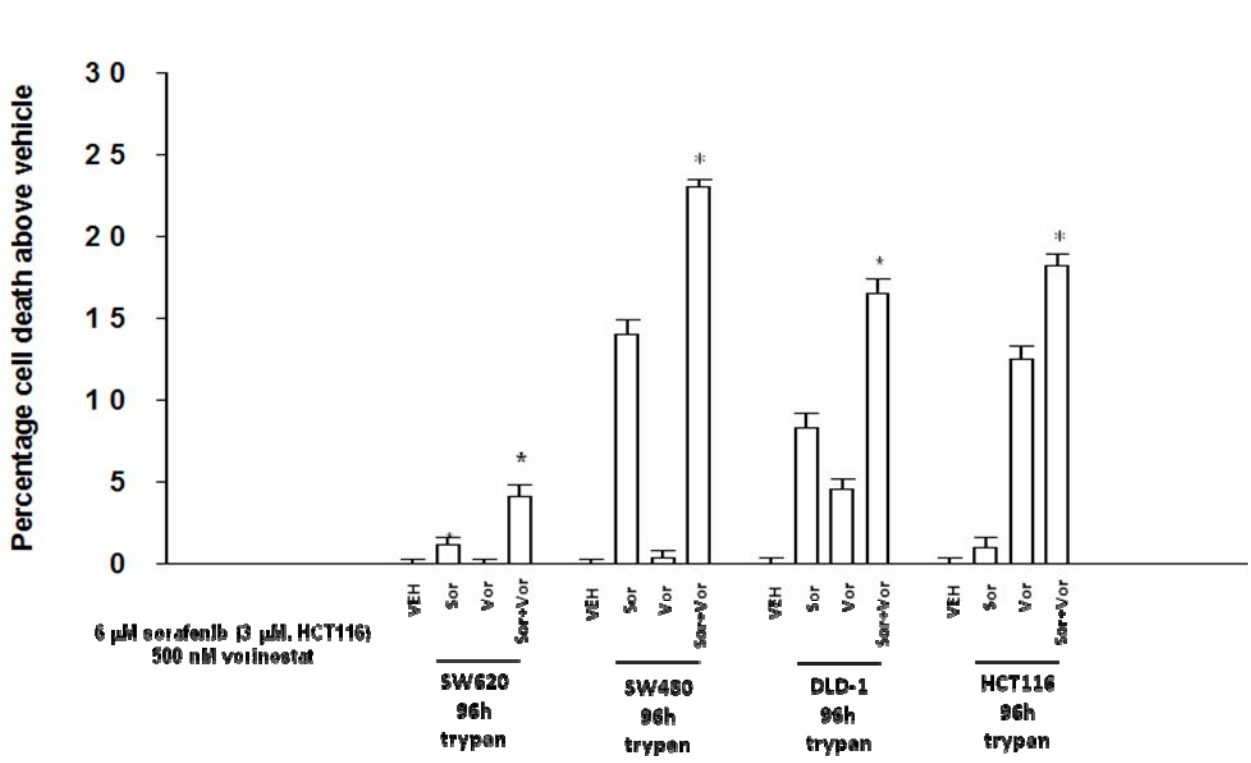

Figure 4.1. Sorafenib and Vorinostat reduce cell viability in colon cancer cells. Colon cancer cells were treated with 6 µM sorafenib (3 µM for HCT116 wt) and 500 nM vorinostat continuously for 96 hours. After drug exposure, the trypan blue exclusion assay was performed. Values represent the means for three separate experiments ± SD. * $p \leq 0.05$, greater cell killing than compared with any other treatment condition.

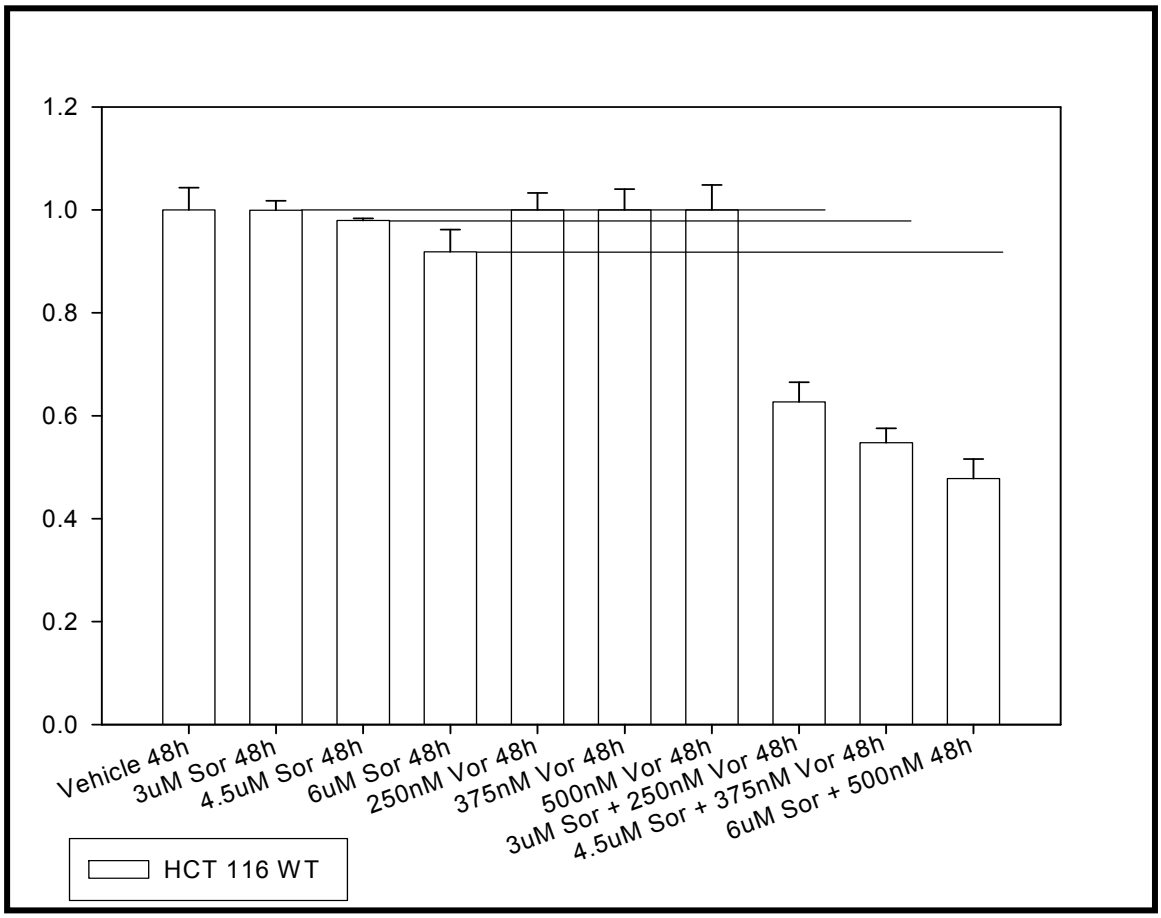

CI For experimental values

Sorafenib (uM)	Vorinostat (uM)	Fa	CI
3.0	0.250	0.39	0.46
4.5	0.375	0.48	0.59
6.0	0.500	0.59	0.66

Figure 4.2. Sorafenib and Vorinostat synergize to kill HCT116 wt cells in colony formation assays. HCT116 wt cells were treated 12h after plating as single cells (250-1500 cells/well) in sextuplicate with vehicle (DMSO), sorafenib (Sor, 3.0-6.0 μM) or vorinostat (Vor. 250-500 nM), or with both drugs combined, as indicated at a fixed concentration ratio to perform median dose effect analyses for the determination of synergy. Combination index (CI) values were determined. CI values less than 1 indicates synergy, equal to 1 indicates additive interactions, and CI values > 1 indicates antagonism.

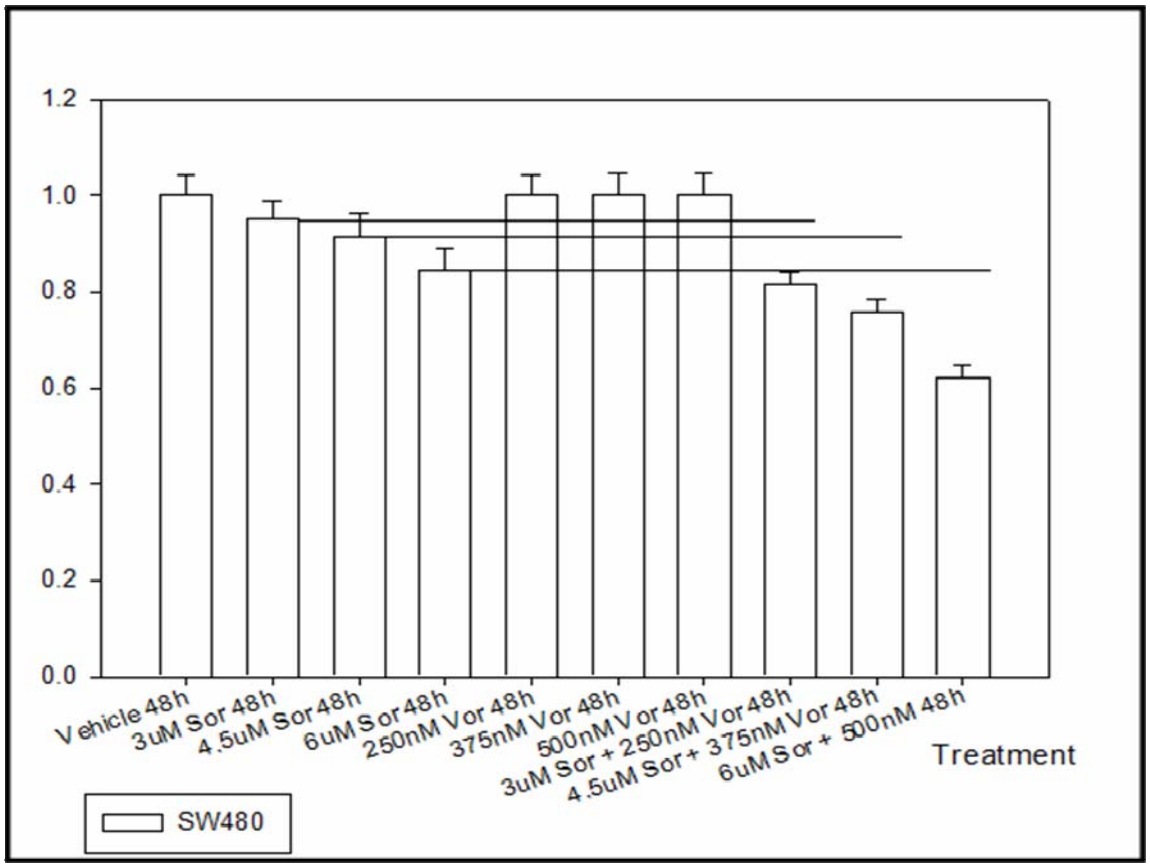

CI For experimental values SW480

Sorafenib (uM)	Vorinostat (uM)	Fa	CI
3.0	0.250	0.16	0.57
4.5	0.375	0.25	0.59
6.0	0.500	0.41	0.49

Figure 4.3. Sorafenib and Vorinostat synergize to kill SW480 cells in colony formation assays. SW480 cells were treated 12h after plating as single cells (250-1500 cells/well) in sextuplicate with vehicle (DMSO), sorafenib (Sor, 3.0-6.0 μM) or vorinostat (Vor. 250-500 nM), or with both drugs combined, as indicated at a fixed concentration ratio to perform median dose effect analyses for the determination of synergy. Combination index (CI) values were determined. CI values less than 1 indicates synergy, equal to 1 indicates additive interactions, and CI values > 1 indicates antagonism.

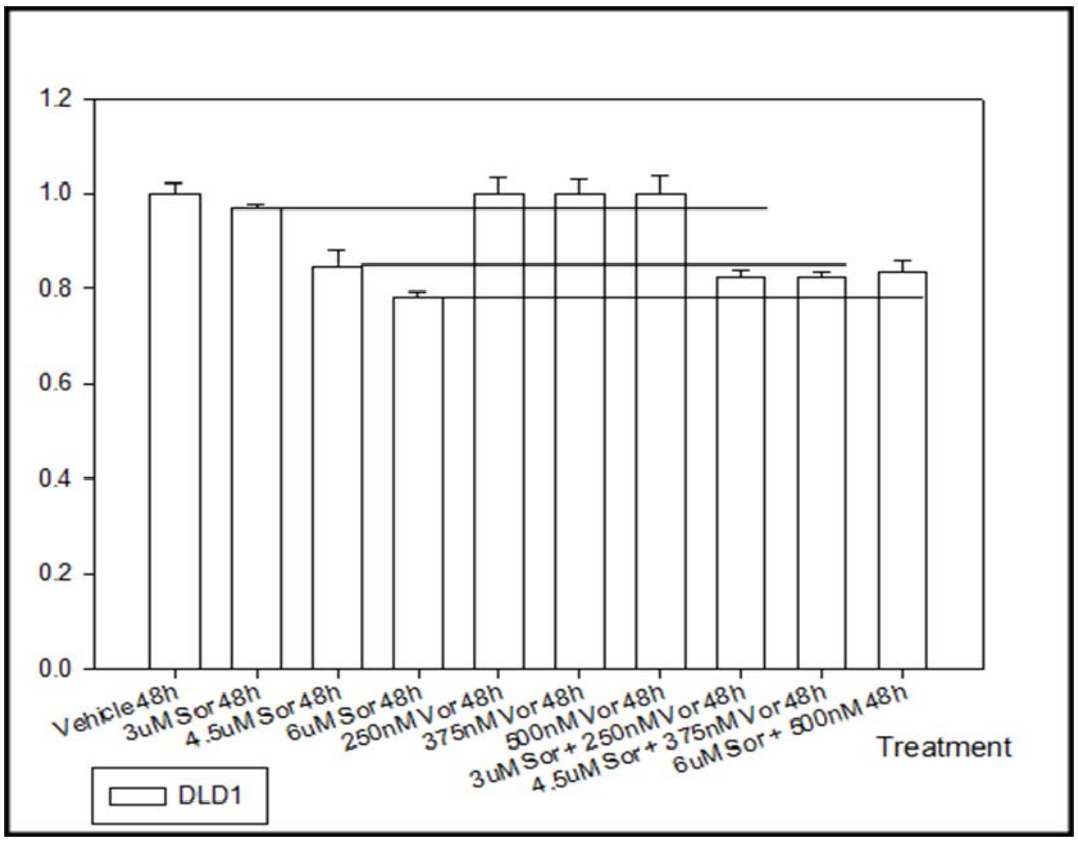

CI For experimental values

Sor (uM)	Vor (uM)	Fa	CI
3.0	0.250	0.16	0.856
4.5	0.375	0.18	1.213
6.0	0.500	0.21	1.500

Figure 4.4. Sorafenib and Vorinostat does not synergize to kill DLD1 cells in colony formation assays. DLD1 cells were treated 12h after plating as single cells (250-1500 cells/well) in sextuplicate with vehicle (DMSO), sorafenib (Sor, 3.0-6.0 μM) or vorinostat (Vor. 250-500 nM), or with both drugs combined, as indicated at a fixed concentration ratio to perform median dose effect analyses for the determination of synergy. Combination index (CI) values were determined. CI values less than 1 indicates synergy, equal to 1 indicates additive interactions, and CI values > 1 indicates antagonism.

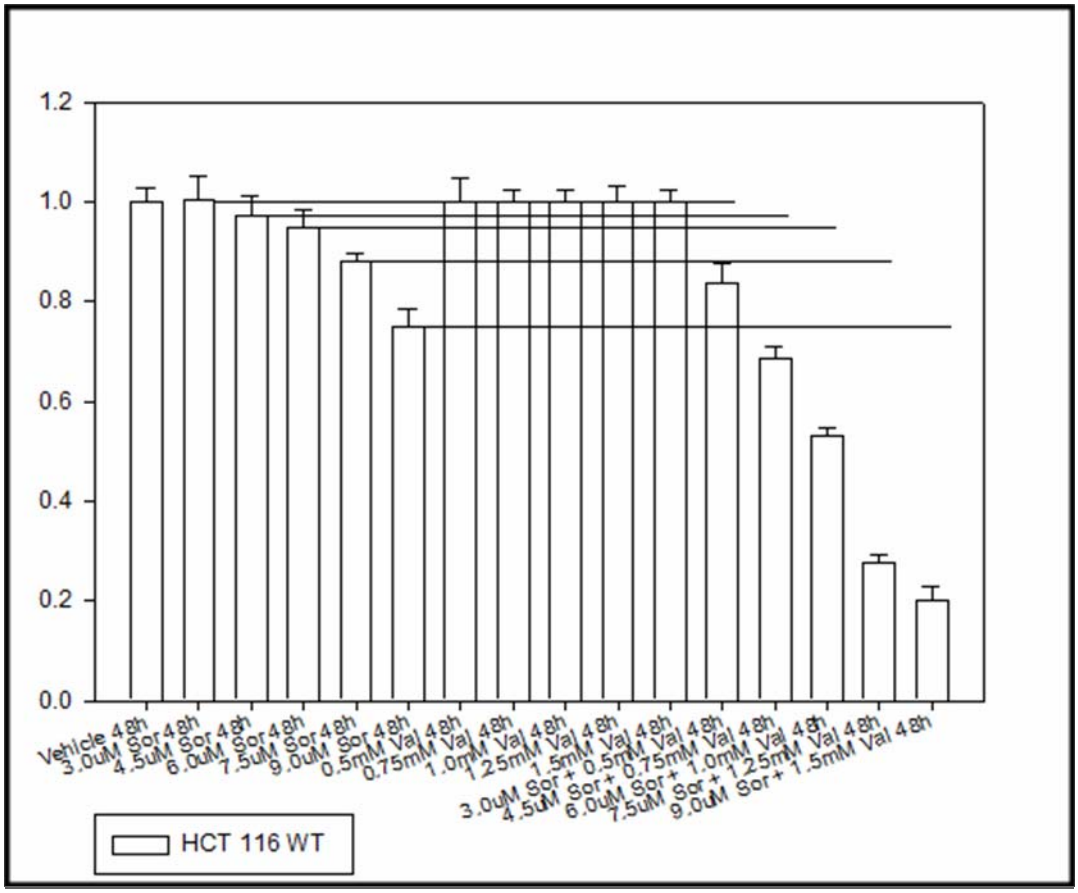

CI For experimental values HCT 116 Wild-type

Sorafenib (uM)	Valproic (mM)	Fa	CI
3.0	0.50	0.18	0.66
4.5	0.75	0.35	0.66
6.0	1.00	0.52	0.65
7.5	1.25	0.77	0.49
9.0	1.50	0.84	0.48

Figure 4.5. Sorafenib and sodium valproate synergize in colony formation assays to kill HCT116 wt cells. HCT116 wt cells were treated 12h after plating as single cells (250-1500 cells/well) in sextuplicate with vehicle (VEH, DMSO), sorafenib (Sor., 3.0-9.0 μM) or sodium valproate (Val. 0.5-1.5 mM), or with both drugs combined, as indicated at a fixed concentration ratio to perform median dose effect analyses for the determination of synergy. Combination index (CI) values were determined. CI values less than 1 indicates synergy, equal to 1 indicates additive interactions, and CI values > 1 indicates antagonism.

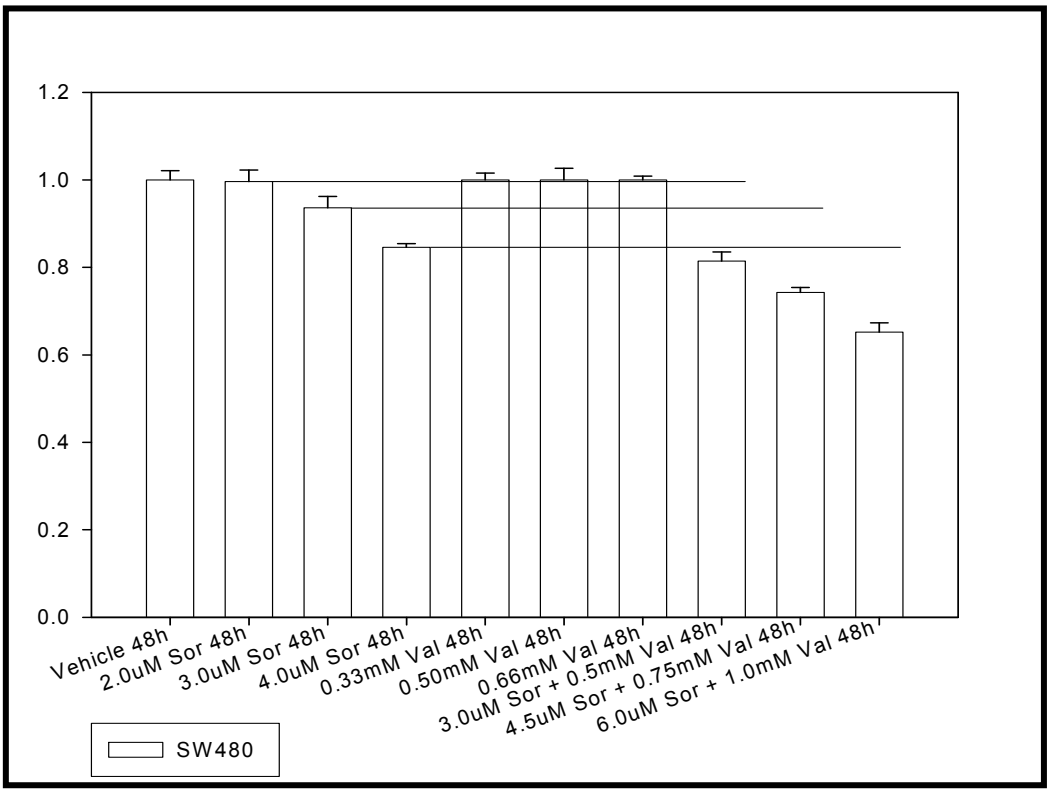

CI For experimental values SW480

Sorafenib (uM)	Valproic (mM)	Fa	CI
2.0	0.33	0.17	0.57
3.0	0.50	0.26	0.69
4.0	0.66	0.37	0.74

Figure 4.6. Sorafenib and sodium valproate synergize in colony formation assays to kill SW480 cells. SW480 cells were treated 12h after plating as single cells (250-1500 cells/well) in sextuplicate with vehicle (VEH, DMSO), sorafenib (Sor., 3.0-9.0 μM) or sodium valproate (Val. 0.5-1.5 mM), or with both drugs combined, as indicated at a fixed concentration ratio to perform median dose effect analyses for the determination of synergy. Combination index (CI) values were determined. CI values less than 1 indicates synergy, equal to 1 indicates additive interactions, and CI values > 1 indicates antagonism.

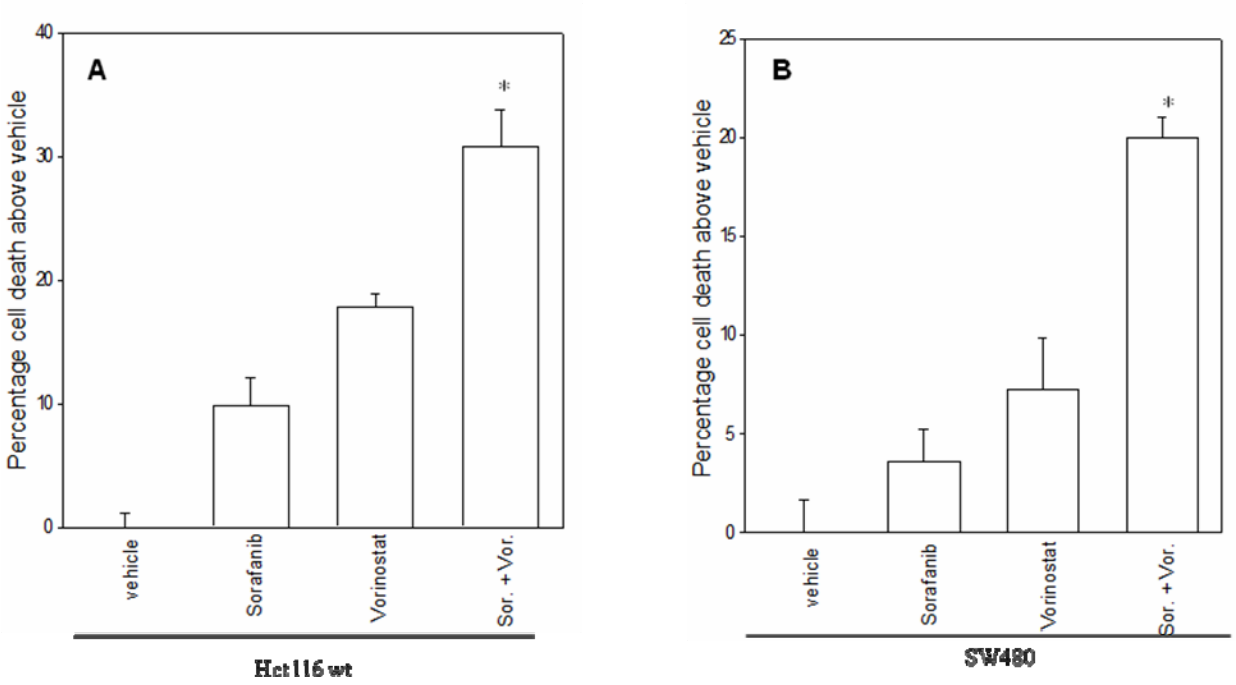

Figure 4.7. Sorafenib and Vorinostat induce cell death in HCT116 wt and SW480 colon cancer cells. *A*, 3 μM sorafenib and 500 nM vorinostat treated continuously for 48 hours. *B*, 6 μM sorafenib and 500 nM vorinostat treated continuously for 48 hours. Cells stained with Annexin V/propidium iodide and subjected to flow cytometry. Values represent the means for three separate experiments ± SD. * $p \leq 0.05$, greater cell killing than compared with any other treatment condition.

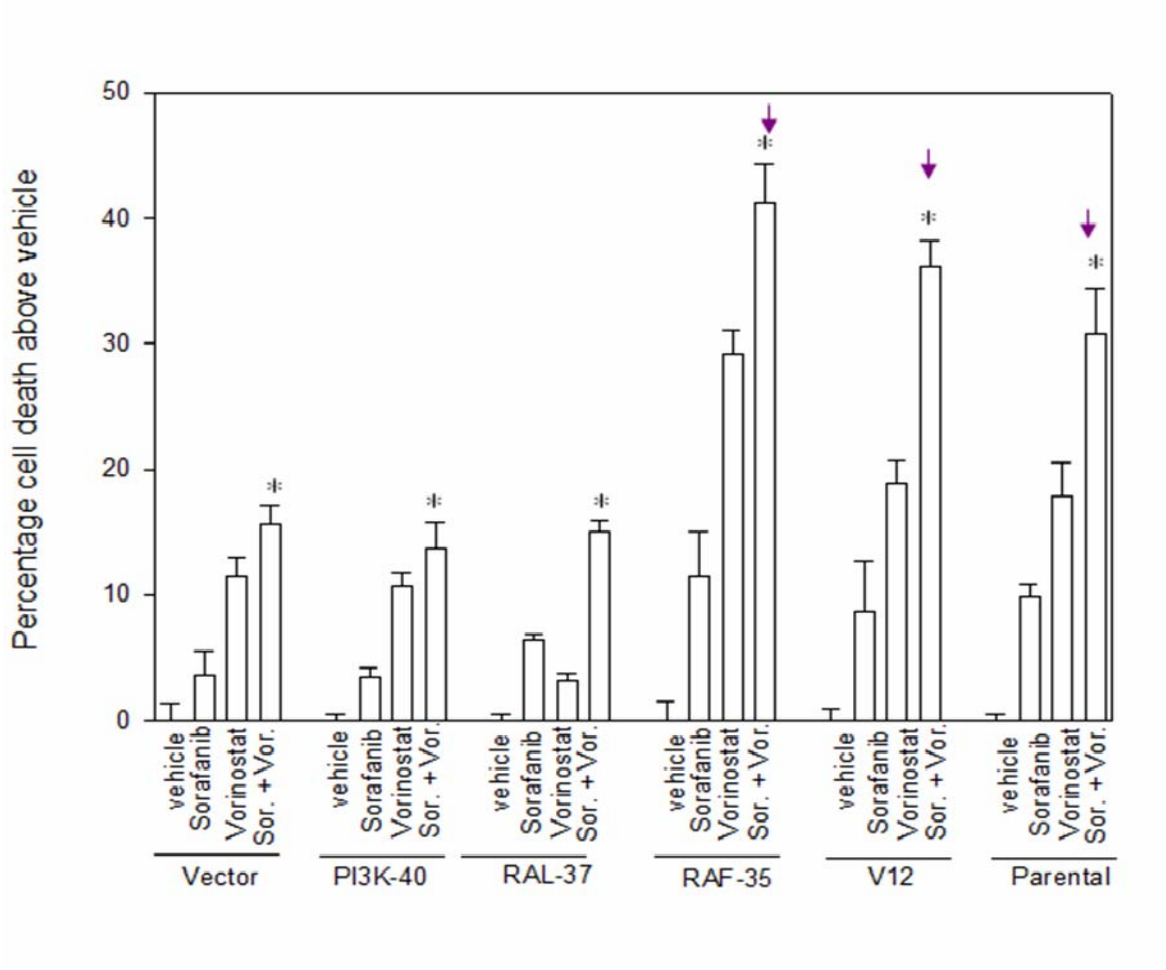

Figure 4.8. Activation of ERK1/2 predicts for a Sorafenib and Vorinostat Response. HCT116 cells (parental expressing K-RAS D13; deleted for K-RAS D12; deleted for K-RAS D12 expressing H-RAS V12 and effector mutants of H-RAS V12), 24h after plating in triplicate, were treated with vehicle (DMSO), sorafenib (3 μM), vorinostat (500 nM) or sorafenib and vorinostat. Forty eight hours after exposure, cells were isolated and stained with Annexin V –propidium iodide and cell viability determined by flow cytometry. Values represent the means for three separate experiments ± SD. * $p \leq 0.05$, greater cell killing than compared with any other treatment condition. Arrows indicate the RAF mutant, V12 cells, and the parental gave significantly more cell death than the other transfectants.

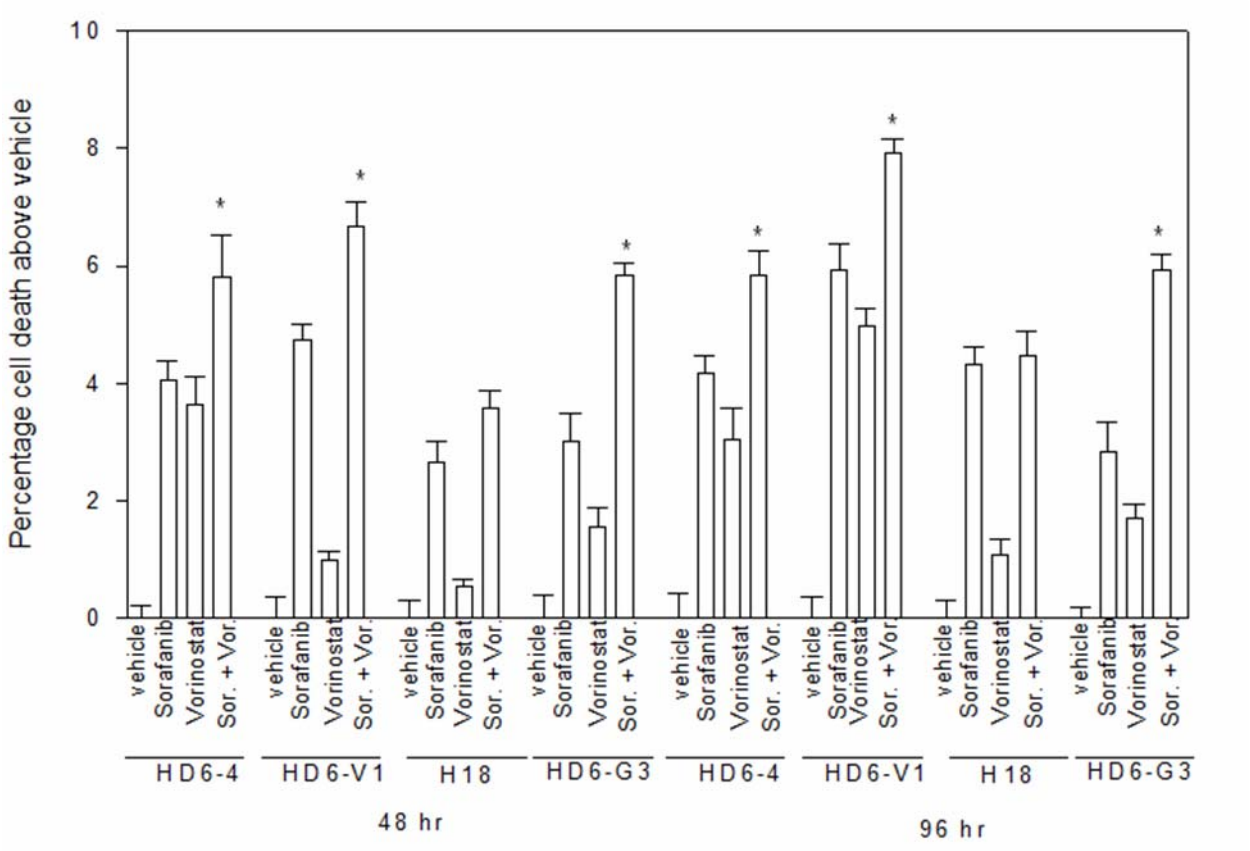

Figure 4.9. Cell viability is slightly reduced in HT29 subclones by Sorafenib and Vorinostat treatment. HT29 cells stably transfected with empty vector (HD6-4), K-RAS V12 (HD6-V1), H-RAS V12 (H18), or K-RAS (HD6-G3), 24h after plating in triplicate, were treated with vehicle (DMSO), sorafenib (3 μM), vorinostat (500 nM) or sorafenib+vorinostat. Forty eight hours after exposure, cells were isolated and viability determined via trypan blue exclusion assay. Values represent the means for three separate experiments ± SD. * $p \leq 0.05$, greater cell killing than compared with any other treatment condition.

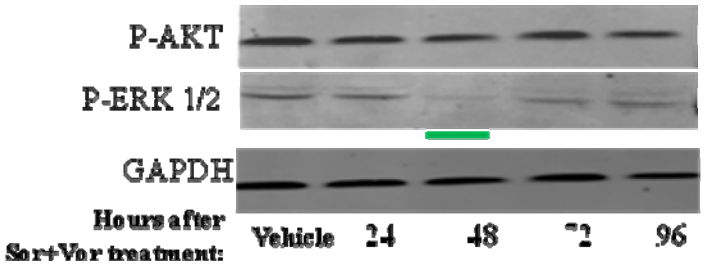

Figure 4.10. Sorafenib and Vorinostat decrease activation of ERK1/2 but not Akt in HCT116 wt cells. HCT116 cells 24h after plating were treated with either vehicle (DMSO) or with sorafenib (3 μM) and vorinostat (500 nM). 24 h – 96h after drug exposure cells were isolated and subjected to SDS PAGE and immunoblotting to determine the phosphorylation of ERK1/2 and Akt (S473). Data are from a representative of 3 independent studies.

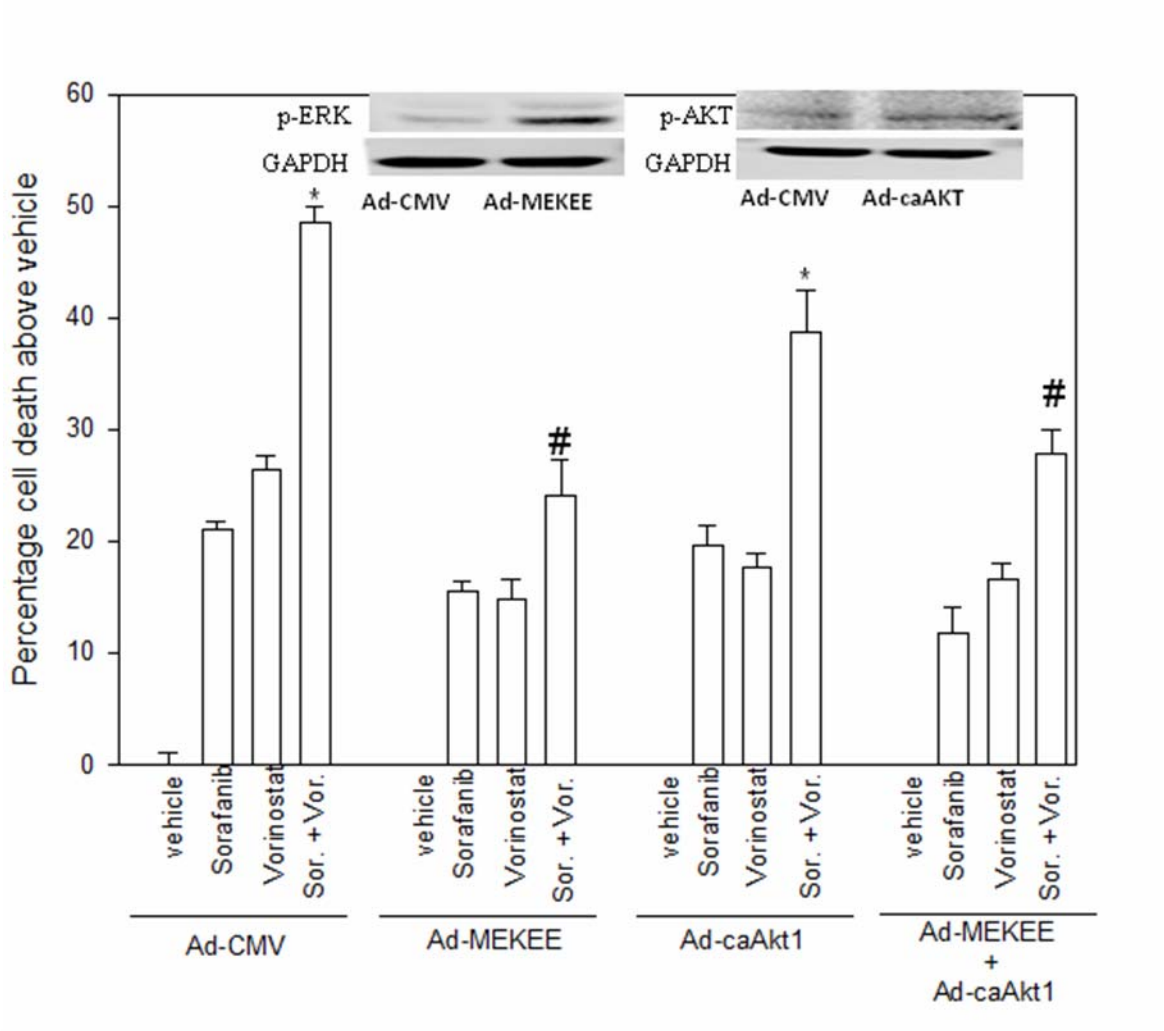

Figure 4.11 Activated MEK1 suppresses the toxicity of Sorafenib and Vorinostat. 3 HCT116 cells 24h after plating were infected with recombinant adenoviruses (empty vector CMV; constitutively active MEK1 EE; constitutively active Akt) at a multiplicity of infection of 25. Twenty four h after infection, cells were treated with vehicle (DMSO), sorafenib (3 μM), vorinostat (500 nM) or both drugs together. Forty eight hours after exposure, cells were isolated and stained with Annexin V – propidium iodide and cell viability determined by flow cytometry. Values represent the means for three separate experiments ± SD. * $p \leq 0.05$, greater cell killing than compared with any other treatment condition. # $p \leq 0.05$, less cell killing than compared with parallel condition in vehicle-treated cells.

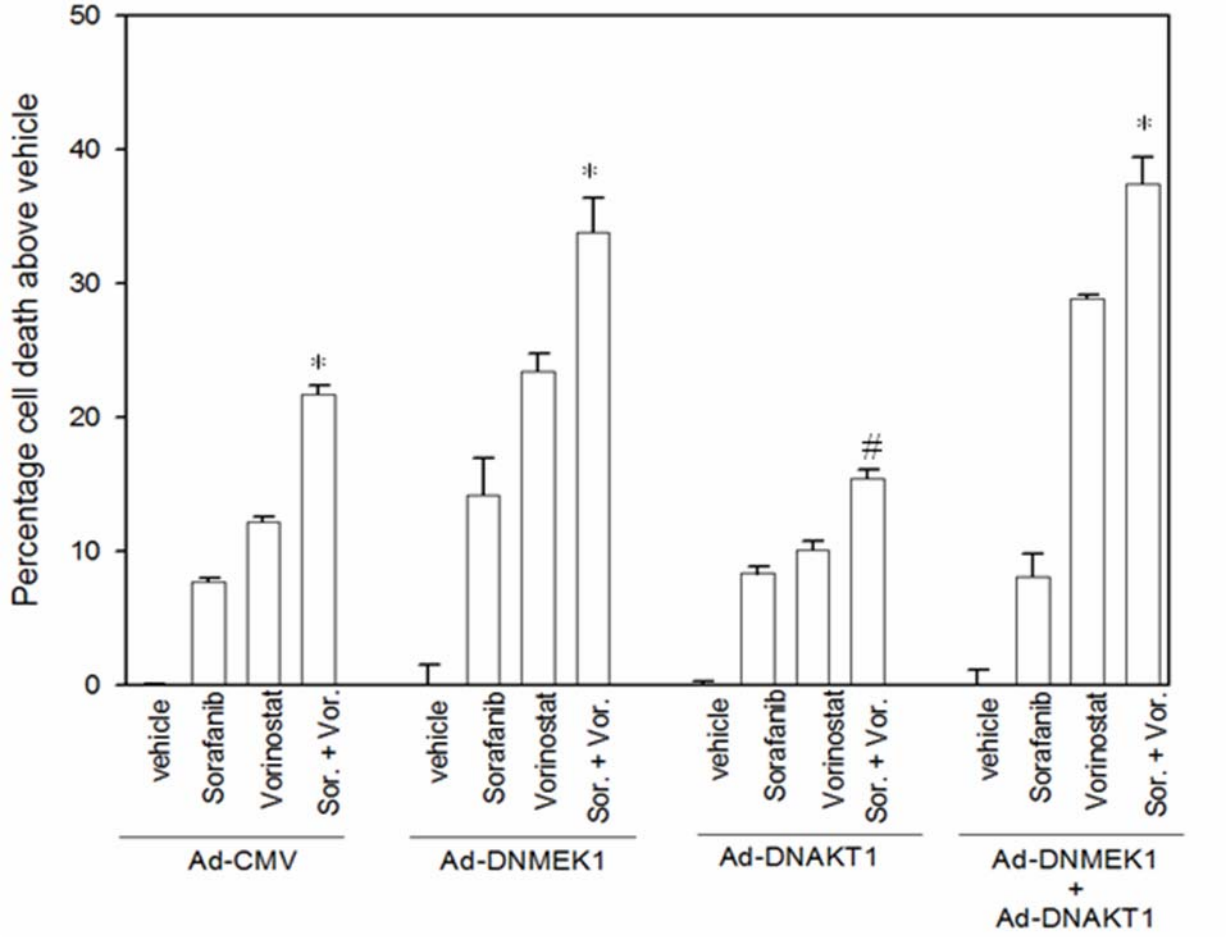

Figure 4.12. DNMEK1 increased Sorafenib and Vorinostat toxicity in HCT116 wt cells. HCT116 cells 24h after plating were, as indicated, infected with recombinant adenoviruses (empty vector CMV; dominant negative MEK1; dominant negative Akt) at a multiplicity of infection of 25. Twenty four h after infection, cells were treated with vehicle (DMSO), sorafenib (3 μM), vorinostat (500 nM) or both drugs together. Forty eight hours after exposure, cells were isolated and stained with Annexin V – propidium iodide and cell viability determined by flow cytometry. Values represent the means for three separate experiments ± SD. * $p \leq 0.05$, greater cell killing than compared with any other treatment condition. # $p \leq 0.05$, less cell killing than compared with parallel condition in vehicle-treated cells.

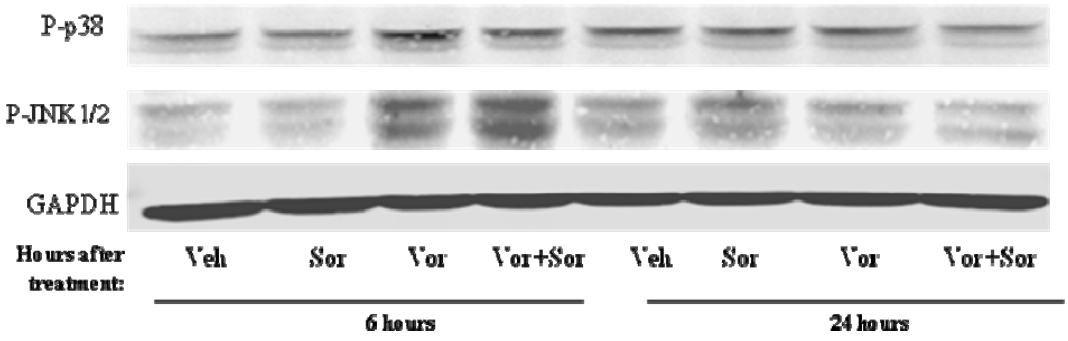

Figure 4.13. Sorafenib and Vorinostat increase the phosphorylation of p38 and JNK in HCT116 wt cells. HCT116 cells 24h after plating were treated with either vehicle (DMSO) or with sorafenib (3 μM) and vorinostat (500 nM). Six h or 24h after drug exposure cells were isolated and subjected to SDS PAGE and immunoblotting to determine the phosphorylation of JNK1/2 and p38. Data are from a representative of 3 independent studies.

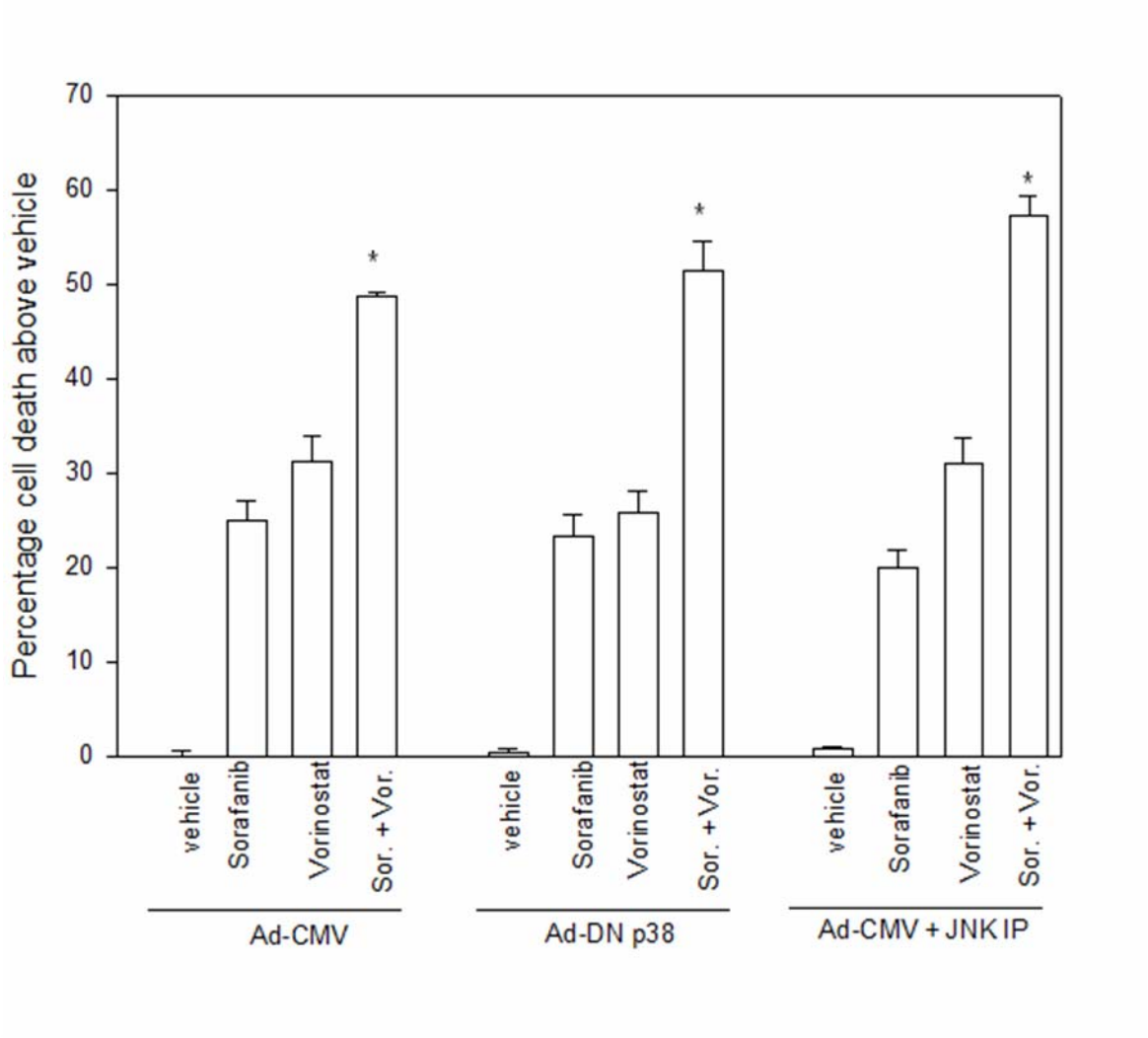

Figure 4.14. DNp38 or JNK IP did not suppress sorafenib and vorinostat lethality in HCT116 wt cells. HCT116 cells 24h after plating were, as indicated, infected with recombinant adenoviruses (empty vector CMV; dominant negative p38 MAPK) at a multiplicity of infection of 25. Thirty minutes prior to drug exposure cells were treated as indicated with vehicle (DMSO) or the JNK inhibitory peptide (JNK-IP, 10 μM). Twenty four h after infection, cells were treated with vehicle (DMSO), sorafenib (3 μM), vorinostat (500 nM) or both drugs together. Forty eight hours after exposure, cells were isolated and stained with Annexin V – propidium iodide and cell viability determined by flow cytometry. Values represent the means for three separate experiments ± SD. * $p \leq 0.05$, greater cell killing than compared with any other treatment condition.

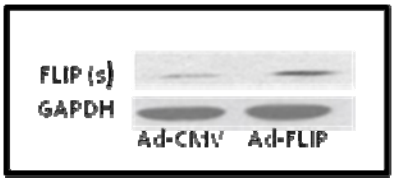

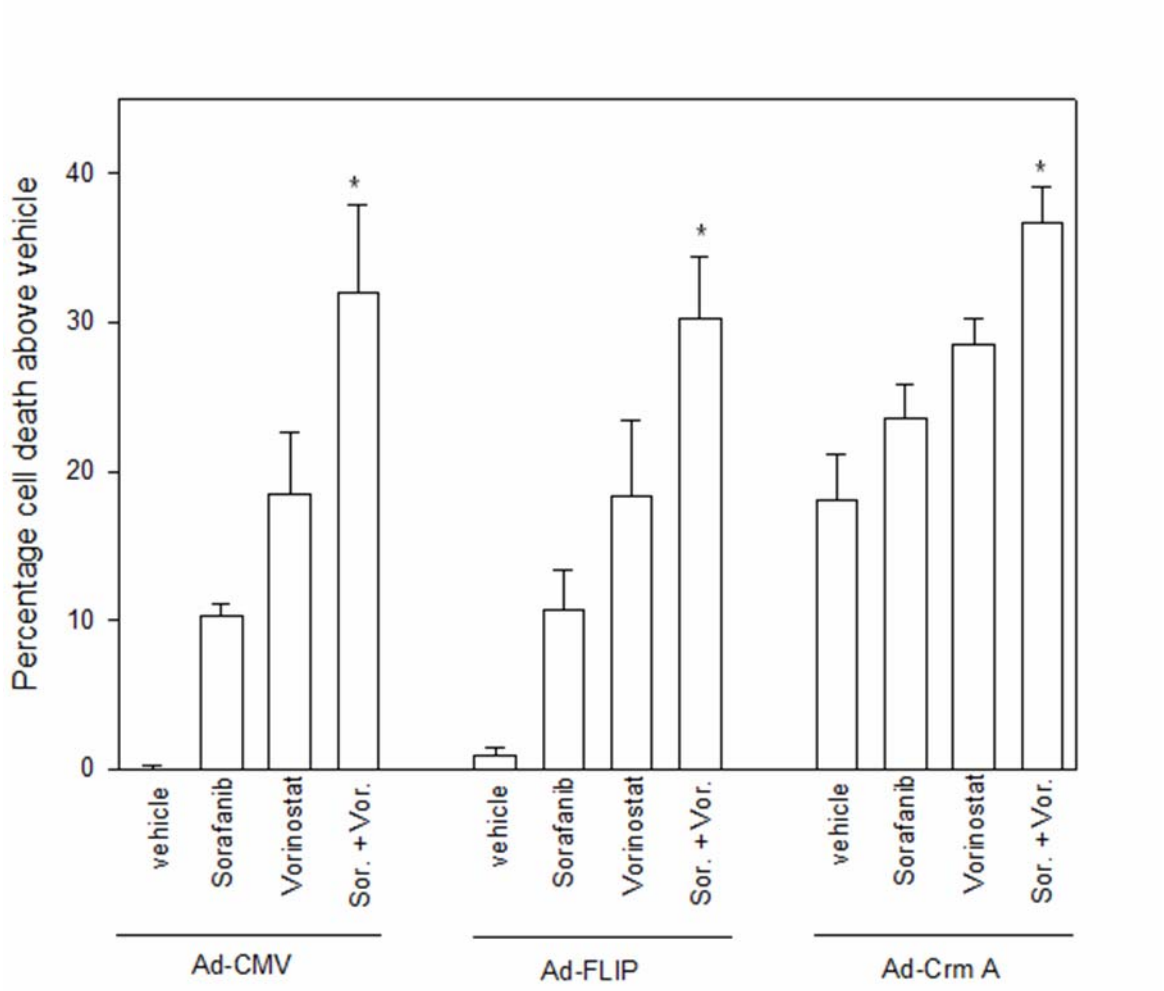

Figure 4.15. Overexpression of FLIP-s or ectopic expression of CrmA did not reduce Sorafenib and Vorinostat lethality in HCT116 wt cells. HCT116 cells 24h after plating were infected with recombinant adenoviruses (empty vector CMV; FLIP; CrmA) at a multiplicity of infection of 25. Twenty four h after infection, cells were treated with vehicle (DMSO), sorafenib (3 μM), vorinostat (500 nM) or both drugs together. Forty eight hours after exposure, cells were isolated and stained with Annexin V – propidium iodide and cell viability determined by flow cytometry. Values represent the means for three separate experiments ± SD. * $p \leq 0.05$, greater cell killing than compared with any other treatment condition.

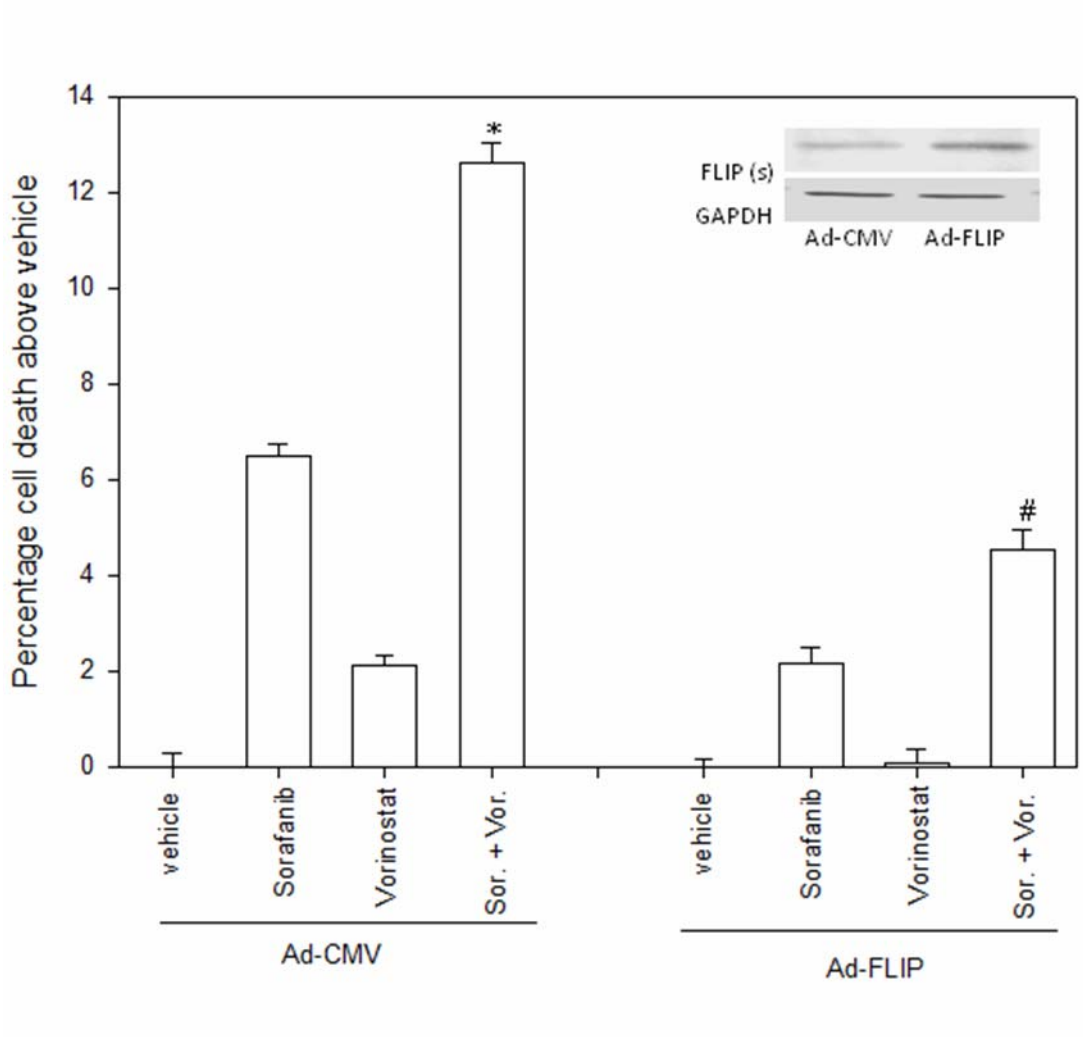

Figure 4.16. Drug lethality was blocked by overexpression of FLIP-s in SW480 cells. SW480 cells 24h after plating were infected with recombinant adenoviruses (empty vector CMV; FLIP) at a multiplicity of infection of 25. Twenty four h after infection, cells were treated with vehicle (DMSO), sorafenib (6 μM), vorinostat (500 nM) or both drugs together. Forty eight hours after exposure, the trypan blue exclusion assay was performed. Values represent the means for three separate experiments ± SD. * $p \leq 0.05$, greater cell killing than compared with any other treatment condition. # $p \leq 0.05$, less cell killing than compared with parallel condition in vehicle-treated cells.

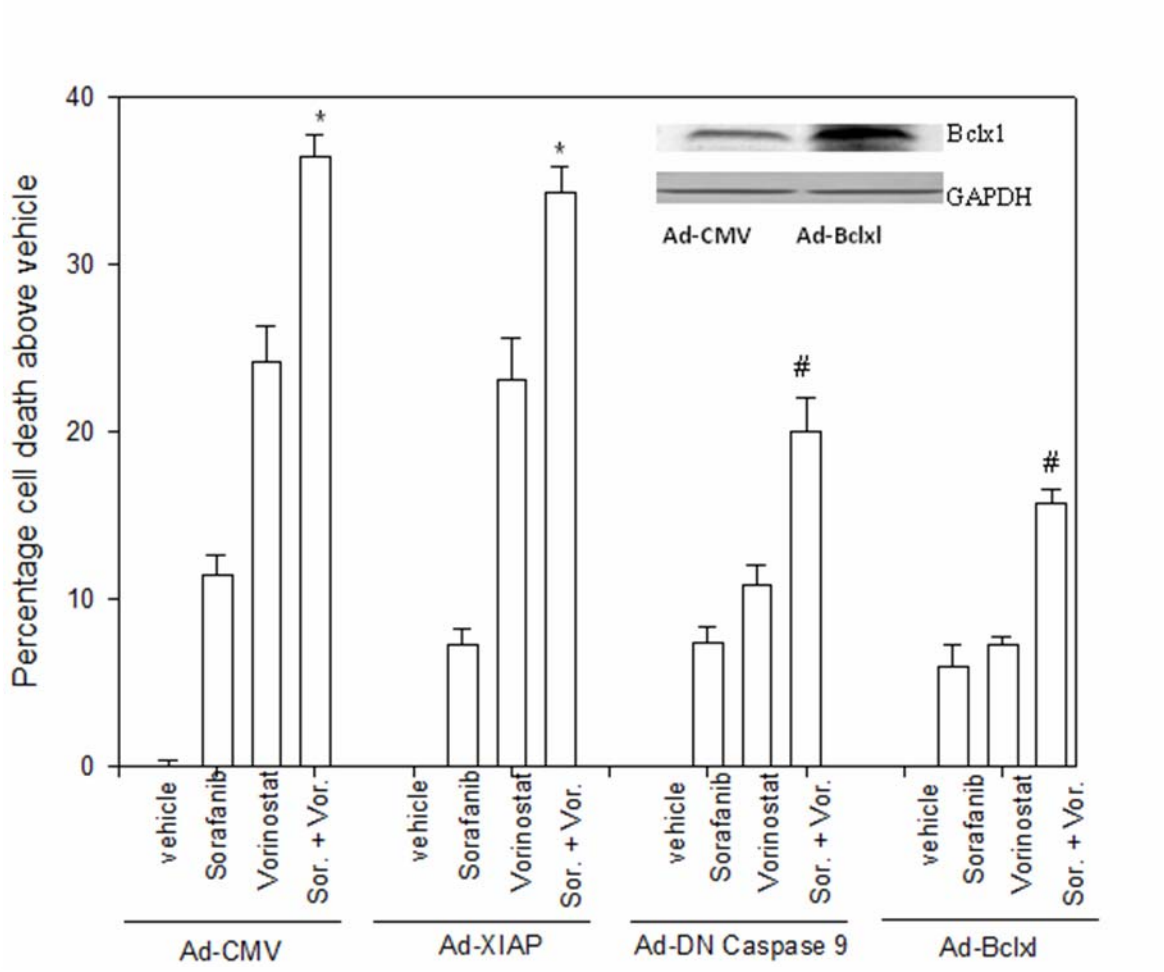

Figure 4.17 Overexpression of XIAP did not reduce sorafenib and vorinostat lethality in HCT116 wt cells, but overexpresion of Bcl-xL or DNCaspase 9 did reduce the toxic effects of combination treatment. HCT116 cells were infected with recombinant adenoviruses (empty vector CMV; caspase inhibitor XIAP; dominant negative caspase 9; Bcl-xL) at a multiplicity of infection of 25. Twenty four h after infection, cells were treated with vehicle (DMSO), sorafenib (3 μM), vorinostat (500 nM) or both drugs together. Forty eight hours after exposure, cells were isolated and stained with Annexin V– propidium iodide and cell viability determined by flow cytometry. Values represent the means for three separate experiments ± SD. * $p \leq 0.05$, greater cell killing than compared with any other treatment condition. # $p \leq 0.05$, less cell killing than compared with parallel condition in vehicle-treated cells.

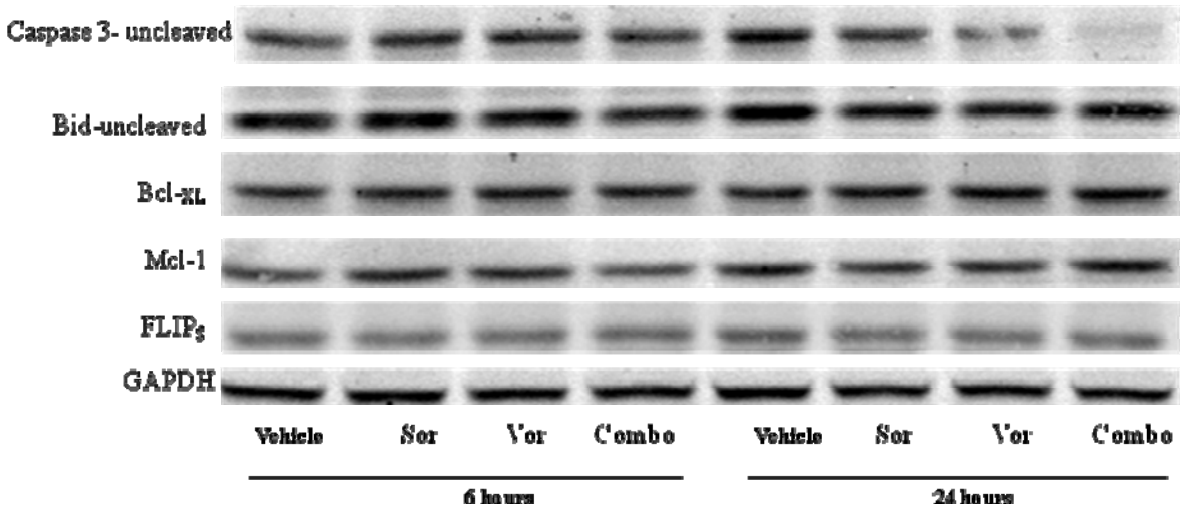

Figure 4.18. Antiapoptotic and Proapoptotic protein expression during Sorafenib and Vorinostat combination response. HCT116 cells 24h after plating were treated with vehicle (DMSO), sorafenib (3 μM), vorinostat (500 nM) or both drugs combined. Cells were isolated 6h and 24h after drug treatment and lysates subjected to SDS PAGE and immunoblotting against the proteins indicated in the Figure panel. Blot shown is a representation of two independent experiments.

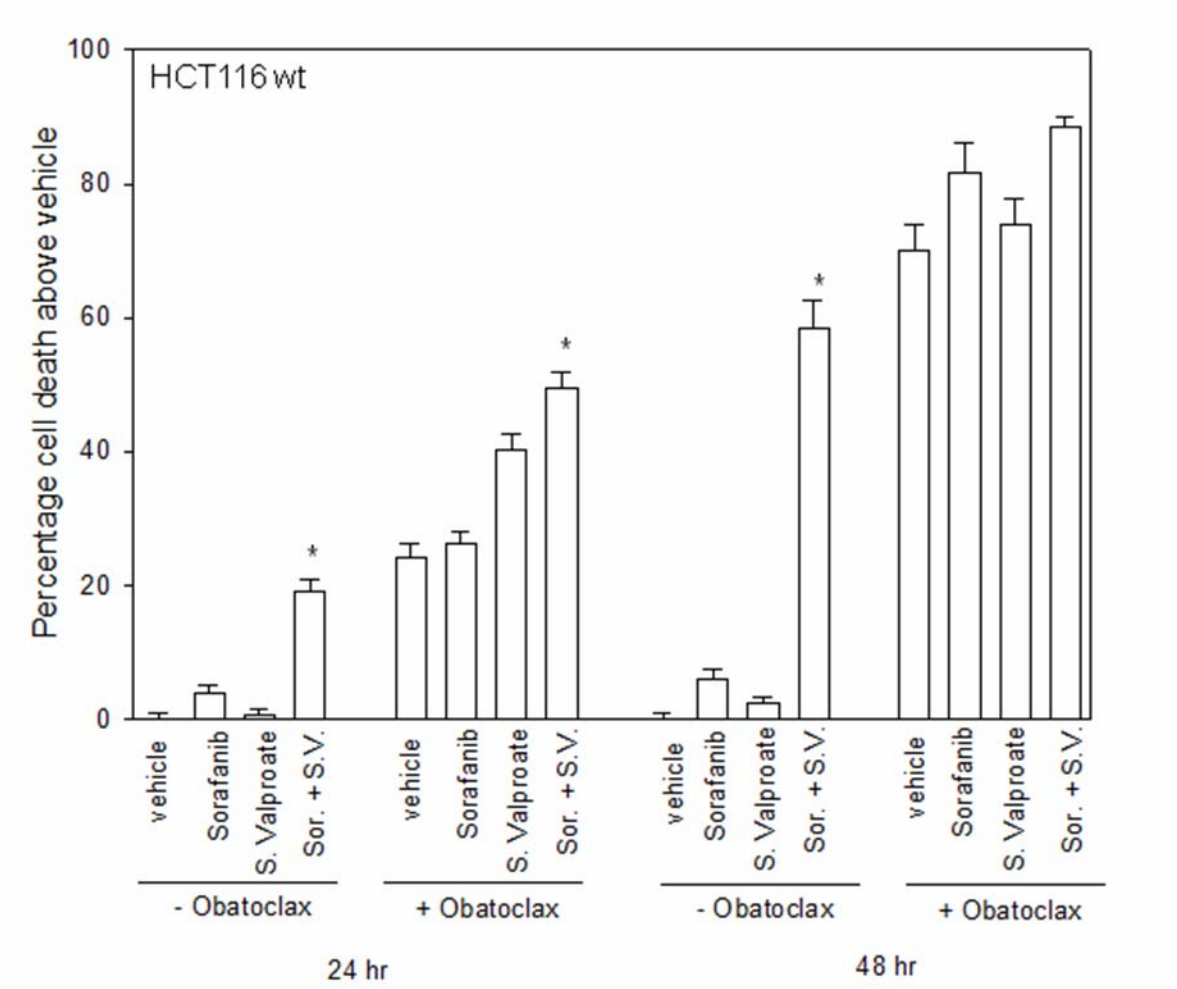

Figure 4.19. BCL-2/Bcl-xL/MCL-1 inhibitor GX15-070 (Obatoclax) increases cell death in HCT116 wt cells. HCT116 cells 24h after plating in triplicate, were treated with vehicle (DMSO) or GX15-070 (100 nM) followed by vehicle (DMSO), sorafenib (3 μM), sodium valproate (1.0 mM) or sorafenib and valproate. Twenty four h and 48h after exposure, cells were isolated and viability determined via trypan blue exclusion assay. Values represent the means for three separate experiments ± SD. * $p \leq 0.05$, greater cell killing than compared with any other treatment condition.

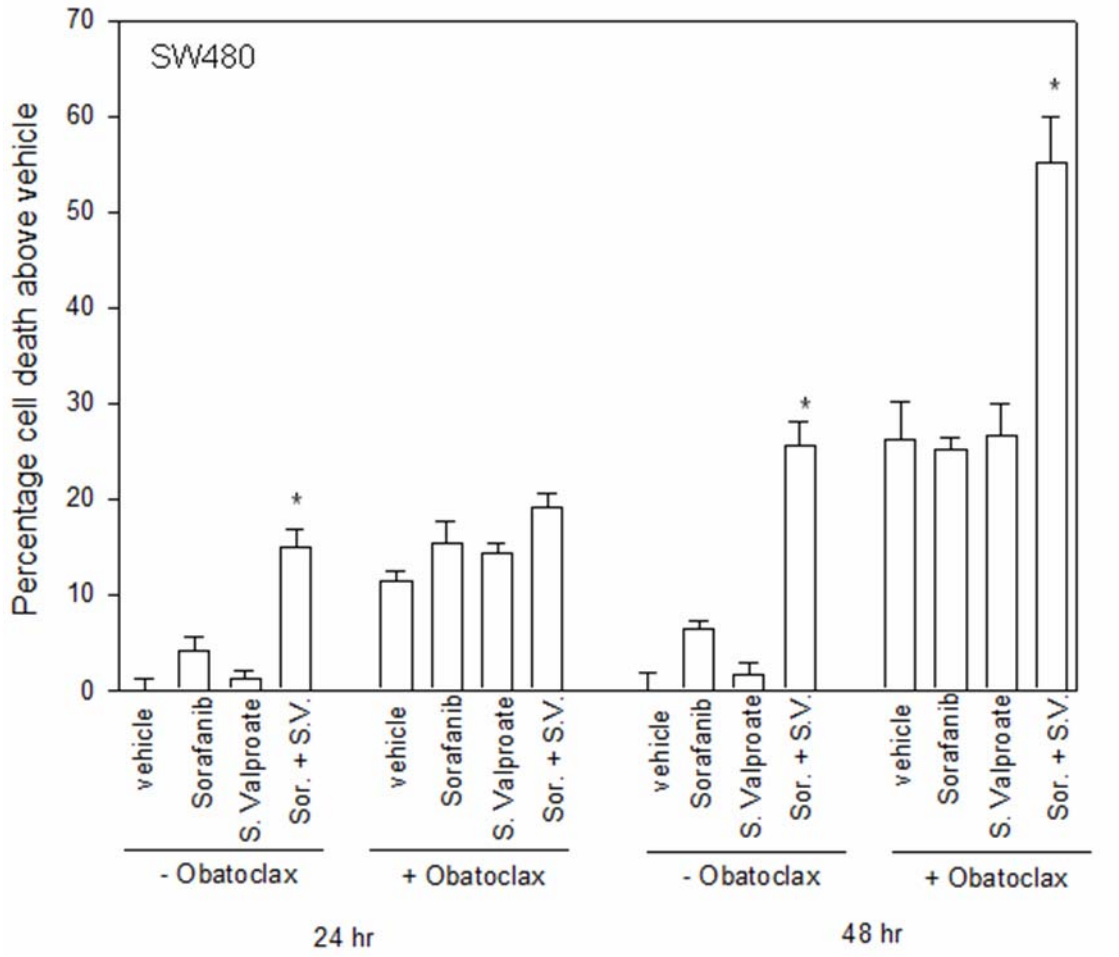

Figure 4.20. BCL-2/Bcl-xL/MCL-1 inhibitor GX15-070 (Obatoclax) increases cell death in SW480 cells. SW480 cells 24h after plating in triplicate, were treated with vehicle (DMSO) or GX15-070 (100 nM) followed by, vehicle (DMSO), sorafenib (6 μM), sodium valproate (1.0 mM) or sorafenib and valproate. Twenty four h and 48h after exposure, cells were isolated and viability determined via trypan blue exclusion assay. Values represent the means for three separate experiments ± SD. * $p \leq 0.05$, greater cell killing than compared with any other treatment condition.

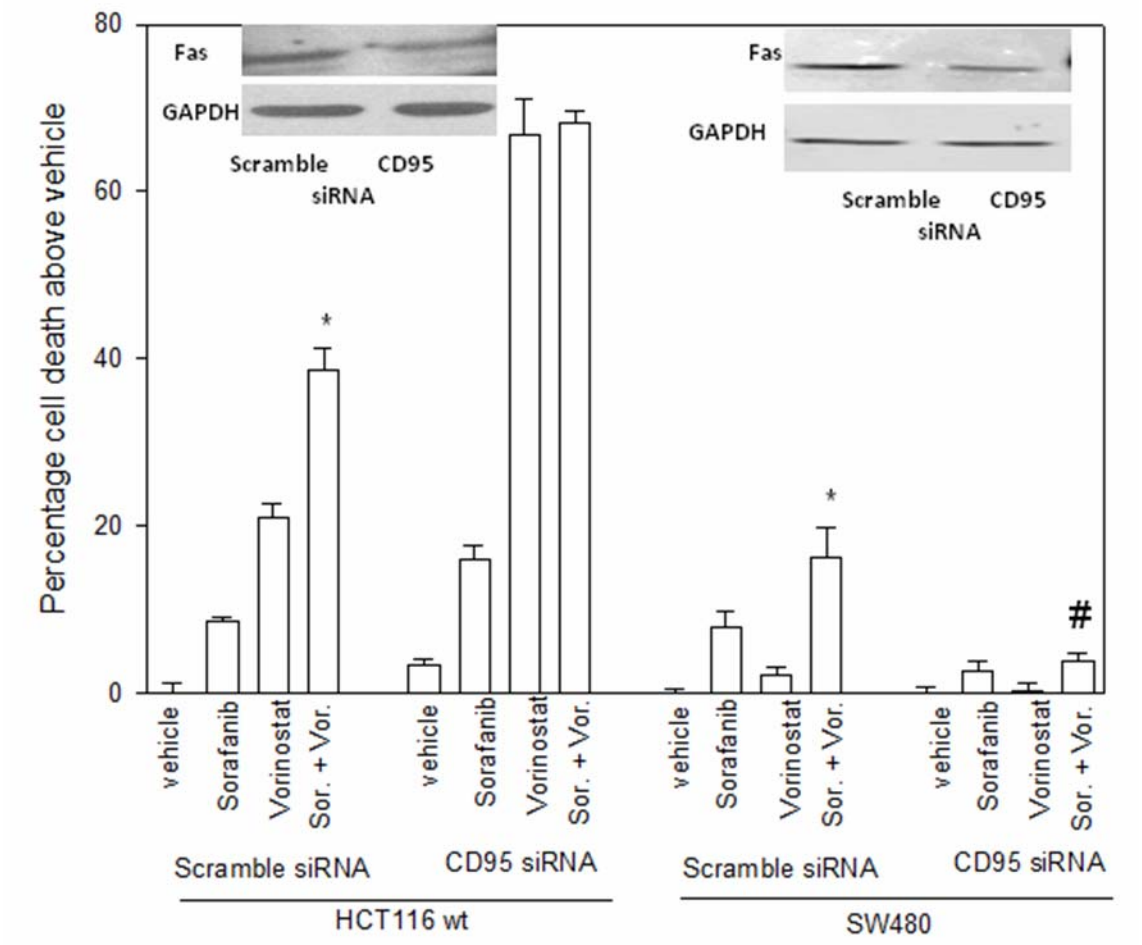

Figure 4.21. HCT116 wt cells mount a death response to Sorafenib and Vorinostat that is Fas-independent; however, SW480 cells have a Fas-dependent mechanism. HCT116 or SW480 cells were transfected with siRNA molecules to knock down CD95 or scrambled siSCR control (20 nM). Twenty four h after infection or transfection, cells were treated with vehicle (DMSO), sorafenib (3 μM, 6 μM for SW480) vorinostat (500 nM) or both drugs together. Forty eight hours after exposure, cells were isolated and stained with Annexin V – propidium iodide and cell viability determined by flow cytometry. Values represent the means for three separate experiments ± SD. * $p \leq 0.05$, greater cell killing than compared with any other treatment condition. # $p \leq 0.05$, less cell killing than compared with any parallel condition in vehicle-treated cells.

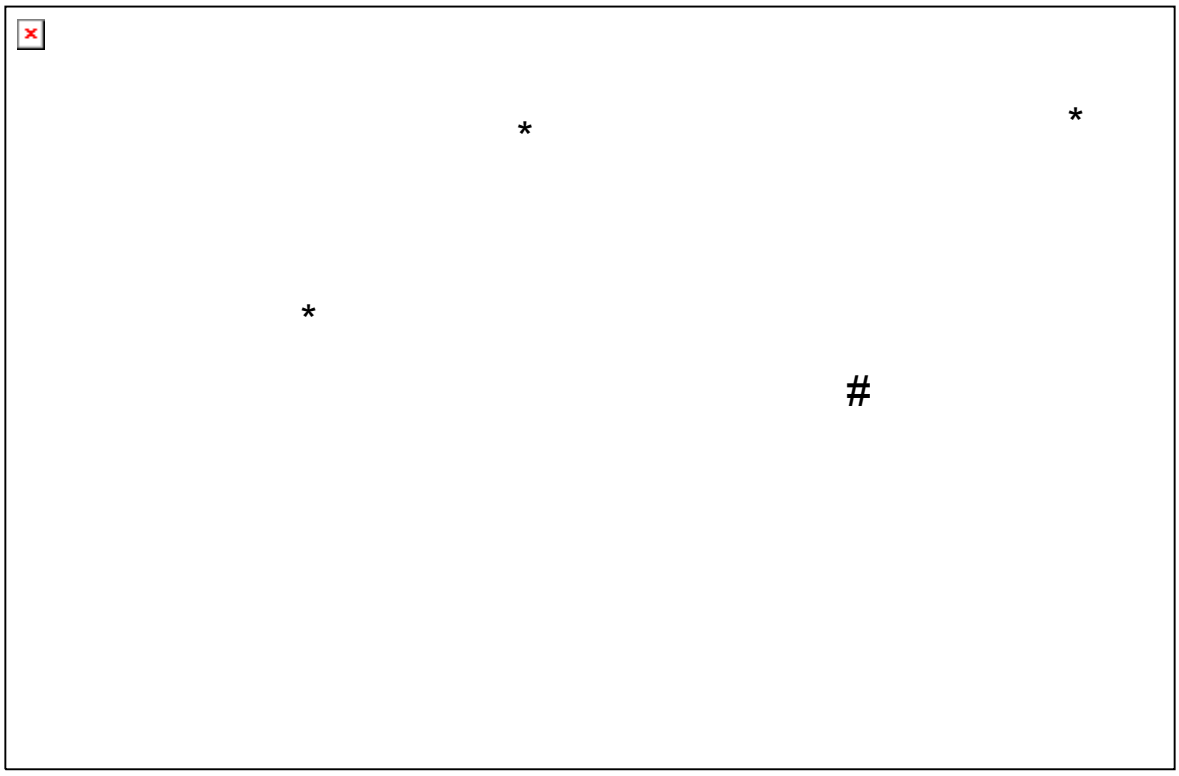

Figure 4.22. Knockdown of CD95 did not rescue cell killing by obatoclax. SW480 cells were transfected with siRNA molecules to knock down CD95 or scrambled siSCR control (20 nM). Twenty four hours after transfection, cells were treated with vehicle, (DMSO) or GX15-070 (100 nM) followed by, vehicle (DMSO), or sorafenib (6 μM) and sodium valproate (1.0 mM). Forty eight hours after exposure, cells were isolated and viability determined via trypan blue exclusion assay (± SEM, n = 2 independent studies). * $p \leq 0.05$, greater cell killing than compared with any other treatment condition. # $p \leq 0.05$, less cell killing than compared with any parallel condition in vehicle-treated cells.

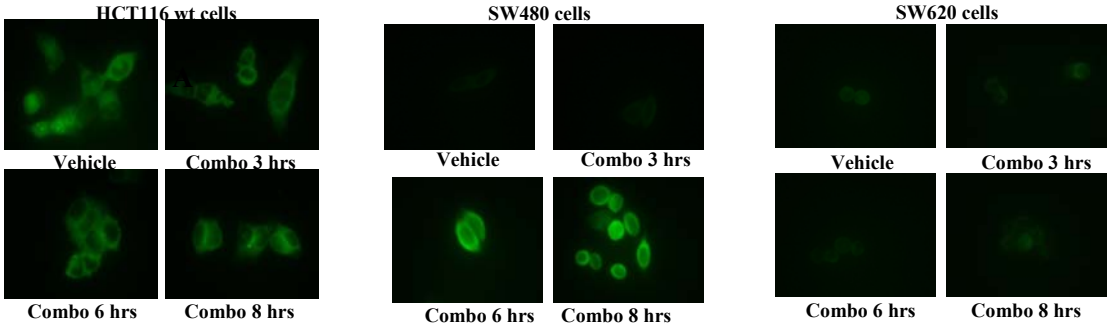

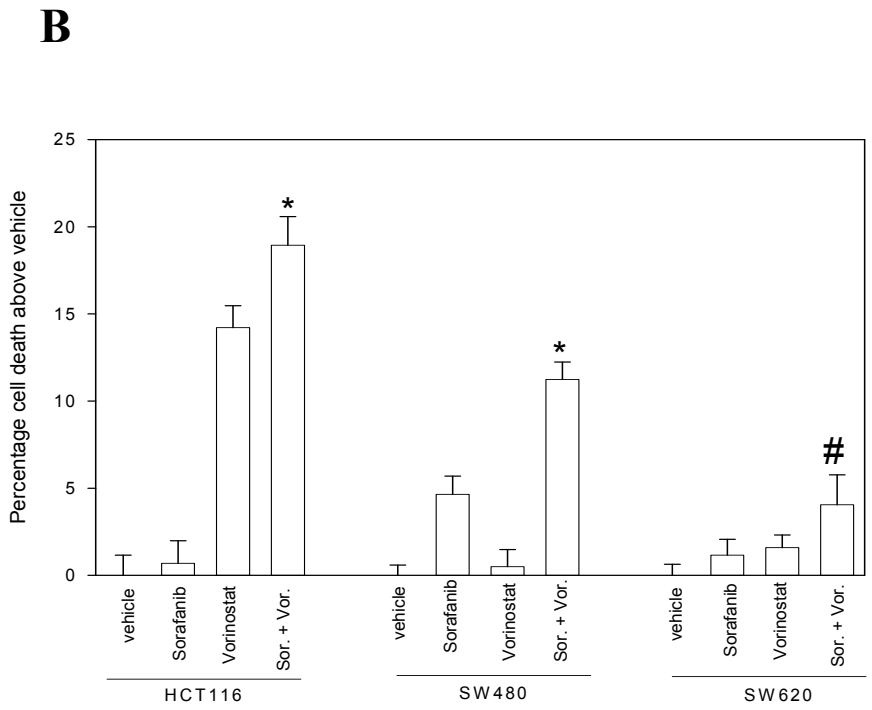

Figure 4.23. Lack of Fas/CD95 surface expression in HCT116 wt cells and SW620 cells, but not in SW480 cells. *A,* HCT116, SW480 and SW620 cells were plated in 4 well glass chamber slides and 24h after plating cells were treated with vehicle (DMSO) or 6μM sorafenib (3 μM, HCT116) and vorinostat (500 nM). Cells were fixed and not permeabilized 0-8h after drug exposure. Fixed cells were immuno-stained for plasma membrane associated CD95 and visualized using an FITC conjugated secondary antibody. Images are representatives from two separate studies. *B*, HCT116, SW480 and SW620 cells were plated and treated with 6 μM sorafenib (3 μM for HCT116 wt) and 500 nM

vorinostat continuously for 48 hours. After drug exposure, the trypan blue exclusion assay was performed. Values represent the means for three separate experiments ± SD * $p \leq 0.05$, greater cell killing than compared with any other treatment condition. # $p \leq 0.05$, less cell killing than compared with any parallel condition in vehicle-treated cells.

A

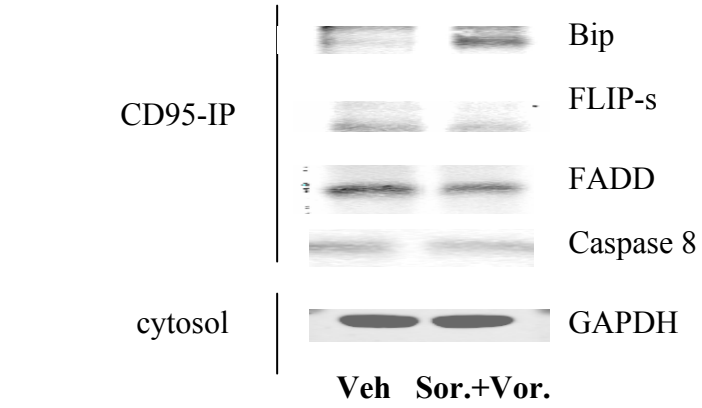

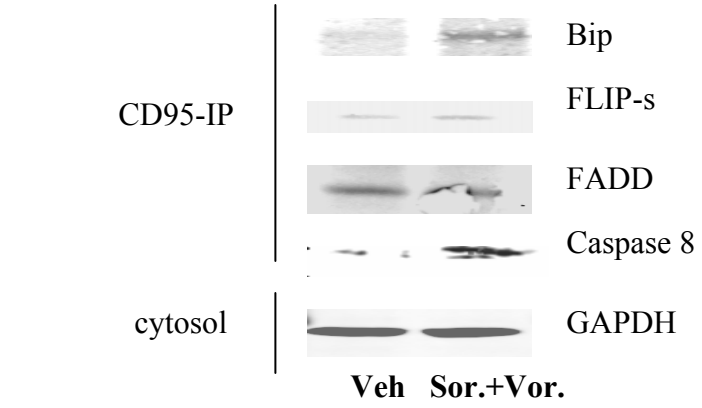

B

Figure 4.24. DISC formation in HCT116 wt and SW480 cells. *A,* HCT116 cells 24h after plating were treated with vehicle (DMSO) or with sorafenib (3 μM) and vorinostat (500 nM). *B, ,* SW480 cells 24h after plating were treated with vehicle (DMSO) or with sorafenib (6 μM) and vorinostat (500 nM). Six h after treatment cells were lysed and CD95 immunoprecipitated. Immunoprecipitates were subjected to SDS PAGE and immunoblotting. A representative CD95 immunoprecipitate is shown (n = 3).

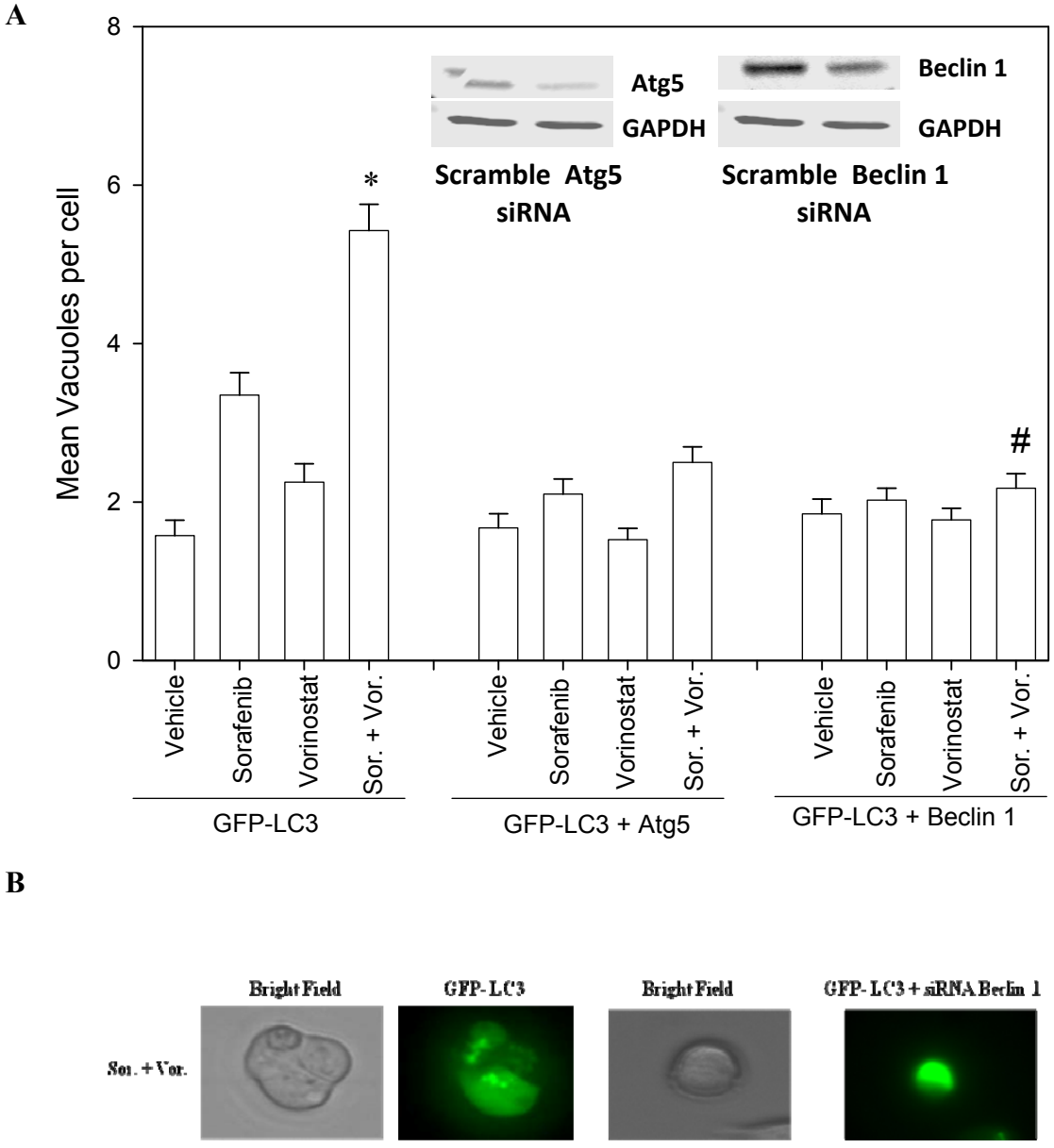

Figure 4.25. Sorafenib and vorinostat stimulate autophagy in the HCT116 wt cells. *A,* HCT116 cells in 4 well chambered glass slides 24h after plating were transfected with siRNA molecules to knock down expression of Atg5 or Beclin1, or with a siScramble control (20 nM). In parallel, cells were co-transfected with a plasmid to express LC3-GFP. Twenty four h after transfection, cells were treated with vehicle (DMSO), sorafenib (3 μM), vorinostat (500 nM) or both drugs combined. Six hours after drug exposure, cells were visualized at 40X using an Axiovert 200 fluorescent microscope under fluorescent light using the FITC filter. The mean number of autophagic vesicles per cell from random fields of 40 cells were counted. * $p \leq 0.05$, greater vesicularization than compared with any

other treatment condition. # $p \leq 0.05$, less cell vesicularization than compared with parallel condition in vehicle-treated cells. *B*, representative microscopic images taken from each of the treatment conditions. Inset Panel: siRNA treatment knocks down of Beclin1 or Atg5 in HCT116 cells 24h after transfection.

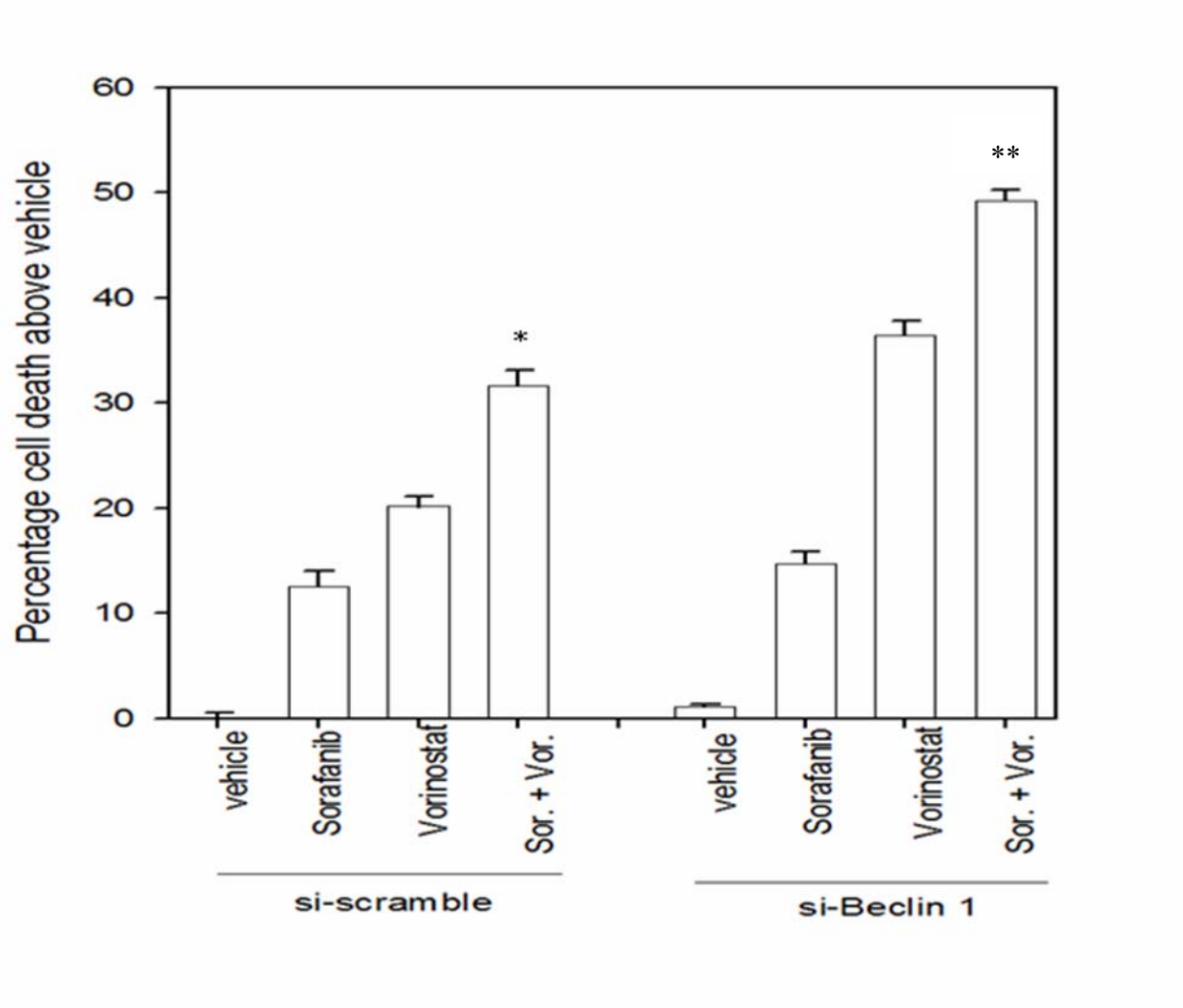

Figure 4.26. Knockdown of Beclin 1 expression enhanced Sorafenib and Vorinostat toxicity. HCT116 cells 24h after plating were transfected with siRNA molecules to knock down expression of Beclin 1, or with a siScramble control (20 nM). Twenty four h after infection or transfection, cells were treated with vehicle (DMSO), sorafenib (3 μM), vorinostat (500 nM) or both drugs together. Forty eight hours after exposure, cells were isolated and stained with Annexin V – propidium iodide and cell viability determined by flow cytometry. Values represent the means for three separate experiments ± SD. * $p \leq 0.05$, greater cell killing than compared with any other treatment condition. **, greater cell killing than si-scramble parallel condition.

A

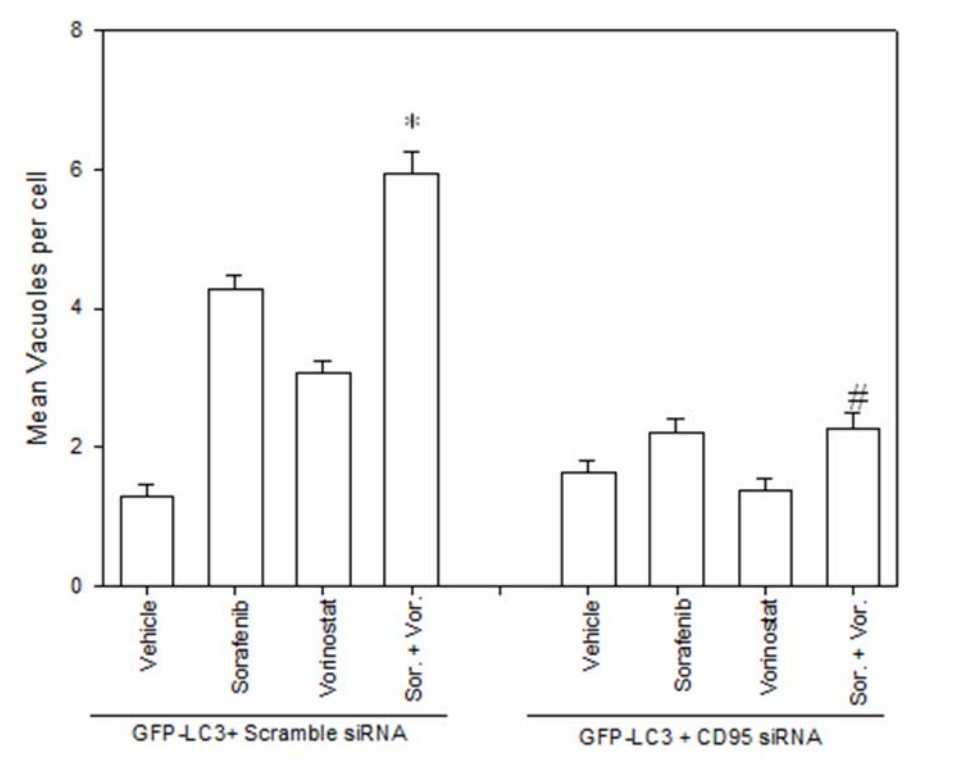

B

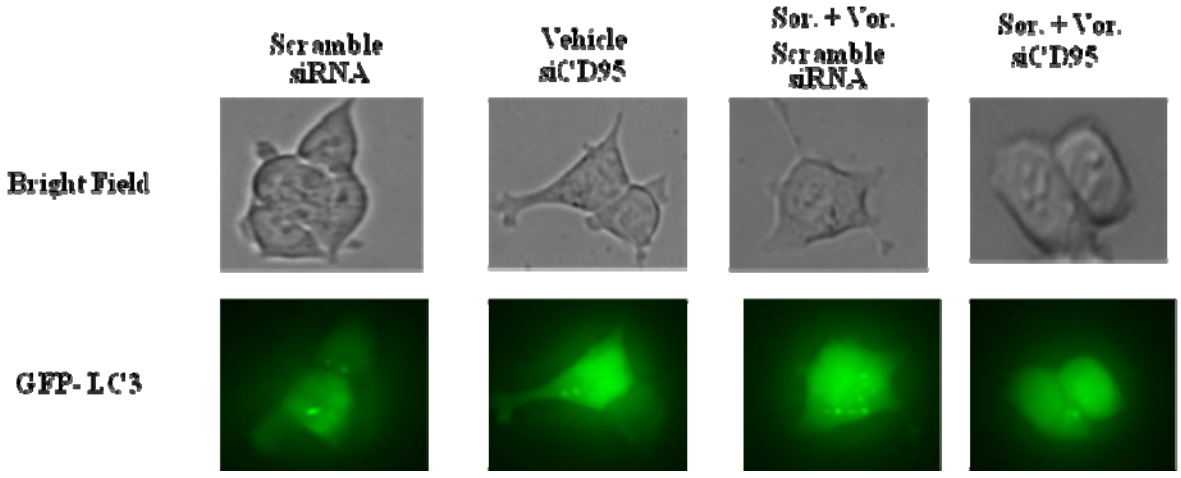

Figure 4.27. Sorafenib and Vorinostat induce autophagy that is CD95 dependent in HCT116 wt cells. *A*, HCT116 cells in 4 well chambered glass slides 24h after plating

were transfected with siRNA molecules to knock down expression of CD95 or with a siScramble control (20 nM). In parallel, cells were co-transfected with a plasmid to express LC3-GFP. Twenty four h after transfection, cells were treated with vehicle (DMSO), sorafenib (3 μM), vorinostat (500 nM) or both drugs combined. Six hours after drug exposure, cells were visualized at 40X using an Axiovert 200 fluorescent microscope under fluorescent light using the FITC filter. The mean number of autophagic vesicles per cell from random fields of 40 cells were counted. * $p \leq 0.05$, greater vesicularization than compared with any other treatment condition. # $p \leq 0.05$, less cell vesicularization than compared with parallel condition in vehicle-treated cells. *B*, representative microscopic images taken from each of the treatment conditions.

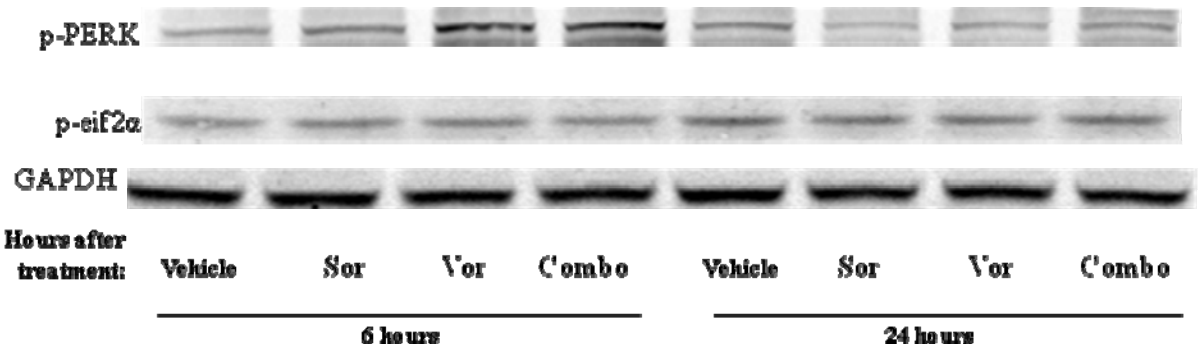

Figure 4.28 Sorafenib and Vorinostat activated PERK but did not alter eif2α phosphorylation in HCT116 wt cells. HCT116 cells 24h after plating were treated with vehicle (DMSO), sorafenib (3 μM), vorinostat (500 nM) or both drugs combined. Cells were isolated 6h and 24h after drug treatment and lysates subjected to SDS PAGE and immunoblotting against the proteins indicated in the Figure panel. Blot shown is a representation of two independent experiments.

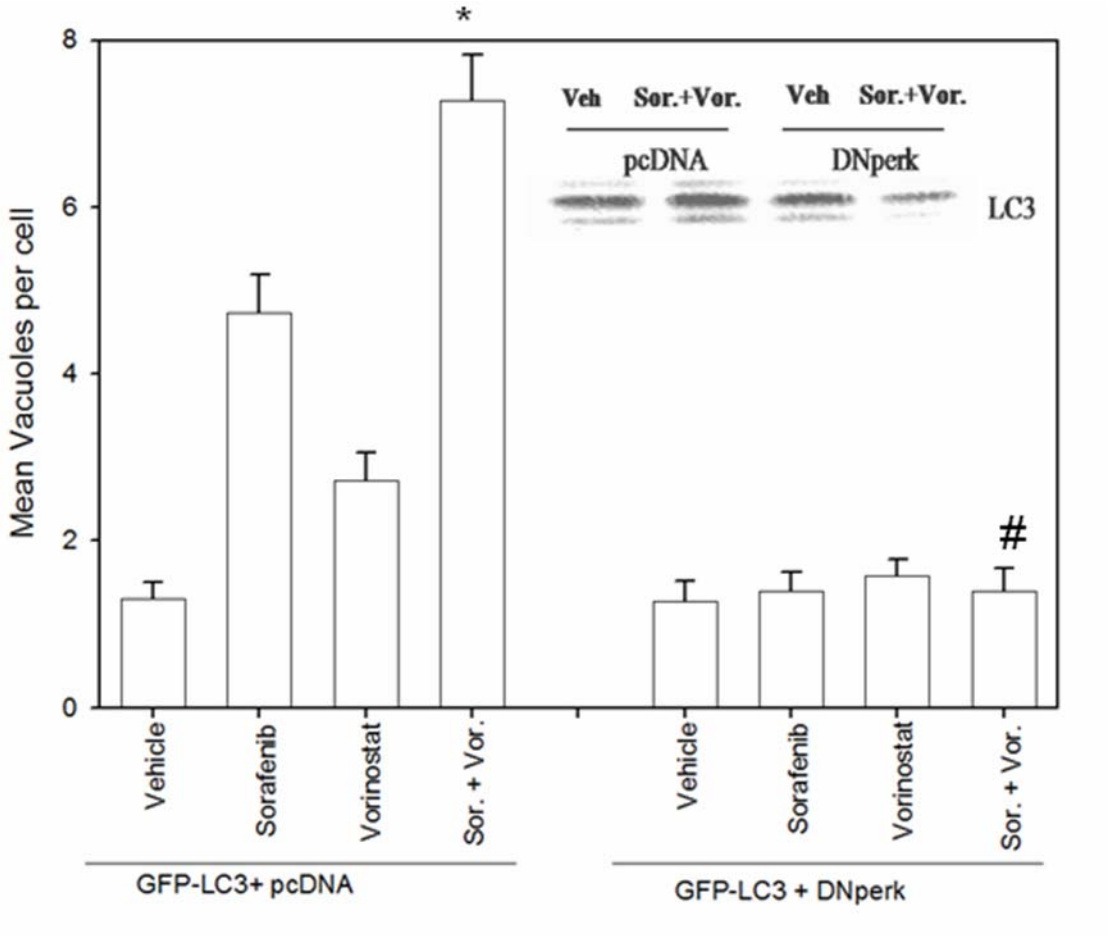

Figure 4.29. DnPERK suppresses Sorafenib and Vorinostat-stimulated autophagy in HCT116 wt cells. HCT116 cells 24h after plating were transfected with either a vector control plasmid (CMV) or a plasmid to express dominant negative PERK. In parallel, cells were co-transfected with a plasmid to express LC3-GFP. Twenty four h after transfection, cells were treated with vehicle (DMSO), sorafenib (3 μM), vorinostat (500 nM) or both drugs combined. Six hours after drug exposure, cells were visualized at 40X using an Axiovert 200 fluorescent microscope under fluorescent light using the FITC filter. The mean number of autophagic vesicles per cell from random fields of 40 cells were counted. * $p \leq 0.05$, greater vesicularization than compared with any other treatment condition. # $p \leq 0.05$, less cell vesicularization than compared with parallel condition in vehicle-treated cells. Inset panel: cells transfected with vector control plasmid (CMV) or a plasmid to express dominant negative PERK (but not LC3-GFP) were isolated 6h after drug exposure and lysates subjected to SDS PAGE and immunoblotting to determine LC3 expression and processing.

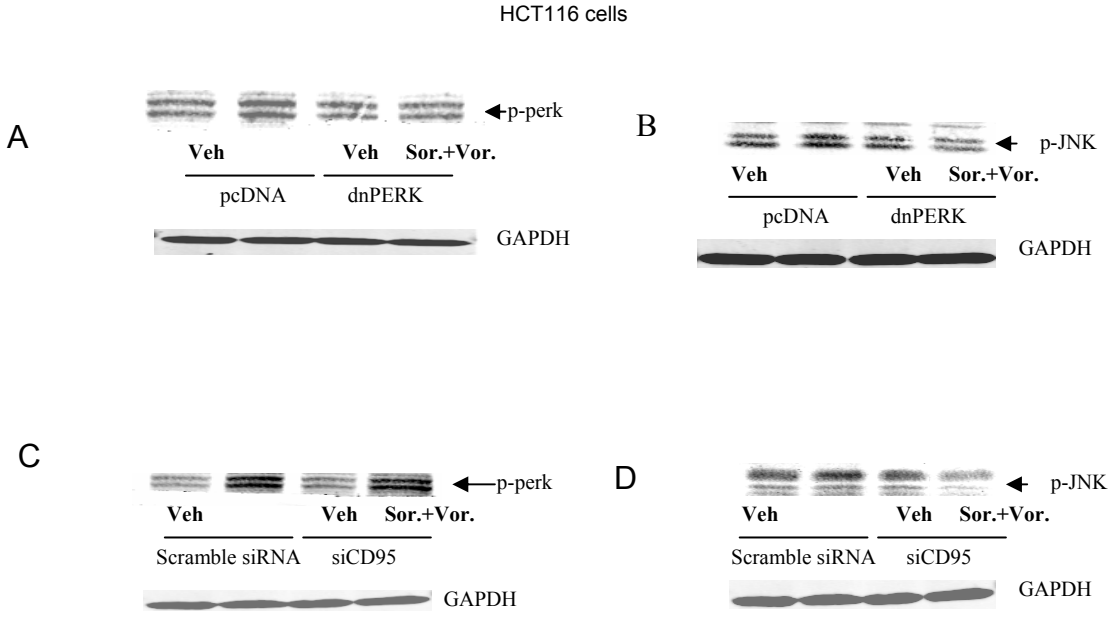

Figure 4.30. Activation of JNK1/2 is dependent on PERK. HCT116 cells 24h after plating were transfected with either: a vector control plasmid (CMV) or a plasmid to express dominant negative PERK; a scrambled siRNA (siSCR) or a siRNA to knock down CD95 expression (20 nM). Twenty four h after infection, cells were treated with vehicle (DMSO) or with sorafenib (3 μM) and vorinostat (500 nM). Six h after drug exposure cells were isolated and lysates subjected to SDS PAGE and immunoblotting to determine the phosphorylation status of PERK and of JNK1/2. Data are from a representative of 2-3 independent studies.

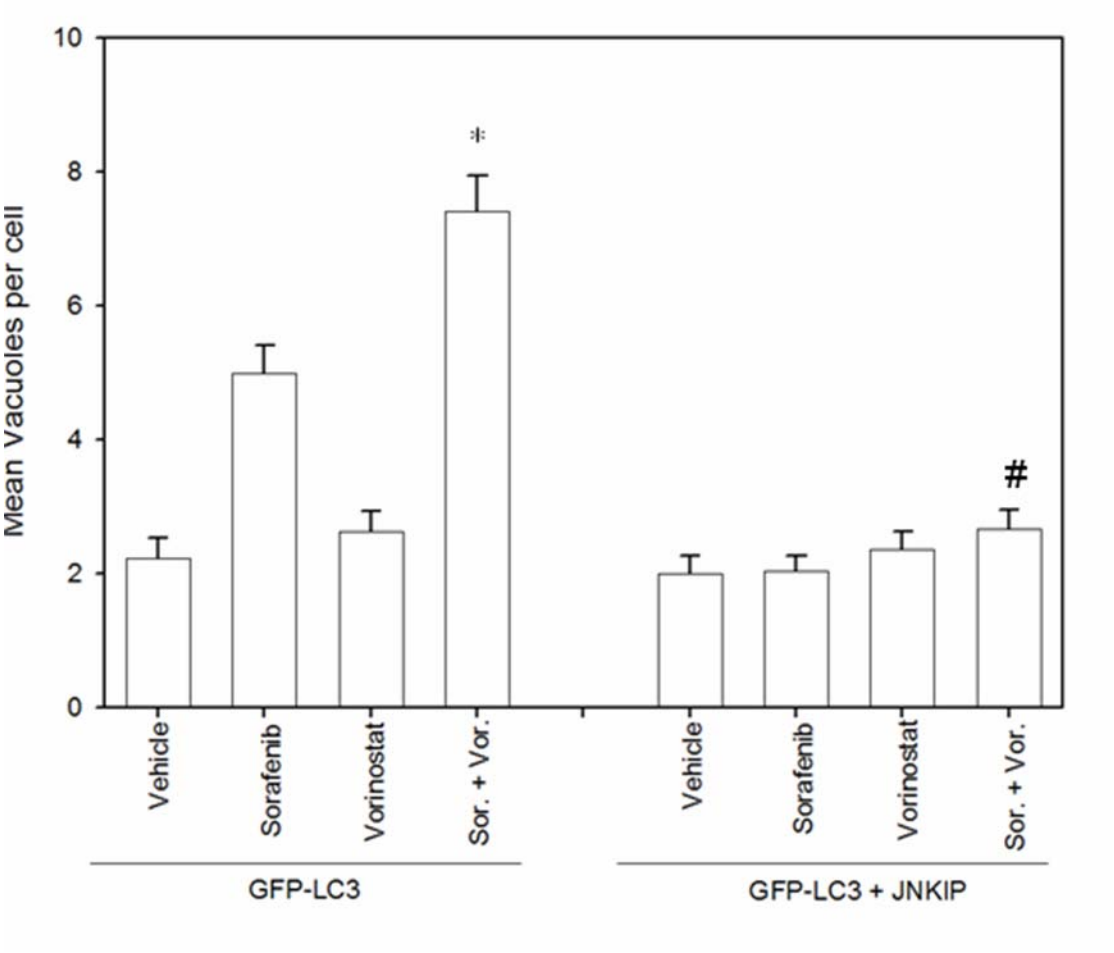

Figure 4.31. Molecular Inhibition of JNK1/2 signaling blocked Sorafenib and Vorinostat-stimulated autophagy. HCT116 cells 24h after plating in 8 well chamber slides were transfected with a plasmid to express LC3-GFP. Thirty minutes prior to drug exposure cells were treated as indicated with vehicle (DMSO) or the JNK inhibitory peptide (JNK-IP, 10 μM). Twenty four h after infection, cells were treated with vehicle (DMSO), sorafenib (3 μM), vorinostat (500 nM) or both drugs combined. Six h after drug exposure cells were visualized at 40X using an Axiovert 200 fluorescent microscope under fluorescent light using the FITC filter. The mean number of autophagic vesicles per cell from random fields of 40 cells were counted. * $p \leq 0.05$, greater vesicularization than compared with any other treatment condition. # $p \leq 0.05$, less cell vesicularization than compared with parallel condition in vehicle-treated cells.

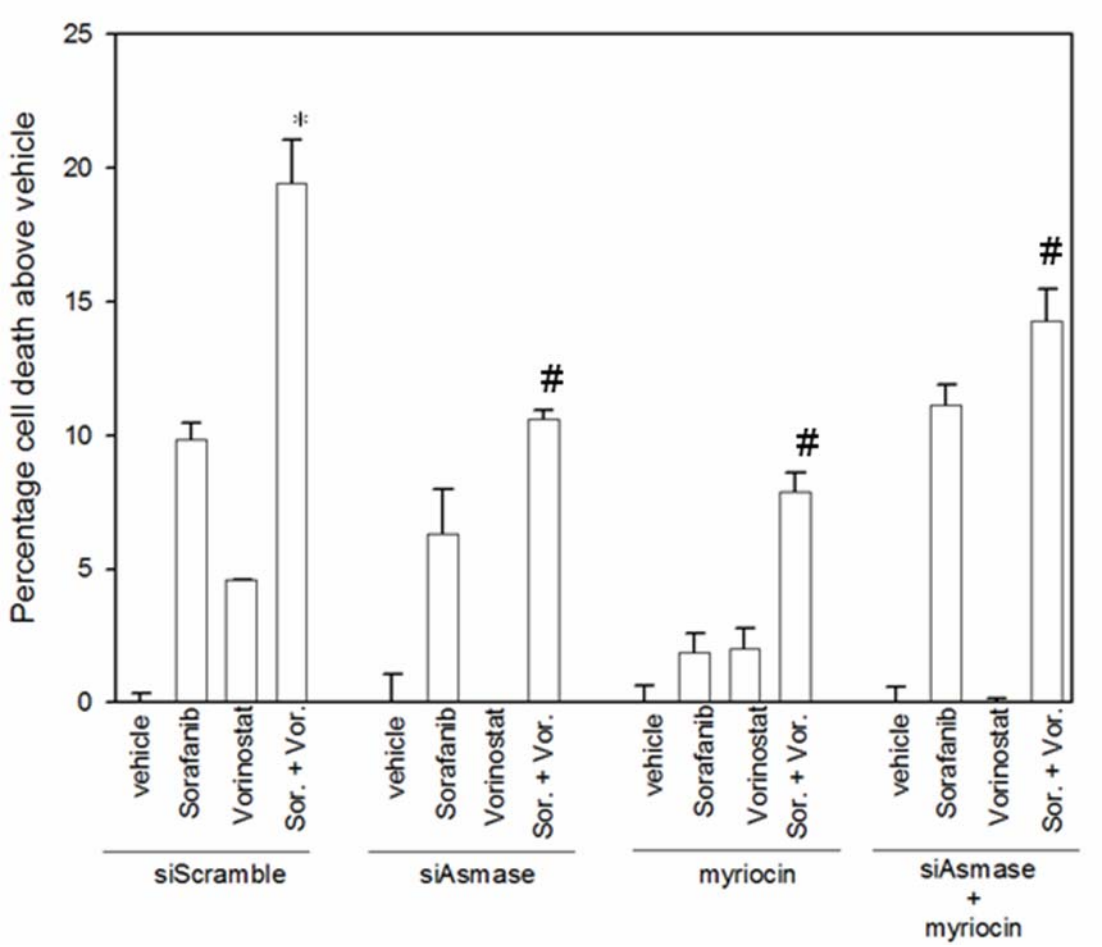

Figure 4.32. Sorafenib and Vorinostat toxicity is acidic sphingomyelinase dependent. SW480 cells 24h after plating were transfected with siRNA molecules to knock down expression of acidic sphingomyelinase (ASMase) or LASS6, or transfected with scrambled siRNA molecules. Twenty four h after transfection cells were treated with vehicle (DMSO) or myriocin (1 μM) and after 30 min, cells then exposed to vehicle (DMSO), sorafenib (6 μM), vorinostat (500 nM) or both drugs combined. Forty eight hours after exposure, cells were isolated and stained with trypan blue dye. * $p \leq 0.05$, greater cell killing than compared with any other treatment condition. # $p \leq 0.05$, less cell killing than compared with any parallel condition in vehicle-treated cells.

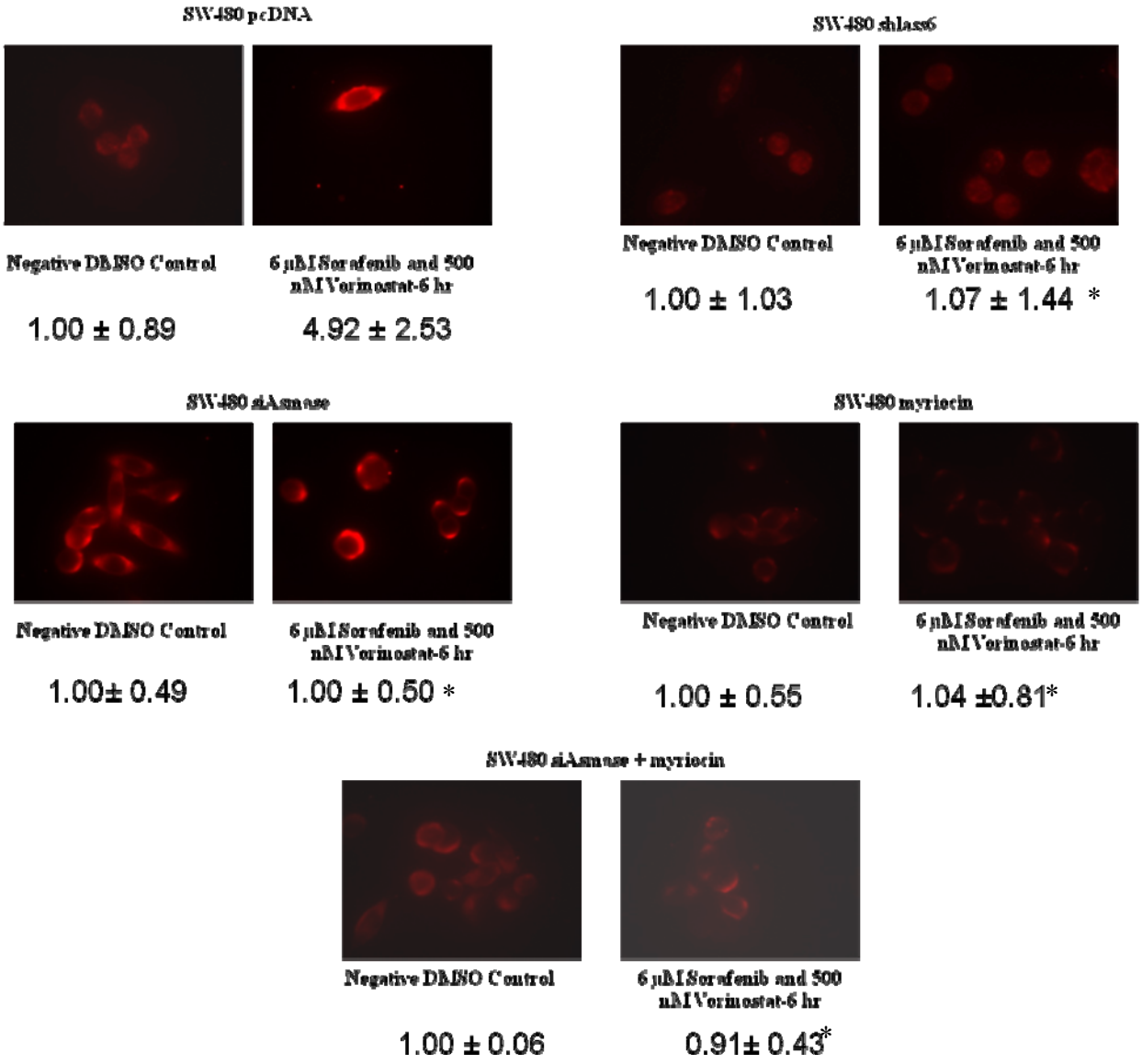

Figure 4.33. CD95 activation is acidic sphingomyelinase dependent. SW480 cells 24h after plating in 4 well chamber slides were transfected with siRNA molecules to knock down expression of acidic sphingomyelinase (ASMase) or LASS6, or transfected with scrambled siRNA molecules. 24 h later cells were exposed to vehicle (DMSO), sorafenib (6 μM), vorinostat (500 nM) or both drugs combined. Cells were fixed 6h after exposure and the amount of plasma membrane associated CD95 determined by immunohistochemistry. * $p \leq 0.05$, value less amount of cell surface CD95 compared to vehicle-treated conditions.

A

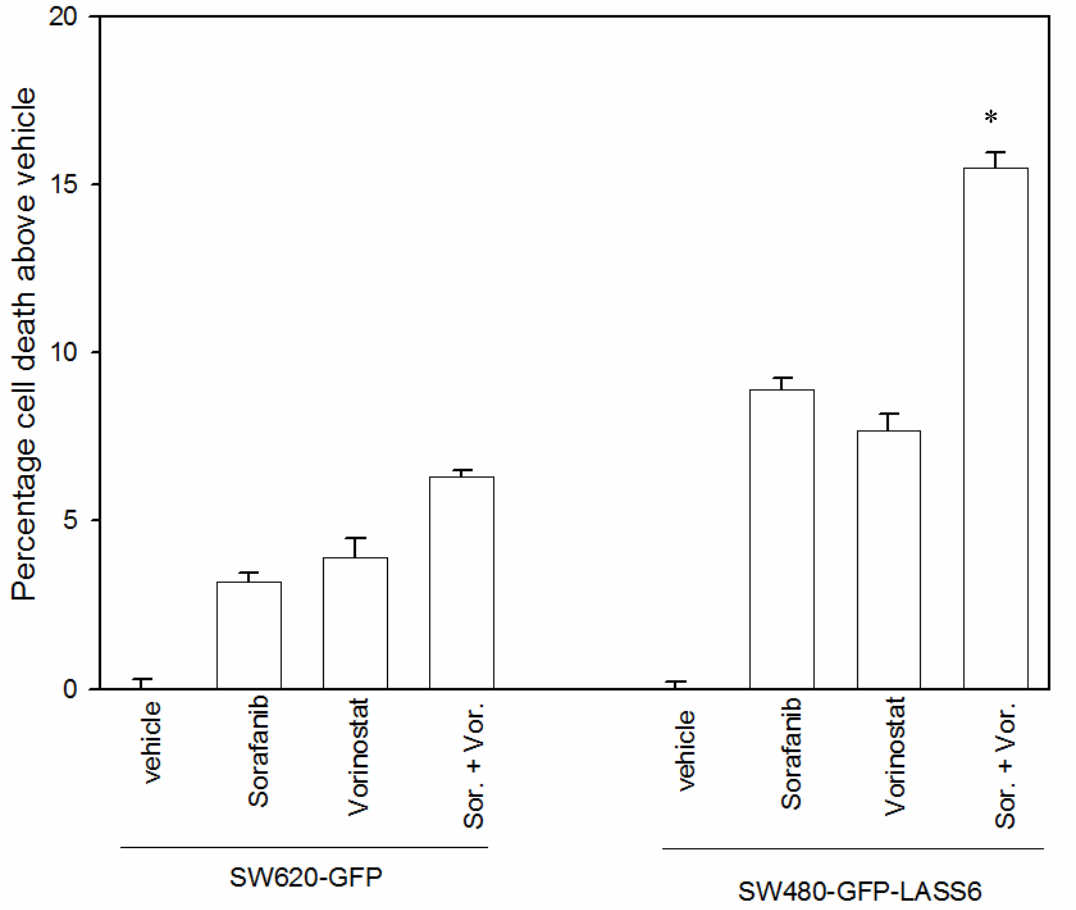

B

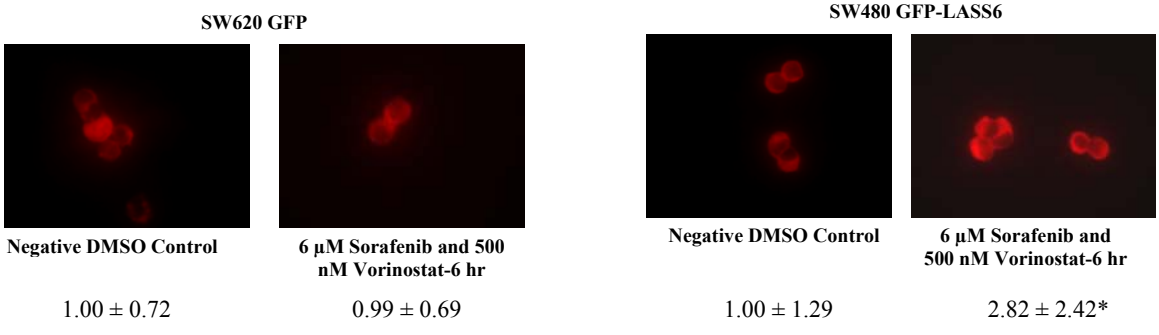

Figure 4.34. Overexpression of LASS6 enhanced Sorafenib and Vorinostat-induced CD95 activation and enhanced tumor cell killing in SW620 cells. *A,* SW620 cells stably

transfected with either vector control plasmid of a plasmid to express LASS6, 24h after plating, were exposed to vehicle (DMSO), sorafenib (6 μM), vorinostat (500 nM) or both drugs combined. Forty eight hours after exposure, cells were isolated and stained with trypan blue dye. * $p \leq 0.05$, greater cell killing than compared with any other treatment condition. *B,* SW620 cells 24h after plating in 4 well chamber slides as above, and exposed to vehicle (DMSO), sorafenib (6 μM), vorinostat (500 nM) or both drugs combined. Cells were fixed 6h after exposure and the amount of plasma membrane associated CD95 determined by immunohistochemistry. * $p \leq 0.05$, value greater amount of cell surface CD95 compared to vehicle-treated conditions.

CHAPTER 5 DISCUSSION: Sorafenib and Vorinostat

Previous studies in our laboratory have shown that sorafenib and vorinostat interact to kill pancreatic, renal, and hepatocellular cancer cells via a CD95 dependent mechanism [107, 108]. The present studies were designed to examine whether sorafenib and HDACIs interact in a synergistic manner to cause cell death in colon cancer cells.

In short term cell viability assays, sorafenib and vorinostat caused an additive to greater than additive increase in colon cancer cell death. However, colony formation assays is deemed as the best in vitro measurements of the impact of tumor cell growth in vivo. In long-term colony formation assays, sorafenib and vorinostat treatment synergized to kill HCT116 wt and SW480 colon cancer cells with CI values of less than 0.70. DLD1 cells have higher levels of AKT, a pro-survival protein, which could be one reason we did not detect synergy with the drug combination in this cell line.

Sodium valproate is an anti-epileptic drug and mood stabilizer that has been rediscovered as and HDACI. Recently, it has been shown that valproic acid may affect the concentration of HDAC2 by inducing its proteasomal degradation [117]. Thus, we used sorafenib and the more specific HDACI inhibitor sodium valproate and also found that this combination synergized to kill colon cancer cells with values of less than 0.75. Collectively, our findings in colon cancer cells with respect to sorafenib and HDACI treatment are in general agreement with those in NSCLC, renal, liver, melanoma and pancreatic cancer cells [107, 108].

In agreement with the concept that *reduced* basal activity in the MEK1/2 and/or PI3K pathways will reduce cellular tumorigenicity and diminish drug toxicity, we found that the lethality of sorafenib or vorinostat, or the drug combination was suppressed by deletion of K-RAS D13 from HCT116 cells. We then investigated the relative importance of three of the best defined pathways downstream of RAS proteins that were likely to be involved in controlling drug toxicity: Raf-MEK1/2 (H-RAS V12 S35); PI3K-Akt (H-RAS V12 C40); RAL GDS (H-RAS V12 G37). We have recently published using these cells in vitro and in vivo that activation of RAS predicted resistance to PI3K inhibitors even in the presence of activating PI3K mutations or loss of PTEN, whereas H-RAS V12 (C40) – induced single activation of PI3K predicted for sensitivity to PI3K inhibitors. Expression of H-RAS V12 but not point effector mutants of H-RAS V12 that activate PI3K-Akt (C40) or RAL GDS (C37) restored the toxicity of sorafenib or vorinostat, and the drug combination, to near those levels observed in wild type cells. Activation of the RAL GDS pathway did not restore vorinostat lethality whereas activation of PI3K-Akt signaling did not restore sorafenib toxicity. Based on the findings of our prior studies, this suggests that inhibition of PI3K signaling would be a rational approach to potentiate sorafenib toxicity. In contrast to data with other effector point mutants, expression of the mutant that elevates Raf-MEK1/2 signaling enhanced both vorinostat and the combination of sorafenib and vorinostat lethality above those in parental cells or cells expressing wild type H-RAS V12. In parental HCT116 cells we noted that sorafenib and vorinostat treatment caused a delayed inactivation of ERK1/2 that was essential for the toxic drug interaction. In HT29

subclones, we found that active K-Ras mutant also enhanced drug lethality with the combination treatment.

In several studies HDACI lethality was shown to be enhanced when ERK1/2 pathway signaling was inhibited using potent small molecule MEK1/2 inhibitors [118, 119]. Expression of dominant negative MEK1, but not dominant negative Akt, enhanced the toxicity of sorafenib, vorinostat, and sorafenib and vorinostat combination. It is likely that DnAKT could protect cells by increasing the activation of JNK, which in turn allows for increased expression of Beclin 1 and more autophagy. Autophagy is protective in these cells. In addition, overexpression of MEK1 suppressed the drug combination. Collectively our data leads us to conclude that while inhibition of ERK1/2 signaling can promote the toxicity of vorinostat and facilitate sorafenib and vorinostat killing, elevated basal/tonic levels of ERK1/2 activity within colon cancer cells are also essential for vorinostat toxicity as well as sorafenib and vorinostat combination toxicity.

In some cell types, the toxicity of vorinostat has been linked to activation of the JNK pathway [120, 121]. In HCT116 cells we noted that vorinostat and sorafenib+vorinostat exposure increased the phosphorylation of p38α/β MAPK as well as that of JNK1/2. Expression of dominant negative p38α MAPK in HCT116 cells had no apparent impact on tumor cell toxicity, in contrast to our recent studies using MEK1/2 inhibitors and 17AAG [122]. Signaling by the JNK pathway has been linked to growth promoting signals as well as both pro- and anti-apoptotic regulation [123-125]. Inhibition of JNK1/2 using a molecular tool modestly enhanced sorafenib+vorinostat toxicity in HCT116 cells; our somewhat surprising finding became more easily understood when we noted that activation of

JNK1/2 was dependent on expression of CD95 and was blocked by expression of dominant negative PERK.

Autophagy in cancer remains to be controversial, as its induction may mediate both cell death and cell survival. Our studies in colon cancer cells indicate that inhibitors of autophagy induce enhanced levels of cell death. In our prior studies combining sorafenib and vorinostat in NSCLC, renal, liver, melanoma and pancreatic cancer cells cell killing was PERK- and CD95 dependent and the induction of protective autophagy was also PERK- and CD95 dependent [107, 108]. In HCT116 cells, although PERK was activated, phosphorylation of eIF2α did not occur. Drug-induced eIF2α phosphorylation was previously noted to be essential for translational repression of c-FLIP-s and Mcl-1 levels and in HCT116 cells, the levels of neither c-FLIP-s nor Mcl-1 were suppressed after drug treatment [107, 108]. This data may explain why CD95-caspase 8 signaling was non-productive in HCT116 cells. To our surprise we found that knock down of CD95 expression in HCT116 cells increased cell killing. Over half of colon cancer patients have mutations in the CD95 receptor. Thus, it is likely that HCT116 wt cells carry a mutation in the CD95 receptor, rendering it cytoprotective. However, we noted that drug exposure promoted a protective form of autophagy that was CD95 dependent. This data confirms our prior work and argues that in some cell types and under certain treatment conditions, CD95 signaling promotes cell survival.

We have shown that bile acids can promote ligand independent, ASMase and ceramide –dependent, activation of CD95 in primary hepatocytes and that generated both toxic signals (caspase 8 and JNK1 activation) as well as protective signals (JNK2

activation [12, 123] The generation of ceramide has been shown by many groups to promote ligand independent activation of several growth factor receptors via the localization / clustering of these receptors and other signal facilitating proteins into lipid rich domains [126, 127]. In melanoma, renal and liver cancer cells, combined but not individual exposure to sorafenib and vorinostat, caused rapid activation of CD95 that did not correlate with altered expression or cleavage of FAS-L [107, 108].

In SW480 cells, sorafenib and vorinostat exposure activated CD95 as judged by increased plasma membrane staining for CD95 as well as increased DISC formation in an ASMase- and de novo –ceramide synthesis pathway dependent fashion. However, in patient matched SW620 cells that have reduced LASS6 expression, CD95 activation was not observed. Our prior analyses in sorafenib and vorinostat treated HEPG2 cells demonstrated that loss of ASMase function reduced formation of C14 and C16 ceramide species whereas inhibition of the de novo synthesis pathway suppressed generation of multiple dihydro-ceramide species, particularly the C12 / C14 / C16 and C20 / C24 / C26 dihydro-ceramides. SW480 cells demonstrated protection from cell death when acidic sphingomyelinase was knocked down or when the pharmacological inhibitor of the de novo pathway, myriocin was used. The combination of both siAsmase and myriocin did not reduce cell death to a greater extent however. This could be due to the compensation of other sphingomyelinases such as neutral or alkaline. The six known ceramide synthase proteins (LASS) are localized in the ER and different LASS proteins have been noted to generate different chain length ceramide forms, with LASS5 and LASS6 being most closely linked to the generation of C14 and C16 dihydro ceramide [128, 129]. In general

agreement with the hypothesis that LASS6 is a key player in the regulation of sorafenib and vorinostat toxicity, knock down of LASS6 in SW480 cells suppressed drug-induced CD95 activation whereas expression of LASS6 in SW620 cells enhanced drug-induced CD95 activation and cell killing. Whether the activities of LASS proteins are regulated by a combination of vorinostat-modulated protein acetylation and sorafenib-induced changes in ROS and Ca^{2+} fluxes in the ER will need to be examined in future studies.

In conclusion, sorafenib and vorinostat interact to kill multiple colon cancer cell types. Unlike tumor cell types previously examined, such as NSCLC, renal, liver, melanoma and pancreatic cancer cells, cell killing occurs via CD95-dependent and CD95-independent mechanisms. Though in all cell types examined thus far, the induction of mitochondrial dysfunction and activation of the intrinsic pathway play central roles in drug lethality.

CHAPTER 6 INTRODUCTION: 17AAG AND PD184352

6.1 Pancreatic Cancer

Pancreatic cancer is a disease in which malignant (cancer) cells are found in the tissues of the pancreas. The pancreas is a large organ that lies horizontally behind the lower part of the stomach and it secretes enzymes that aid in digestion and hormones (i.e. insulin) that help regulate the metabolism of sugars. The digestive juices are produced by exocrine pancreas cells and the hormones are produced by endocrine pancreas cells. About 95% of pancreatic cancers begin in exocrine cells [130].

Pancreatic cancer typically spreads rapidly and is seldom detected in its early stages, thus it is one of the deadliest of all the solid malignancies. The five year survival rate is only 4% [131]. For those patients with localized disease and small cancers (<2 cm) with no lymph node metastases and no extension beyond the capsule of the pancreas, complete surgical resection can yield 5-year survival rates of 18% to 24% [132]. Nearly 34,000 patients die from pancreatic cancer, and it is the fourth leading cause of cancer death in the United States [131].

6.2 Hepatocellular Carcinoma

Hepatocellular carcinoma (HCC), also called malignant hepatoma is cancer of the liver. Most cases of hepatoma are secondary to cancers caused by viral hepatitis (20%), primarily hepatitis B and C, or cirrhosis (80%). The most common cause for cirrhosis in the United States is alcohol abuse. In the United States, it was estimated that there would be 21,370 new cases diagnosed and 18,410 deaths due to this disease in 2008 [131]. There is

also a distinct male preponderance among all ethnic groups in the United States. Although this hepatoma is rare in the United States, it is one of the most common tumors worldwide. It is the fourth most common cancer in the world. HCC is especially prevalent in parts of Asia and Africa. The male preponderance is most marked among Chinese Americans, in whom the annualized rate of HCC among men is 20.9 per 100,000 and among women 8.0 per 100,000 population. HCC is one of the deadliest cancers in China [133]. One of the most common risk factors is the production of aflatoxins in food. Aflatoxins, which are mycotoxins formed by certain Aspergillus species, are a frequent contaminant of improperly stored grains and nuts. In parts of Africa, the high incidence of HCC in individuals may be related to ingestion of foods contaminated with aflatoxins [134].

Treatment options depend on the tumor size and staging, but the prognosis is usually poor with hepatomas. Only 10-20% of hepatomas can be removed completely by surgery. If the cancer is not removed completely, the survival rate is usually only about 3 to 6 months. Liver transplantation is also an option and may be curative for relatively small tumors. However, even liver transplantation is not typically possible in most cases as early diagnosis is somewhat rare. Most patients receive chemotherapy, precutaneous ethanol injection, transcatheter arterial chemoembolization (TACE), or radiotherapy which may relieve symptoms and prolong life but these procedures are not curative [135] .

6.6 Hsp90 inhibitors

The highly conserved N-terminal domain of hsp90 is the binding site for geldanamycin (GA), an ansamycin drug which specifically targets hsp90 [136]. GA inhibits the hsp90 ATPase with nanomolar affinity. This drug occupies the nucleotide-binding

cleft within in the N-terminal domain [68]. Radicicol is a macrocyclic antifungal structurally unrelated to GA but posses the same function as GA. Radicicol can compete with GA for the N-terminal domain of hsp90 [137]. Thus, both of these inhibitors act like nucleotide mimetics that lock hsp90 in an ADP-bound state. A major consequence of this action is inhibition of p23-hsp90 interaction [138]. Like many chemotherapeutic agents, GA has a dose-dependent selectivity for tumor cells. In cancer cells, Hsp90 has a higher affinity for N-terminal ligands than in normal cells [139]. Thus, GA would preferentially target cancer cells rather than normal cells since it binds the N-terminus of hsp90. GA however was found to be too toxic for clinical development [140]. Its derivative, 17-allylamino-17-demethoxygeldanamycin (17-AAG), a reversible Hsp90 inhibitor, as well as the more water-soluble compound 17-dimethoxygeldanamycin (17-DMAG) posses anti-tumor activity and is currently undergoing clinical phase I trials. However, 17-AAG seems to undergo extensive metabolism that can result in the generation of toxic species [141] (Figure 6.1).

6.7 PD184352 (CI-1040)

PD184352 is a second generation MEK1/2 inhibitor with enhanced bioavailability (Figure 6.2). This drug does not compete with ATP for the binding site, thus PD184352 acts as an allosteric inhibitor, binding outside the ATP and ERK1/2 binding sites on MEK1/2. PD184352 inhibits activation of MEK1 in cells by 50% at 2nM, a concentration over 100 fold lower than that which inhibits MEK 1 activity in vitro. This drug is also highly specific for MEK 1 and 2. When given orally every 12 hours for 2 weeks,

PD184352 exhibits a growth inhibitory effect on human colon tumor xenografts in mice. This drug also decreases invasiveness and motility of HT29 cells [142].

6.8 Basis for 17AAG and PD184352 Project

We recently published that 17AAG and PD184352 interact to kill in hepatoma cells via activation of the CD95 extrinsic apoptotic pathway [122]. The present studies determined whether the same killing mechanisms apply after 17AAG and PD184352 treatment in colon cancer cells. Additional studies were designed to mechanistically advance our knowledge of 17AAG and PD184352 in pancreatic and hepatoma cell lines.

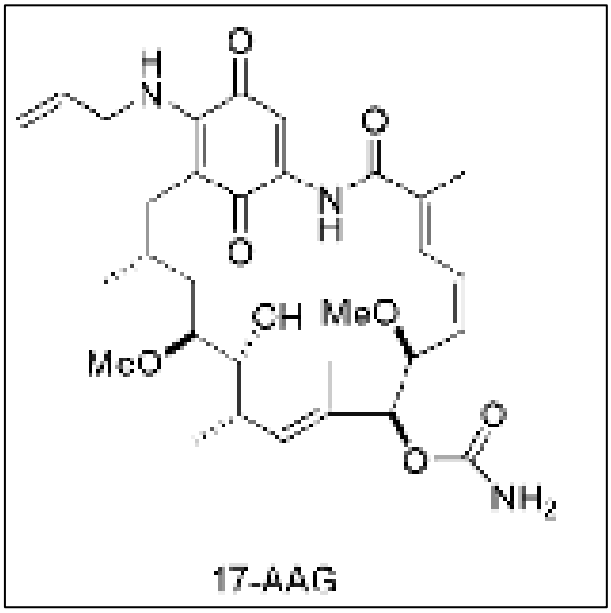

Figure 6.1. Chemical Structure of 17-allylamino-17-demethoxygeldanamycin[143].

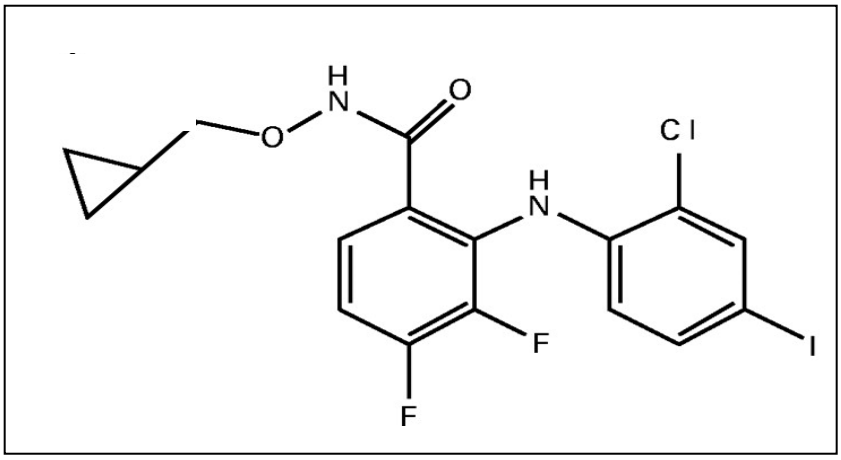

Figure 6.2. Chemical Structure of PD184352 (CI-1040) [142].

CHAPTER 7 MATERIALS AND METHODS: 17AAG AND PD184352

7.1 Materials

Dulbecco's Modified Eagle's Medium (DMEM), RPMI 1640 medium, Minimum Essential Medium Alpha (MEMα), sodium bicarbonate, trypsin-EDTA, and penicillin-streptomycin were purchased from GIBCOBRL (GIBCOBRL Life Technologies, Grand Island, NY. Minimum Essential Medium (MEM), Non-essential amino acids (NEAA) and sodium pyruvate were from Cellgro (Herndon, VA). Trypan blue solution, formaldehyde, acetic acid, 6-Diamidino-2-Phenylidole (DAPI), and dimethyl sulfoxide (DMSO) were all obtained from Sigma Chemical (St. Louis, MO).

17AAG was supplied by Calbiochem (San Diego, CA) as a powder, dissolved in sterile DMSO, and stored frozen under light-protected conditions at -80˚C. PD184352 was purchased from Upstate Biotechnology (Lake Placid, NY).

Anti-Beclin-1 (60 kDa, 1:1000, rabbit polyclonal), phospho-/total-p38α/β (38 kDa, 1:1000, rabbit polyclonal), phospho-/total-JNK1/2 (46, 54 kDa, 1:1000, rabbit polyclonal), anti-Bcl-xL (30 kDa, 1:1000, rabbit polyclonal), anti-FAS receptor (48 kDa, 1:1000, rabbit polyclonal), were obtained from Cell Signaling Technology (Worcester, MA). Anti-GAPDH (37 kDa, 1:1000, mouse monoclonal), phospho-PERK (125 kDa, 1:500, rabbit polyclonal), phospho-/total ERK1/2 (42, 44 kDa, 1:1000, mouse monoclonal), phospho-/total-Akt (60 kDa, 1:1000, rabbit polyclonal), phospho-MEK and all of the secondary antibodies (anti-rabbit-HRP, anti-mouse-HRP, and anti-goat-HRP) were obtained from Santa Cruz Biotechnology (Santa Cruz, CA). Commercially available siRNA duplexes to

knockdown RNA/protein levels were from Qiagen (Valencia, Ca): CD95 (SI02654463), Beclin-1 (SI00055573).

7.2 Cell Culture

HCT116 (p53 wild type) cells are a colon cancer cell line from ATCC. HCT116 stably transfected cell lines were previously generated. Cell lines were maintained in DMEM medium with L-glutamine and supplemented with 10% (v/v) fetal bovine serum and 2% (v/v) penicillin/streptomycin according to supplier instructions. SW480 cells are from ATCC. These cells were maintained in RPMI medium with L-glutamine and supplemented with 10% (v/v) fetal bovine serum and 2% (v/v) penicillin/streptomycin according to supplier instructions. SW620 cells (ATCC), patient matched to SW480 cells were maintained in DMEM with L-glutamine and supplemented with 10% (v/v) fetal bovine serum and 2% (v/v) penicillin/streptomycin according to supplier instructions. HEPG2 (hepatoma) and MiaPaCa2 (pancreatic), were purchased from ATCC as well. All cells were routinely subcultured and maintained in a 10 % CO_2/90 % air/37^{o}C humidified incubator. In addition, all cells were examined frequently for contamination with bacteria or fungus by visual inspection. Also, cells were routinely tested for mycoplasma contamination. Cells were not cultured in reduced serum media during any study in this manuscript.

7.3 Assessment of Cell Viability

A method used for evaluating cell viability involves the trypan blue inclusion/exclusion of isolated cells under light microscopy and scoring the percentage of cells exhibiting blue staining indicative of cell death. Cells were washed once with PBS

and trypsinized to detach cells from 12 well plates. Cells were centrifuged for 4 minutes at 1400 rpm at 25º C (room temperature). The media was then aspirated off and trypan blue was added to the tube depending on pellet size. The trypan blue inclusion/exclusion represents the integrity of the cellular membrane in that healthy, viable cells contain intact cell membranes and thus reject the trypan blue stain, while damaged cells exhibit a blue color due to a compromised cellular membrane that allows the trypan blue stain to be incorporated into the cell. Viable cells and trypan blue stained cells were counted in a hemacytometer viewed under a microscope. Calculations of cell death were made using the number of trypan blue positive cells divided by alive cell number multiplied by 100 to get the percentage of cell death.

7.4 Western Blot Analysis for Protein Expression

a.) Protein Isolation

Cells were plated at an appropriate density and treated with drug. At the indicated times after drug exposure, cells were washed in PBS and then scraped from the using whole-cell lysis buffer (0.5 M Tris-HCl, pH 6.8, 2% (w/v) SDS, 10% (v/v) glycerol, 1% (v/v) β-mercaptoethanol, 0.02% (w/v) bromophenol blue). A 1:20 dilution of protease inhibitor cocktail (Roche) and a 1:100 dilution of phosphatase inhibitor cocktail (Roche) was also added to the lysis buffer. The samples were then vortexed to dislodge the pellet, heated at 95-100 ºC for 5 minutes and placed immediately on ice.

b.) Electrophoresis

50-100 µg aliquots of cell protein (depending on the protein analyzed) were loaded onto a polyacrylamide gel (10-15%, depending on the size of the protein analyzed). Samples

were run in a SDS-PAGE running buffer (3.02g Tris-base, 14.40g glycine, 1.0g SDS, QS to 1 L deionized water) for approximately 6 hours with a constant current of 60 mA. Proteins were transferred onto a nitrocellulose membrane electrophoretically for 4 hours on ice at 450 mA in transfer buffer (5.8g Tris-base, 2.9 g glycine, milli-Q water to 800 ml, 1.8 ml 20% (w/v) SDS, 200 ml methanol.)

c.) Immunoblotting

The membrane was blocked in TBS-tween buffer containing 5% (w/v) non-fat dry milk for 30 minutes. After removal of the blocking solution, the primary antibody was added at a certain dilution to fresh block solution. After an overnight exposure with the primary antibody at 4ºC with orbital shaking, the antibody/wash solution was removed and the membrane was washed with blotto wash (5 x 5 minutes). The membrane was then incubated with the corresponding goat anti-mouse or rabbit secondary antibody for 2 hours at room temperature with orbital shaking. The secondary antibody was then removed and the membrane washed in blotto wash again, 5 x 5 minutes. All immunoblots were visualized by ECL. For presentation, immunoblots were digitally scanned at 600 dpi using Adobe PhotoShop CS2, and their color removed and Figures generated in Microsoft PowerPoint.

7.5 Colony Formation Assay for Cell Survival

Cells were plated as single cells (100– 125 cells/well) in a 6 well plate. Twenty four hours after plating, cells were treated with three different drug concentrations of each drug as well as the combination of both drugs for 48 h. After 48 h, the drug-containing

media was carefully removed, the cells were washed once, and fresh media lacking drugs were added. Colony formation assays were cultured for an additional 10 to 14 days. Upon colony formation, the medium was removed and the cells washed in 1X PBS. The cells were then fixed on the dish by adding 100% methanol for 10 minutes. The methanol was then removed and the cells were placed in a 0.1% (v/v) crystal violet (Sigma-Aldrich) staining solution for 1 h. Colonies containing more than 50 cells were then counted and normalized to the control cell survival sample. The survival data shown includes individual assays performed at multiple dilutions with a total of six plates per data point, repeated for a total of three experiments.

7.6 Recombinant Adenoviral Vectors: Infection in Vitro

We purchased recombinant adenoviruses to express (CrmA, c-FLIPs, Bcl-xL, XIAP) or to express dominant negative (p38, caspase 9, or activated MEK1) as well as a negative control using CMV (Vector Biolabs, Philadelphia, PA). *In vitro* adenoviral infections were performed 24 hours after plating cells. Monolayer cultures were washed in PBS prior to infection and specific virus was added to the monolayer cultures in serum-free growth medium at an m.o.i. (multiplicity of infection) of 25 (m.o.i. = # of virus per cell). The dishes were then placed on a rocker for 4 hours in a humidified atmosphere of 5% (v/v) CO_2 at 37ºC. The serum free growth medium was removed after 4 hours and the appropriate medium was added back to the cells and allowed to incubate overnight in the same humidified atmosphere. The expression of the recombinant viral transgene was allowed to occur for 24 h to ensure adequate expression of transduced gene products before drug exposures.

7.7 Transfection using Small Interfering RNA Molecules (siRNA) or plasmids

RNA interference or gene silencing for down-regulating the expression of specific siRNA was performed using validated target sequences designed by Ambion (Austin, TX). Plasmids were used at a concentration of 1 μg/μl or appropriate vector control plasmid DNA. For transfection, 10 nM concentration of the annealed siRNA or the negative control (a "scrambled" sequence with no significant homology to any known gene sequences from mouse, rat, or human cell lines) were used. The siRNA molecules were transfected into cells according to the manufacturer's instructions.

Briefly, cells were plated and allowed to sit overnight until about 80% confluent. For each well 2 μl of siRNA was diluted in 100 μl pen-strep-and-FBS-free medium (100 μl for chamber slides), in a 96 well plate. For each well, 2 μl of lipofectamine 2000 reagent (Invitrogen, Carlsbad, CA) was diluted into 100 μl pen-strep-and-FBS-free medium in a separate tube. The two solutions were incubated separately for approximately 5 minutes, then combined and incubated at room temperature for 30 minutes. After incubation, the total mix (400 μl) was added to each well. Cells were incubated for 4 hours at 37ºC with gentle rocking. After 4 hours, the media was then replaced with 1 ml of its regular media with antibiotics and FBS.

7.8 Immunohistochemistry: CD95 surface localization

Cells were plated on chamber slides, collected from the culture the next day, and washed once with DPBS (Dulbecco’s PBS without calcium and magnesium, Mediatech, Inc, Herndon, VA). The cells were then fixed in a solution of 4% paraformaldehyde in PBS

for twenty minutes. Cells were washed again in DPBS and nonspecific binding was blocked with a 1% (v/v) BSA and 2% (v/v) rat serum DPBS solution for 1 hour. Slides were then incubated with a 1:100 dilution of the primary anti-Fas in block solution overnight in a humidified chamber. The next day, slides were washed once in DPBS and incubated for 1 hour with secondary goat anti-mouse Alexa 488/647 at a dilution of 1:500 in block solution. Slides were washed after an hour, and coverglasses were mounted onto the glass slides using Vectashield with Dapi (Calbiochem, Madrid, Spain). Preparations were observed in a Zeiss LCM 510 meta-confocal microscope and analyzed using the Axio 2.0 software. No labeling was observed when using the secondary antibodies alone.

7.9 Statistical Analyses

The effects of various treatments were analyzed using one-way ANOVA and a two-tailed t test. Differences containing a p-value less than 0.05 were considered statistically significant. The experiments shown are the means of multiple individual points (+/-SEM).

CHAPTER 8 RESULTS: 17AAG and PD184352

8.1 17AAG and PD184352 decreases cell viability in HCT116 wt cells

HCT116 wt cells were plated at a density of $1x10^4$ cells per well in a 12 well plate. Cells were treated with vehicle (DMSO), 0.1 μM 17AAG, 0.5 μM PD184352, or the combination of both drugs. After 48 hours, the trypan blue exclusion assay was performed as described in materials and methods. Treatment of the HCT116 wt cells resulted in a greater than additive induction of cell killing than either individual agent alone (Figure 8.1).

8.2 17AAG and PD184352 synergize to kill HCT116 wt cells in colony formation assays

We next used colony formation assays to determine long term effects on cell survival. Colon cancer cells were plated as single cells (100-125 cells/well) in a 6 well plate. There was one treatment condition per plate. Twenty four hours after plating, cells were treated with either 17AAG (33, 66, 99 nM) or PD184352 (0.5, 1.0, 1.5 μM) and the combination of both drugs as indicated at a fixed concentration ratio to perform median dose effect analysis for the determination of synergy. Forty eight hours after drug exposure, the media was changed and the cells were cultured in drug free media for an additional 10-14 days. Cells were fixed, stained with crystal violet, and colonies >50 cells/colony counted as described in materials and methods under colony formation assay. Colony formation data was entered into the Calcusyn program and combination index (CI)

values determined. CI values less than 1 indicates synergy, equal to 1 indicates additive interactions, and CI values > 1 indicates antagonism (Figure 8.2 and 8.3).

8.3 Active Mutant Ral significantly sensitizes cells to 17AAG and PD184352

We next used RAS effector mutants to decipher the mechanism of action of this drug combination. HCT116 wt, HCT116 V12, as well as the HCT116 V12 transfectants were plated at a density of $1x10^4$ cells per well in a 12 well plate. Cells were treated vehicle (DMSO), 0.1 μM 17AAG, 0.5 μM PD184352, or the combination of both drugs. After 48 or 96 hours, the trypan blue exclusion assay was performed as described in materials and methods. The RAL active mutant (HCT116-HRAS-V12-RAL) significantly enhanced cell death at the 48 and 96 hour time points (Figure 8.4, 8.5).

8.4 DNp38 or JNK inhibitory peptide (JNK IP) does not significantly reduce cell death in the HCT116 wt cells

Previous studies in our laboratory have shown that in hepatoma cells, the combination of 17AAG and PD184352 induced rapid phosphorylation of p38 and no relative changes in JNK activation [122]. We tested whether inhibition of p38 or JNK affected the cell death response with combination treatment. HCT116 wt and HCT116-HRAS-V12-RAL cells were plated at a density of 2.5×10^4 in 12 well plates. Cells were allowed to attach overnight and the next day cells were infected with adenovirus dominant negative p38 (dnp38) or a CMV control adenovirus. Cells were infected as described in materials and methods. The next day, cells were treated with vehicle (DMSO), 0.1 μM 17AAG, 0.5 μM PD184352, or the combination of both drugs. After 48 hours, the trypan blue exclusion assay was performed as described in materials and methods. There was no

significant difference among the HCT116 wt cells or the HCT116-HRAS-V12-RAL cells in terms of p38 activity; p38 does not play a significant role in 17AAG and PD184352 lethality (Figure 8.6). In a separate experiment, cells were plated and treated with JNK IP for two hours followed by vehicle (DMSO) or 0.1 μM 17AAG + 0.5 μM PD184352. The JNK IP did not affect the lethality of the drug combination in the HCT116wt cells, although there was an inhibitory effect with the HCT116-HRAS-V12-RAL cells (Figure 8.7).

8.5 Activated MEK1 suppresses the toxicity of 17AAG and PD184352

We next determined whether expression of constitutively activated MEK1 protected cells from 17AAG and PD184352 exposure. HCT116 wt cells and HCT116-V12-RAL were plated at a density of $2.5x10^4$ cells per well in a 12 well plate. Cells were infected 24 hours after plating with empty vector control virus (CMV) or virus to express constitutively active MEKEE (ca-MEKEE) as described in materials and methods. The next day, cells were treated with vehicle (DMSO), 0.1 μM 17AAG, 0.5 μM PD184352, or the combination of both drugs. After 48 hours, the trypan blue exclusion assay was performed as described in materials and methods. Activated MEK1 protected the cells from the increase in cell death seen in the CMV control (Figure 8.8).

8.6 Protein expression of MAP Kinase members during 17AAG and PD184352 combination response

To further define the process of cell death, immunoblotting analysis in 17AAG and PD184352 treated HCT116 wt and HCT116-HRAS-V12-RAL cells were performed. Cells were plated at 1.0×10^6 in 10 cm dishes. Twenty four hours after plating, cells were

treated with vehicle (DMSO), 0.1 μM 17AAG, 0.5 μM PD184352, or the combination of both drugs. Forty eight hours later, cells were isolated and western blot analysis was performed as described in materials and methods. Many studies have argued that the inhibition of the PI3K/Akt pathway is a key component in the toxicity of 17AGG rather than RAF/MEK/ERK pathway [144, 145], thus we analyzed the phosphorylation of Akt, p38, ERK, and JNK. Unfortunately, p-Akt and p-p38 were undetectable and p-JNK remained constant in cell lysates. The constant levels of JNK in the colon cancer cells correlated with previous studies with hepatoma cells in which the JNK1/2 pathway was not activated. The phosphorylation of p-ERK correlated with 17AAG and PD184352 toxicity (Figure 8.9).

8.7 17AAG and PD184352 induced CD95 activation in HCT116 wt cells

Based upon prior studies in which 17AAG and PD184352 induced CD95 activation in hepatoma cells, we determined whether treatement of the drug combination elevated CD95 plasma membrane levels (indicative of activation) in colon cancer cells. HCT116 wt cells 24h after plating in 4 well chamber slides were exposed to vehicle (DMSO) or the combination of 17AAG (0.1 μM) and PD184352 (0.5 μM). Cells were fixed 3-8h after exposure and the amount of plasma membrane associated CD95 determined by immunohistochemistry (± SEM, n = 2). HCT116 wt cells induced plasma membrane CD95 activation (Figure 8.10).

8.8 Overexpression of LASS6 enhanced 17AAG and PD184352 tumor cell killing in SW620 cells

We determined whether expression of LASS6 in SW620 cells facilitated drug-induced cell death. SW620 cells were stably transfected with either vector control plasmid of a plasmid to express LASS6. Twenty four hours after plating, cells were exposed to vehicle (DMSO), 0.1 μM 17AAG, 0.5 μM PD184352, or both drugs combined. Forty eight hours after exposure, cells were isolated and stained with trypan blue dye and cell viability determined by visible light microscopy (± SEM, n = 2). Overexpression of LASS6 in SW620 cells enhanced the toxicity of the drug combination (Figure 8.11). Collectively, this data argues that activation of enzymes within the de novo ceramide pathway represents a key step in the toxic actions of 17AAG and PD184253 in pancreatic cancer cells.

8.9 Overexpression of LASS6 enhanced 17AAG and PD184352-induced CD95 activation

We determined whether expression of LASS6 in SW620 cells facilitated drug-induced CD95 activation. SW620 cells were stably transfected with either vector control plasmid of a plasmid to express LASS6. SW620 cells 24h after plating in 4 well chamber slides were exposed to vehicle (DMSO), 0.1 μM 17AAG, 0.5 μM PD184352, or both drugs combined. Cells were fixed 3-8h after exposure and the amount of plasma membrane associated CD95 determined by immunohistochemistry (± SEM, n = 2). Overexpression of LASS6 increased activation of CD95 (Figure 8.12).

8.10 c-FLIP and CrmA significantly reduced lethality in MiaPaca2 cells

We decided to direct our attention to the mechanisms of drug toxicity in pancreatic cells. Previous studies in our laboratory have shown that overexpression of c-FLIP-s abolished lethality in 17AAG and PD184352 combination treatment in hepatoma cell lines [122]. Thus we decided to review this in MiaPaca2 cells. Cells were plated at a density of 2.5 x 10^4 in 12 well plates. Cells were allowed to attach overnight and the next day cells were infected with adenovirus FLIP, cytokine response modifier A (CrmA), as well a CMV control adenovirus. Cells were infected as described in materials and method. The next day, cells were treated with vehicle (DMSO), 0.1 μM 17AAG, 0.5 μM PD184352, or the combination of both drugs. After 48 hours, trypan blue exclusion assays were performed as described in materials and methods. Overexpression of FLIP-s inhibited cell killing in MiaPaca2 cells (Figure 8.13). CrmA also suppressed cell death. Total cell lysates were analyzed by immunoblotting with anti-FLIP to assess the levels of expression of infected Flip in both cell lines (Figure 8.13, inset).

8.11 Overexpression of Bcl-xL or DNCaspase 9 reduced the toxic effects of combination treatment in MiaPaca2 cells

To further investigate the apoptotic pathway and its role in 17AAG and PD184352 combination treatment, we tested the effects of overexpression of Bcl-xL or DNcaspase 9 on 17AAG and PD184352 lethality. MiaPaca2 cells were plated at a density of 2.5 x 10^4 in 12 well plates. Cells were allowed to attach overnight and the next day cells were infected with adenovirus dominant negative caspase 9 (DNcaspase 9), Bcl-xL, as well a CMV control adenovirus. Cells were infected as described in materials and methods. The next

day, cells were treated with vehicle (DMSO), 0.1 μM 17AAG, 0.5 μM PD184352, or the combination of both drugs. After 48 hours, the trypan blue exclusion assay was performed as described in materials and methods. Overexpression of Bcl-xL or expression of dominant negative caspase 9 suppressed 17AAG+PD184352 toxicity in MiaPaca2 cells, arguing that the drugs were using the intrinsic pathway to kill this tumor cell type (Figure 8.14). Total cell lysates were analyzed by immunoblotting with anti-Bcl-xL to assess the levels of expression of infected Bcl-xL in both cell lines (Figure 8.14, inset).

8.12 MiaPaca2 cells demonstrate a Fas-dependent mechanism

Prior studies have demonstrated in hepatoma cells that 17AAG and PD184352 toxicity was dependent on activation of CD95 [122]. We decided to test this in MiaPaca2 cells. Cells were plated at a density of 2.5 x 10^4 in 12 well plates. Cells were allowed to attach overnight and the next day cells were transfected with siScramble, or knockdown of CD95 (siCD95), a death receptor and part of the extrinsic apoptotic pathway. Cells were transfected as described in materials and method. The next day, cells were treated with vehicle (DMSO), 0.1 μM 17AAG, 0.5 μM PD184352, or the combination of both drugs. After 48 hours, the trypan blue exclusion assay was performed as described in materials and methods. In MiaPaca2 cells, knockdown of CD95 decreased cell death compared to Si-scramble group (Figure 8.15).

8.13 MiaPaca2 cells enhanced 17AAG and PD184352-induced CD95 activation

MiaPaca2 cells 24h after plating in 4 well chamber slides were exposed to vehicle (DMSO), 0.1 μM 17AAG, 0.5 μM PD184352, or both drugs combined. Cells were fixed 3-8h after exposure and the amount of plasma membrane associated CD95 determined by

immunohistochemistry (± SEM, n = 2), (Figure 8.16). MiaPaca2 cells increased plasma membrane levels in a time-dependent fashion.

8.14 Knockdown of Beclin 1 expression enhanced 17AAG and PD184352 toxicity in HepG2 cells

We decided to investigate the effect of knockdown beclin 1 on cell death in HepG2 cells. Cells were plated at a density of 2.5 x 10^4 in 12 well plates. Cells were allowed to attach overnight and the next day cells were transfected with siScramble or knockdown of beclin1 (si-beclin1). Cells were transfected as described in materials and methods. The next day, cells were treated with vehicle (DMSO), 0.1 μM 17AAG, 0.5 μM PD184352, or the combination of both drugs. After 48 hours, trypan blue exclusion assays were performed as described in materials and methods. Knockdown of Beclin 1 increased cell death, with knockdown of beclin 1 increasing the toxicity of PD184253 as well (Figure 8.17).

8.15 DnPERK protected HepG2 cells from 17AAG and PD18435 toxicity

We next determined whether knockdown of PERK function could alter 17AAG and PD184352 lethality in hepatoma cells. Cells were plated at a density of 2.5 x 10^4 in 12 well plates. The next day, cells were transiently transfected with pcDNA or DnPERK as described in materials and methods. The next day, cells were treated with vehicle (DMSO), 0.1 μM 17AAG, 0.5 μM PD184352, or the combination of both drugs. After 48 hours, the trypan blue exclusion assay was performed as described in materials and methods. DnPERK suppressed cell death as compared to the pcDNA control (Figure 8.18).

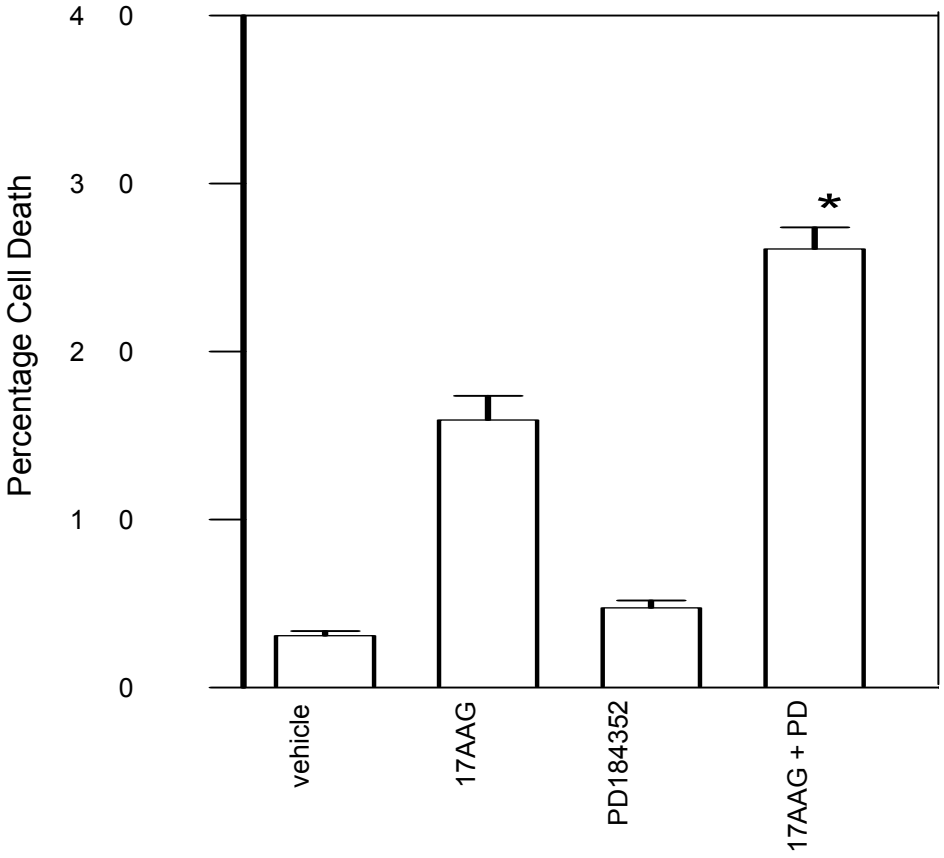

Figure 8.1. 17AAG and PD184352 reduce cell viability in HCT116 cells. Colon cancer cells were treated with 0.1μM 17AAG and 500 nM PD184352 continuously for 48 hours. After drug exposure, the trypan blue exclusion assay was performed. Values represent the means for three separate experiments ± SD. * $p \leq 0.05$, greater cell killing than compared with any other treatment condition.

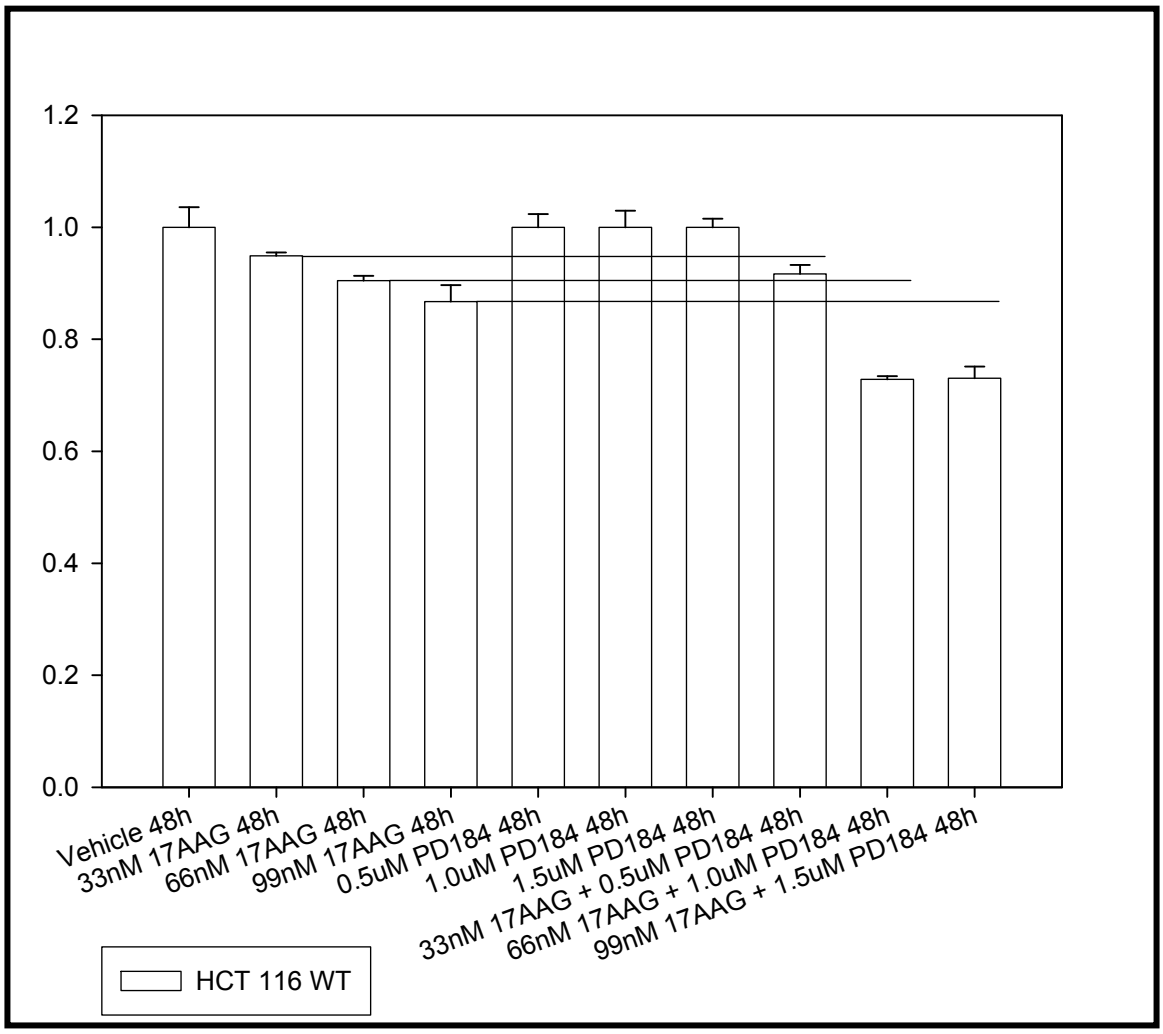

CI For experimental values HCT 116 wt

17AAG (nM)	PD184352 (uM)	Fa	CI
33.0	0.5	0.22	0.58
66.0	1.0	0.40	0.38
99.0	1.5	0.48	0.37

Figure 8.2. 17AAG and PD184352 synergize to kill HCT116 wt cells in colony formation assays. HCT116 wt cells were treated 12h after plating as single cells (250-1500 cells/well) in sextuplicate with vehicle (DMSO), 17AAG (33, 66, 99 nM) or PD184352 (0.5, 1.0, 1.5 μM), or with both drugs combined, as indicated at a fixed concentration ratio to perform median dose effect analyses for the determination of synergy. Combination index (CI) values were determined. CI values less than 1 indicates synergy, equal to 1 indicates additive interactions, and CI values > 1 indicates antagonism.

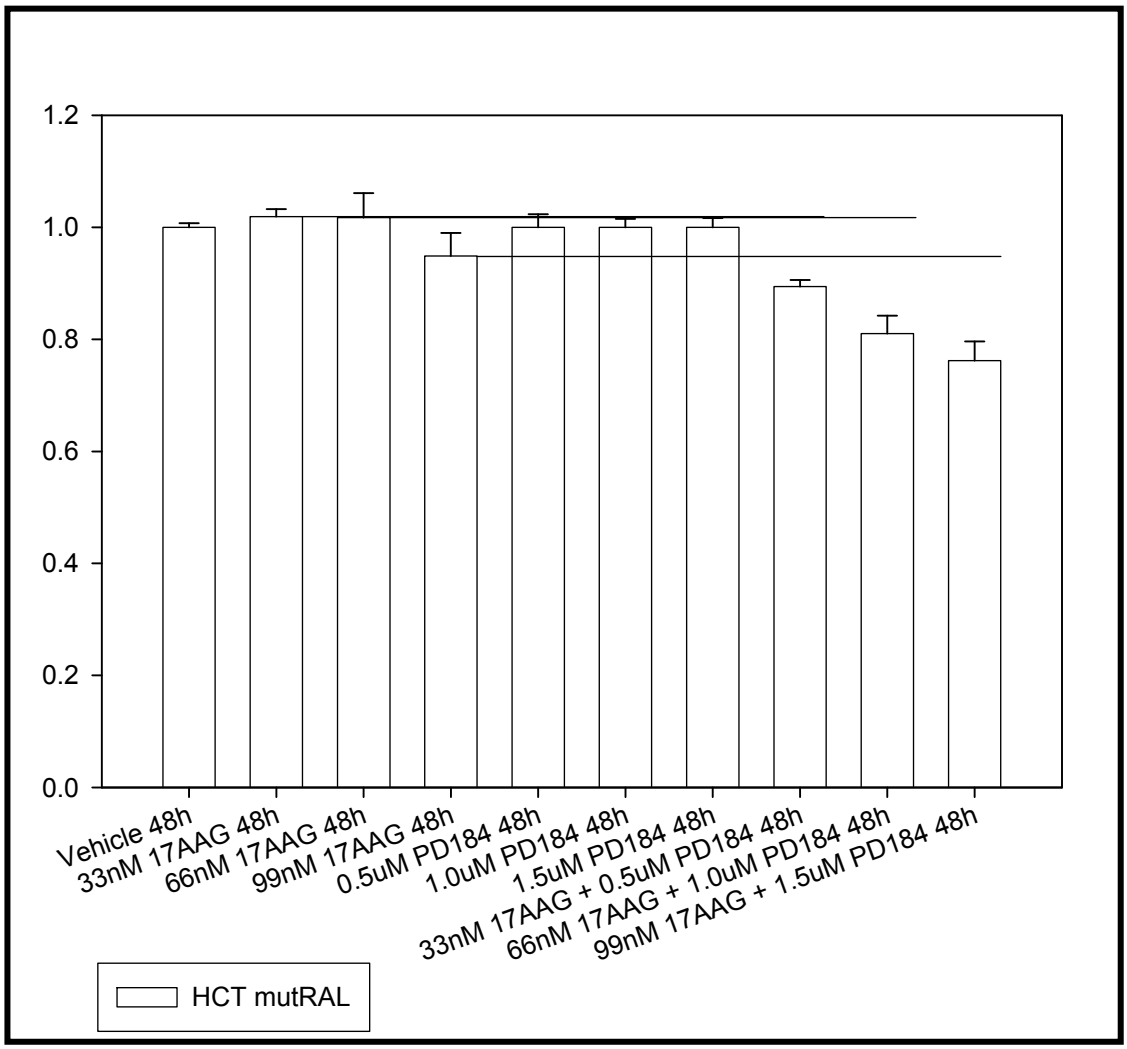

CI For experimental values HCT116-HRASV12-RAL

17AAG (nM)	PD184352 (uM)	Fa	CI
33.0	0.5	0.09	0.37
66.0	1.0	0.21	0.27
99.0	1.5	0.30	0.26

Figure 8.3. 17AAG and PD184352 synergize to kill HCT116-HRASV12-RAL cells in colony formation assays. HCT116-HRASV12-RAL cells were treated 12h after plating as single cells (250-1500 cells/well) in sextuplicate with vehicle (DMSO), 17AAG (33, 66, 99 nM) or PD184352 (0.5, 1.0, 1.5 μM), or with both drugs combined, as indicated at a fixed concentration ratio to perform median dose effect analyses for the determination of synergy. Combination index (CI) values were determined. CI values less than 1 indicates synergy, equal to 1 indicates additive interactions, and CI values > 1 indicates antagonism.

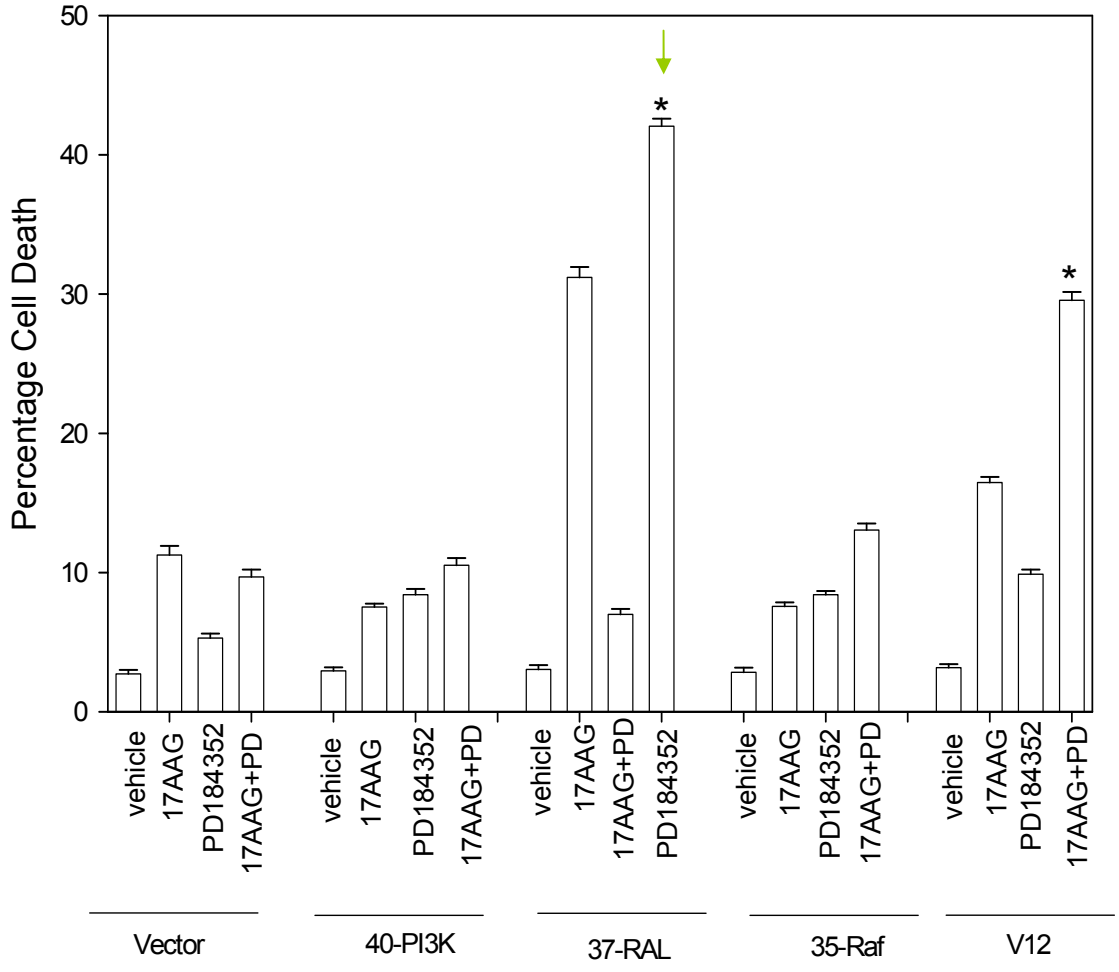

Figure 8.4. Active mutant HCT116-HRAS-V12-RAL significantly sensitizes cells to 17AAG and PD184352. HCT116 cells (parental expressing K-RAS D13; deleted for K-RAS D12; deleted for K-RAS D13 expressing H-RAS V12 and effector mutants of H-RAS V12), 24h after plating in triplicate, were treated with vehicle (DMSO), 17AAG (0.1 μM), PD184352 (500 nM) or the combination of both drugs. Forty eight hours after exposure, the trypan blue exclusion assay was performed. Values represent the means for three separate experiments ± SD. * $p \leq 0.05$, greater cell killing than compared with any other treatment condition. Arrows indicate the RAL mutant gave significantly more cell death than the other transfectants.

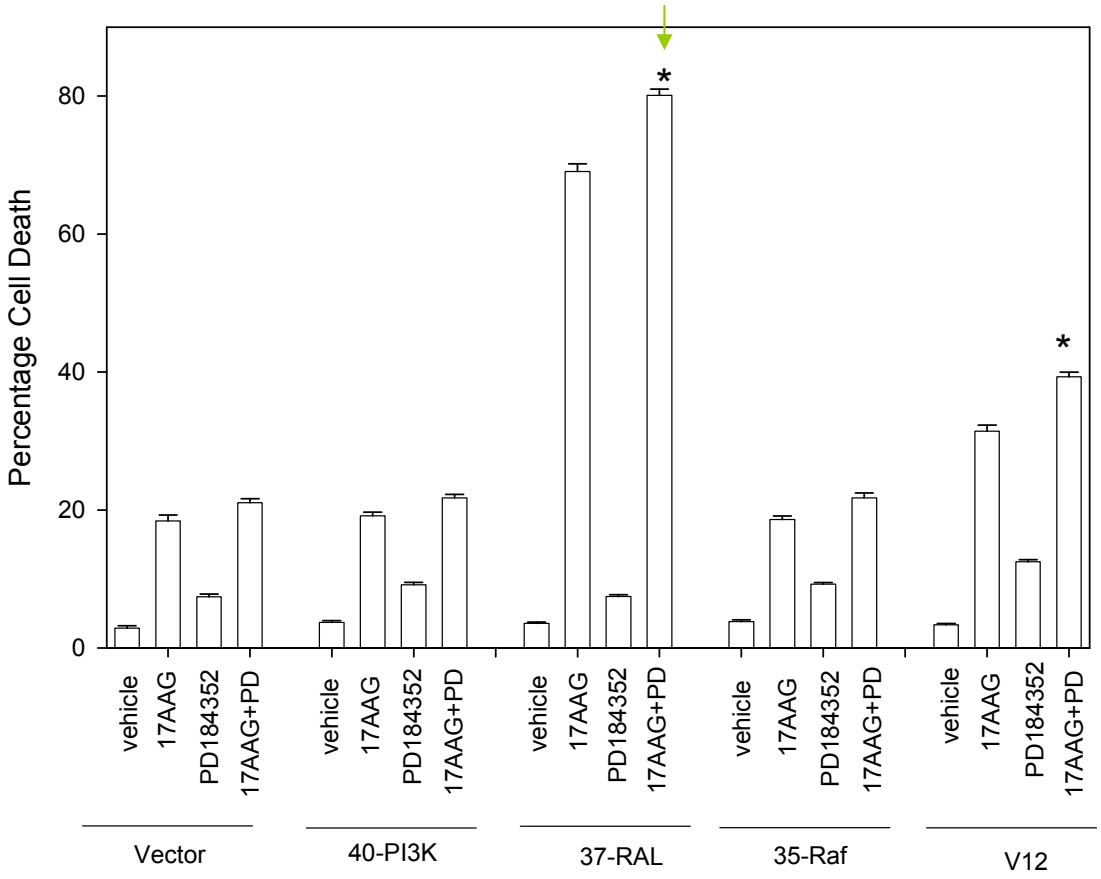

Figure 8.5. Active mutant HCT116-HRAS-V12-RAL significantly increases toxic effects of 17AAG and PD184352. cells (parental expressing K-RAS D13; deleted for K-RAS D12; deleted for K-RAS D13 expressing H-RAS V12 and effector mutants of H-RAS V12), 24h after plating in triplicate, were treated with vehicle (DMSO), 17AAG (0.1 μM), PD184352 (500 nM) or the combination of both drugs. Ninety six hours after exposure, the trypan blue exclusion assay was performed. Values represent the means for three separate experiments ± SD. * $p \leq 0.05$, greater cell killing than compared with any other treatment condition. Arrows indicate the RAL mutant gave significantly more cell death than the other transfectants.

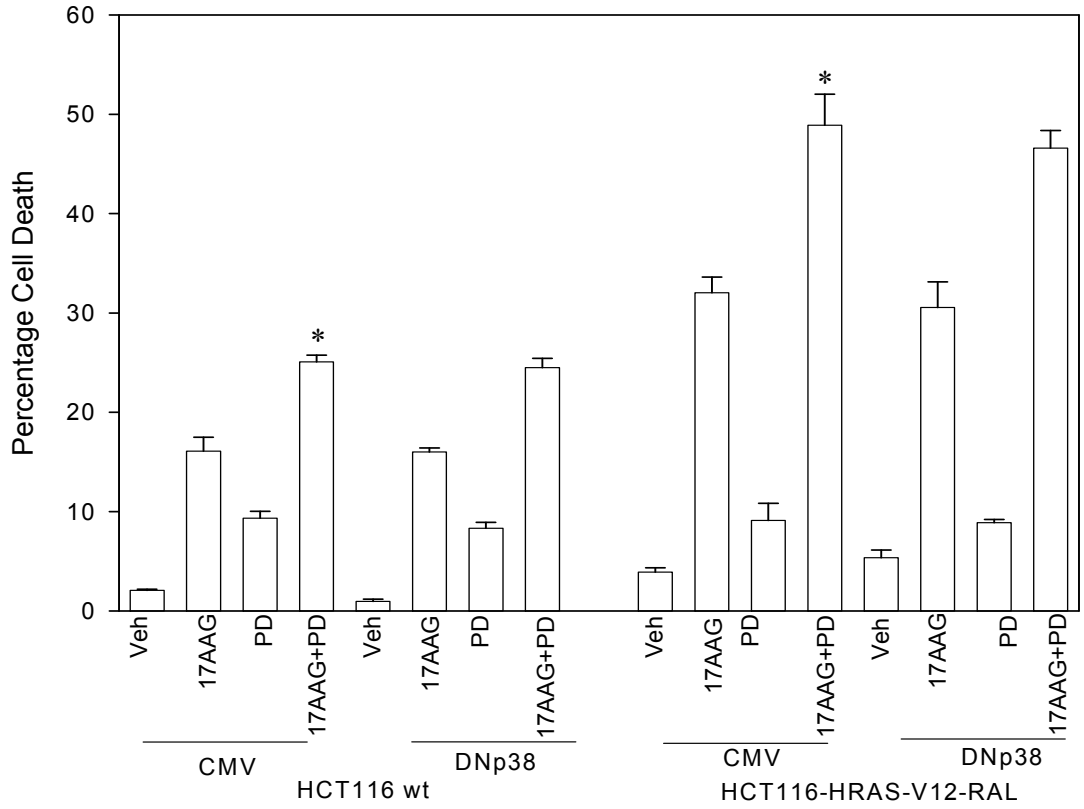

Figure 8.6 DNp38 did not significantly suppress 17AAG and PD184352 lethality in HCT116 wt or HCT116-HRAS-V12-RAL cells. Cells 24h after plating were, infected with recombinant adenoviruses (empty vector CMV; dominant negative p38 MAPK) at a multiplicity of infection of 25. Twenty four h after infection, cells were treated with vehicle (DMSO), 17AAG (0.1 μM), PD184352 (500 nM) or the combination of both drugs. Forty eight hours after exposure, the trypan blue exclusion assay was performed. Values represent the means for two separate experiments ± SD. * $p \leq 0.05$, greater cell killing than compared with any other treatment condition.

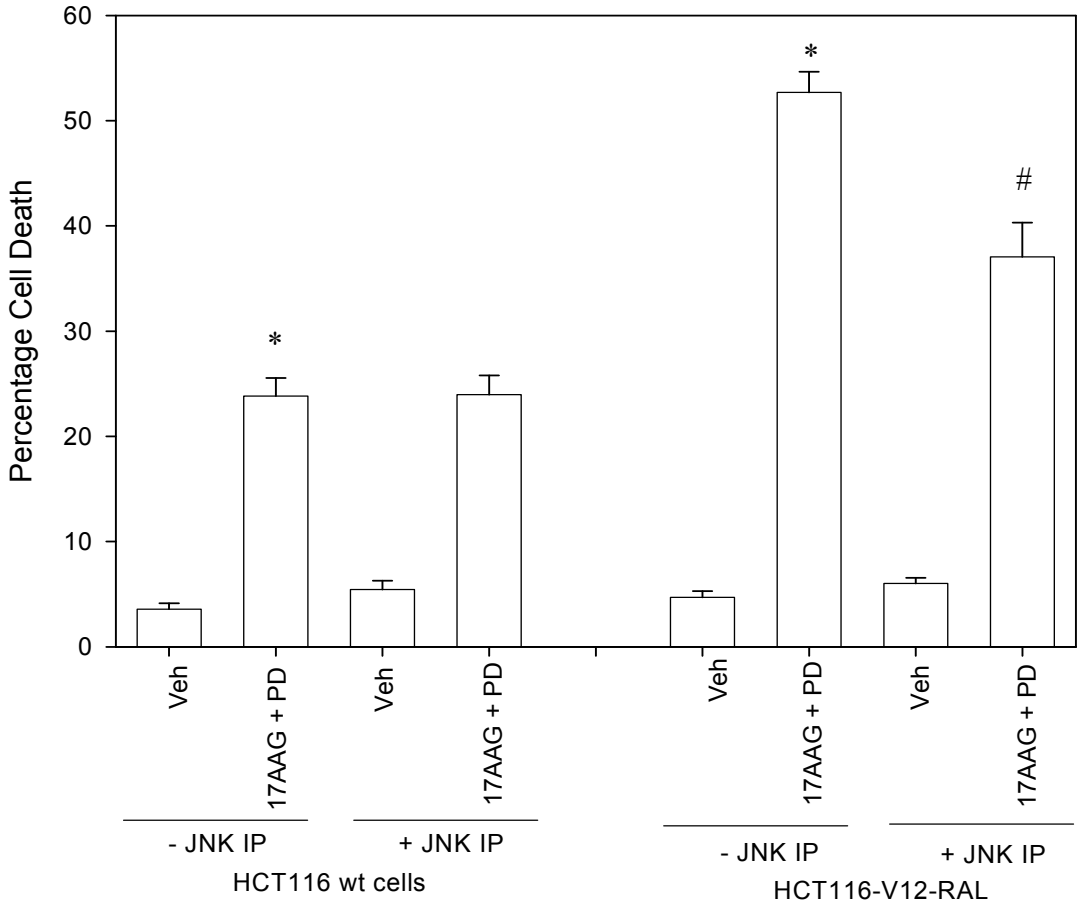

Figure 8.7 JNK IP did not significantly suppress 17AAG and PD184352 lethality in HCT116 wt or HCT116-HRAS-V12-RAL cells. Cells 24h after plating were treated two hours prior to drug exposure to vehicle (DMSO) or the JNK inhibitory peptide (JNK-IP, 10 μM). Cells were then treated with vehicle (DMSO), or 17AAG (0.1 μM) and PD184352 (500 nM). Forty eight hours after exposure, the trypan blue assay was performed. Values represent the means for two separate experiments ± SD. # $p \leq 0.05$, less cell killing than compared with any other treatment condition.

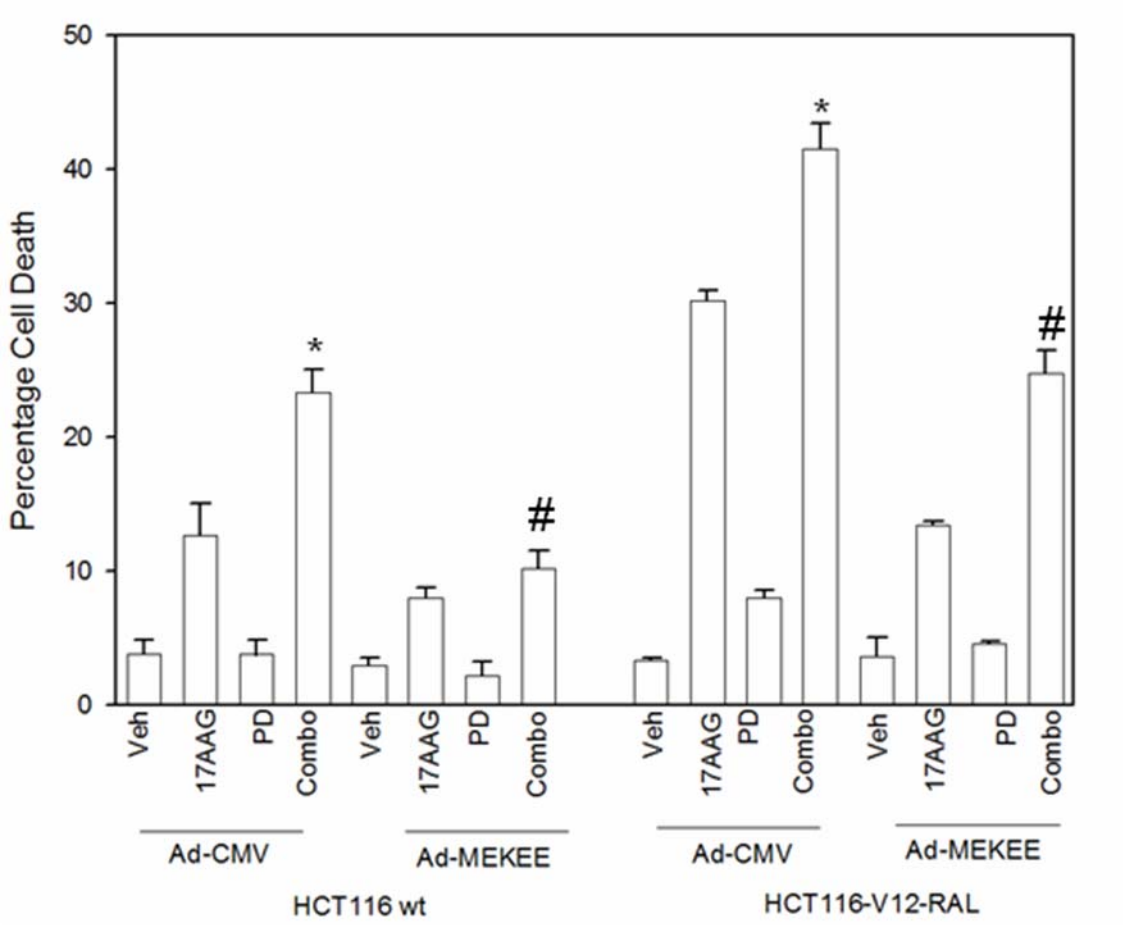

Figure 8.8 Activated MEK1 suppresses the toxicity of 17AAG and PD184352. HCT116 cells 24h after plating were infected with recombinant adenoviruses (empty vector CMV; constitutively active MEK1 EE) at a multiplicity of infection of 25. Twenty four h after infection, cells were treated with vehicle (DMSO), 17AAG (0.1 μM), PD184352 (500 nM) or the combination of both drugs. Forty eight hours after exposure, the trypan blue exclusion assay was performed. Values represent the means for two separate experiments ± SD. * $p \leq 0.05$, greater cell killing than compared with any other treatment condition. # $p \leq 0.05$, less cell killing than compared with any other treatment condition.

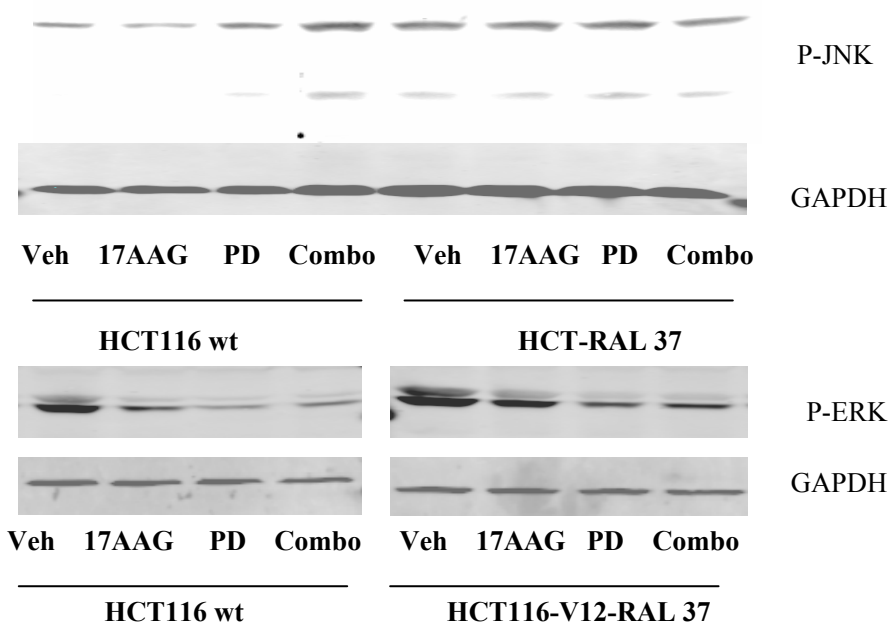

Figure 8.9. Protein expression of MAP Kinase members during 17AAG and PD184352 combination response. HCT116 and HCT-RAL cells 24h after plating were treated with vehicle (DMSO), 17AAG (0.1 μM), PD184352 (500 nM) or both drugs combined. Cells were isolated 24h after drug treatment and lysates subjected to SDS PAGE and immunoblotting against the proteins indicated in the Figure panel. Blot shown is a representation of two independent experiments.

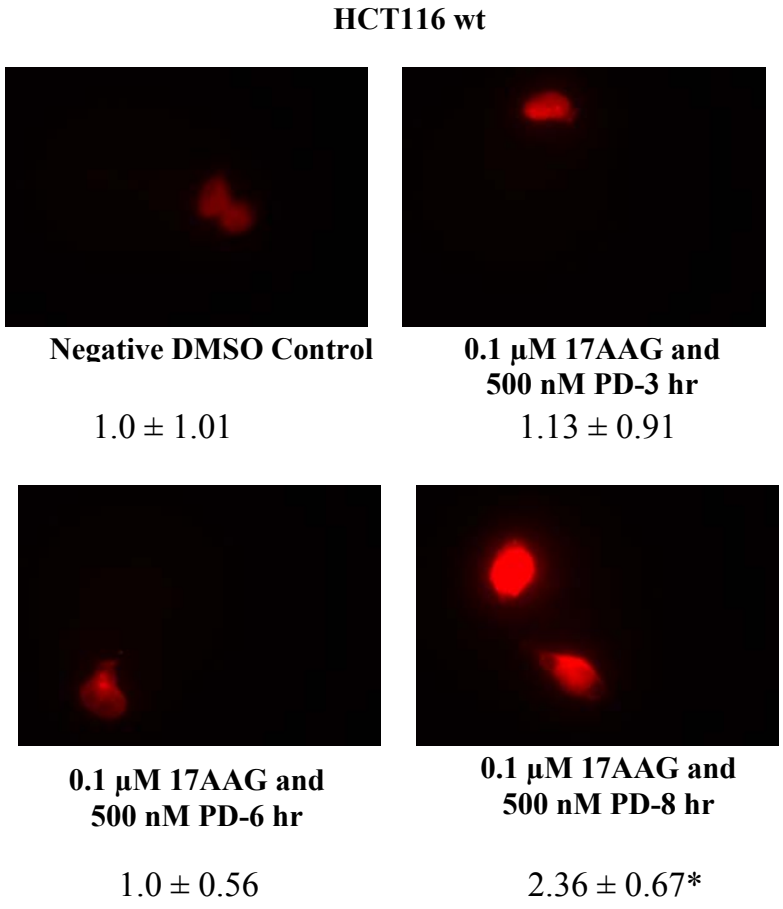

Figure 8.10. Fas/CD95 surface expression in HCT116 wt cells. HCT116 cells were plated in 4 well glass chamber slides and 24h after plating cells were treated with vehicle (DMSO) or 0.1 µM 17AAG and 500 nM PD184352. Cells were fixed and not permeabilized 0-8h after drug exposure. Fixed cells were immuno-stained for plasma membrane associated CD95 and visualized using an FITC conjugated secondary antibody. Images are representatives from two separate studies. * $p \leq 0.05$, value greater amount of cell surface CD95 compared to vehicle-treated conditions.

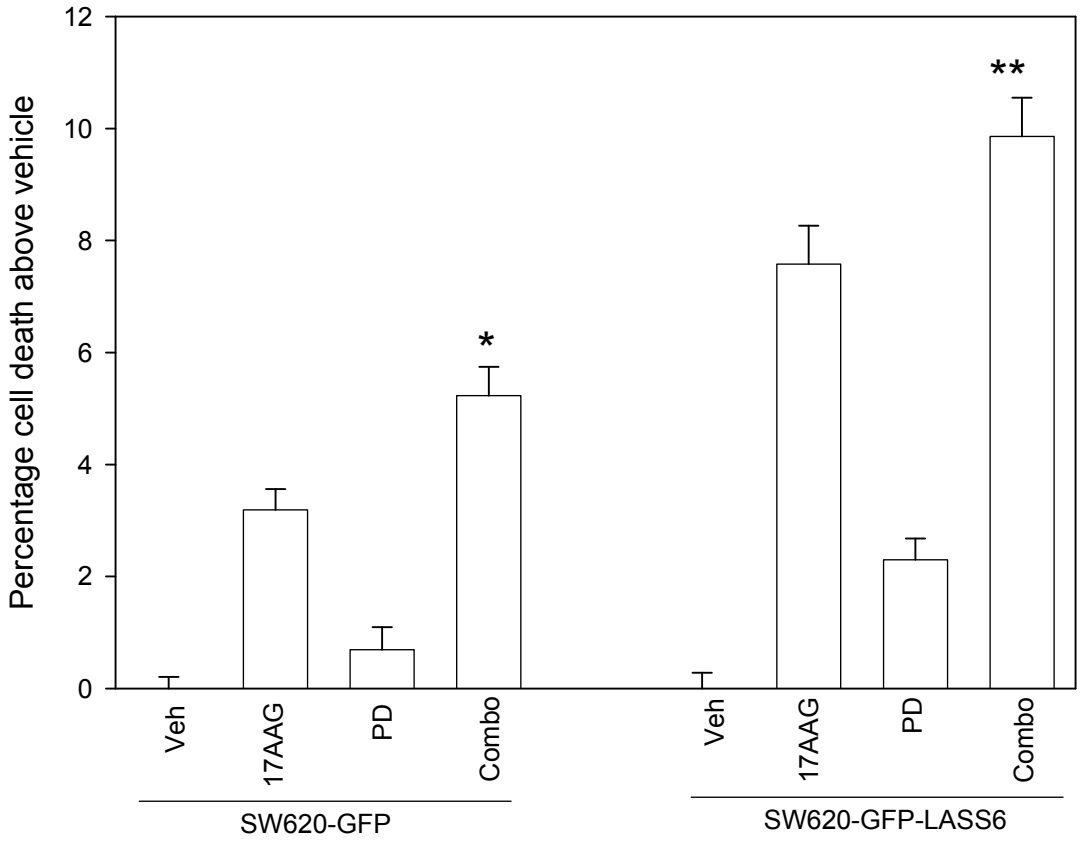

Figure 8.11. Overexpression of LASS6 enhanced 17AAG and PD184352 tumor cell killing in SW620 cells. SW620 cells stably transfected with either vector control plasmid of a plasmid to express LASS6, 24h after plating, were exposed to vehicle (DMSO), 17AAG (0.1 μM), PD184352 (500 nM) or the combination of both drugs. Forty eight hours after exposure, cells were isolated and stained with trypan blue dye. * $p \leq 0.05$, greater cell killing than compared with any other treatment condition. **, greater cell killing than compared with SW620-GFP parallel condition.

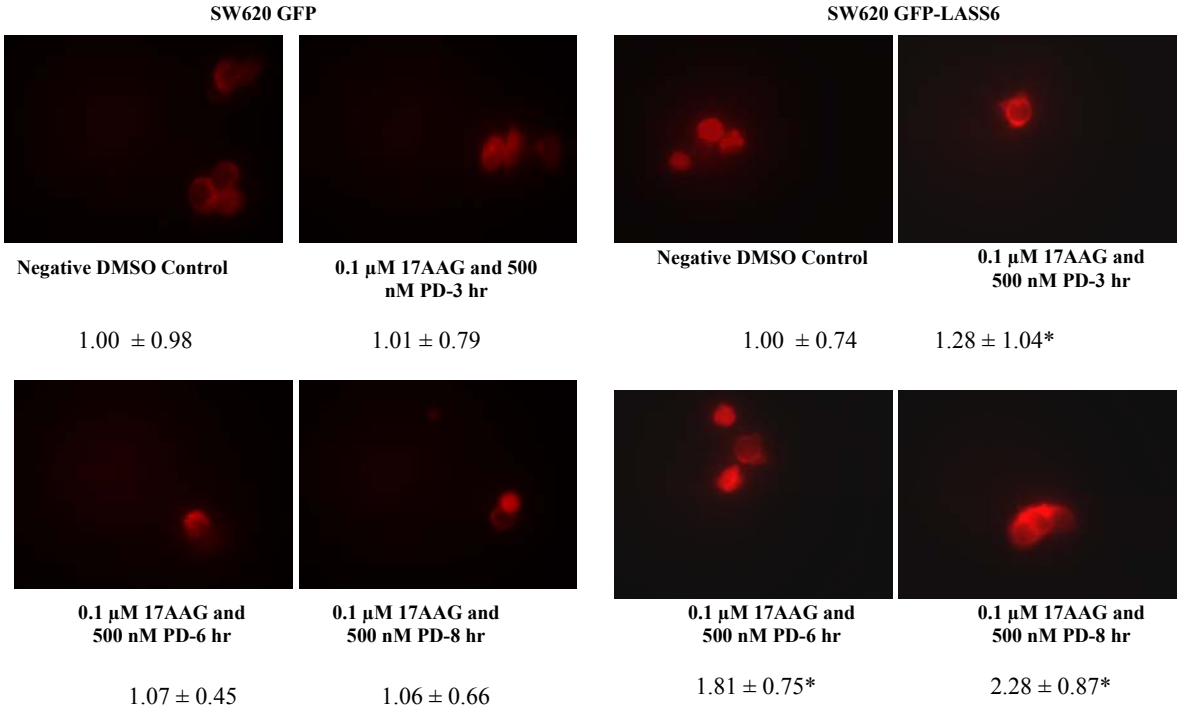

Figure 8.12. Overexpression of LASS6 enhanced 17AAG and PD184352-induced CD95 activation. SW620 cells stably transfected with either vector control plasmid of a plasmid to express LASS6, 24h after plating in 4 well chamber slide , cells were exposed to vehicle (DMSO) or 0.1 µM 17AAG and 500 nM PD184352. Cells were fixed and not permeabilized 0-8h after drug exposure. Fixed cells were immuno-stained for plasma membrane associated CD95 and visualized using an FITC conjugated secondary antibody. Images are representatives from two separate studies. * $p \leq 0.05$, value greater amount of cell surface CD95 compared to vehicle-treated conditions.

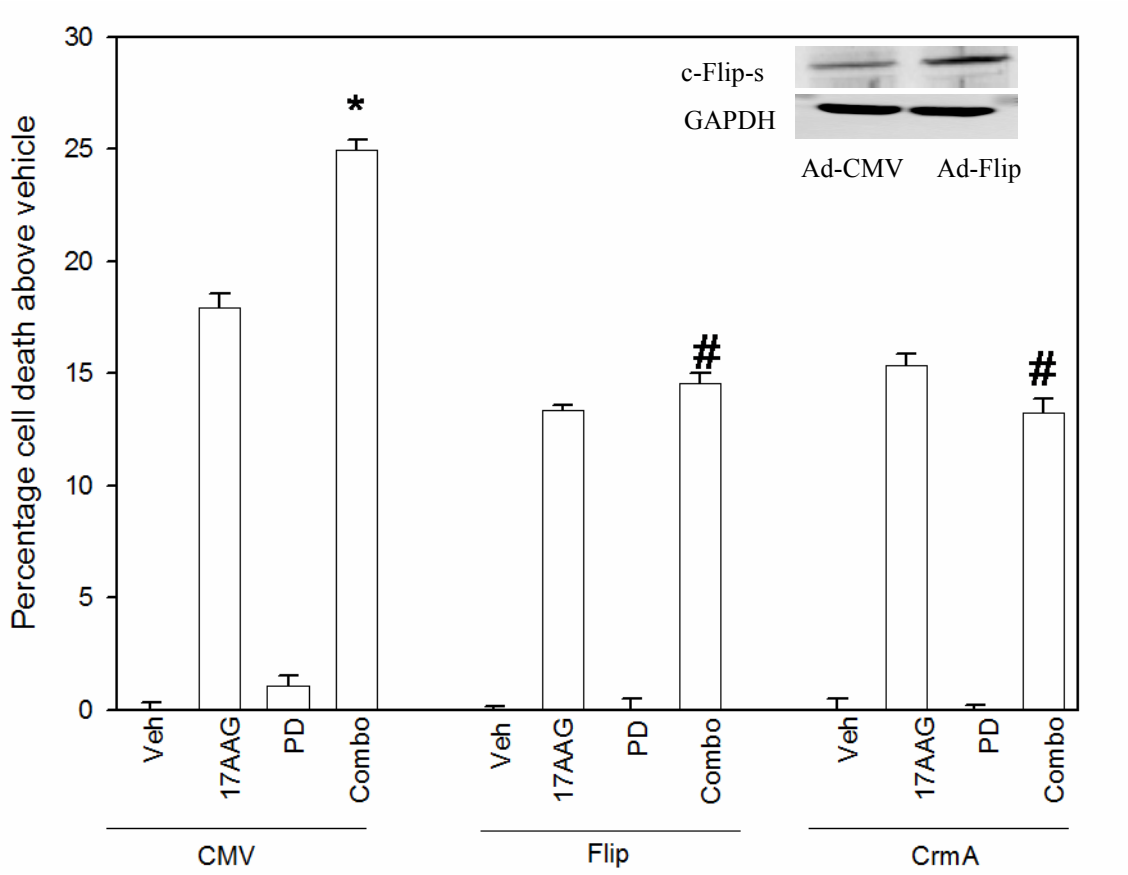

Figure 8.13. Overexpression of c-FLIP-s or ectopic expression of CrmA reduced 17AAG and PD184352 lethality in MiaPaca2 cells. MiaPaca2 cells 24h after plating were infected with recombinant adenoviruses (empty vector CMV; FLIP; CrmA) at a multiplicity of infection of 25. Twenty four h after infection, cells were treated with vehicle (DMSO), 0.1 μM 17AAG, 0.5 μM PD184352, or both drugs together. Forty eight hours after exposure, the trypan blue exclusion assay was performed. Values represent the means for three separate experiments ± SD. * $p \leq 0.05$, greater cell killing than compared with any other treatment condition. # $p \leq 0.05$, less cell killing than compared with any parallel condition in vehicle-treated cells.

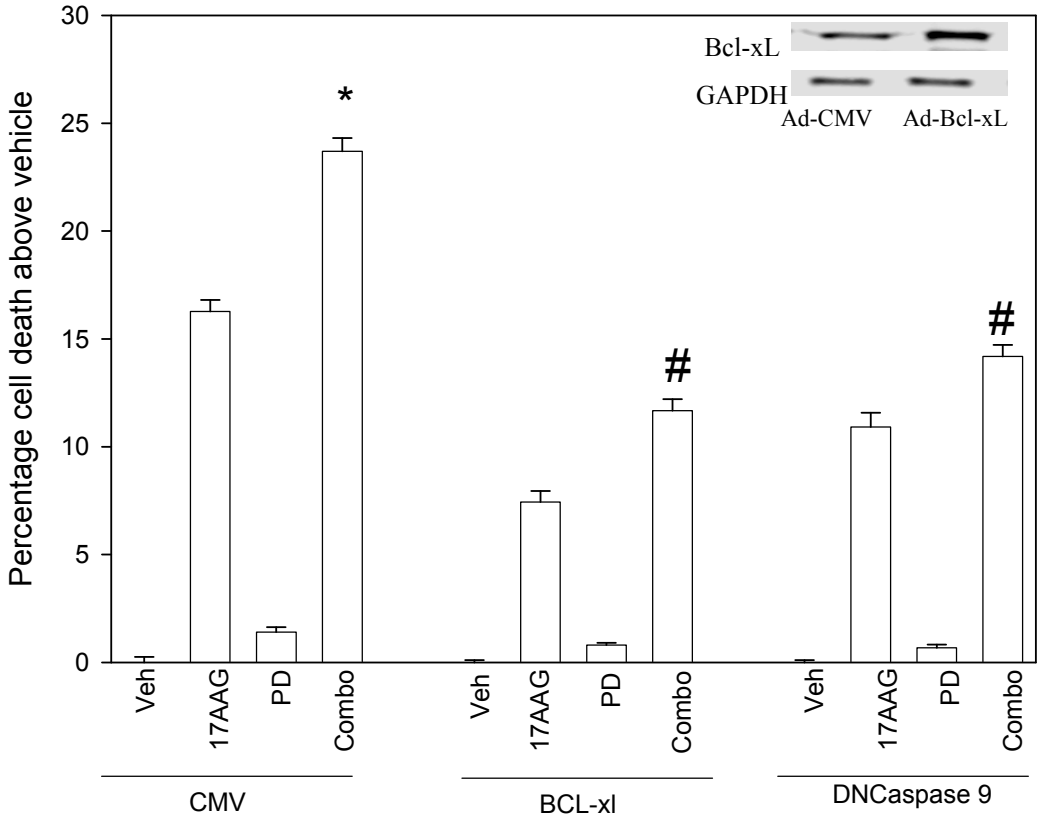

Figure 8.14. Overexpression of Bcl-xL or DNCaspase 9 reduced the toxic effects of combination treatment in MiaPaca2 cells. MiaPaca2 cells were infected with recombinant adenoviruses (empty vector CMV; dominant negative caspase 9; Bcl-xL) at a multiplicity of infection of 25. Twenty four h after infection, cells were treated with vehicle (DMSO), 0.1 μM 17AAG, 0.5 μM PD184352 or both drugs together. Forty eight hours after exposure, cells were isolated and the trypan blue exclusion assay was performed. Values represent the means for two separate experiments ± SD. * $p \leq 0.05$, greater cell killing than compared with any other treatment condition. # $p \leq 0.05$, less cell killing than compared with parallel condition in vehicle-treated cells.

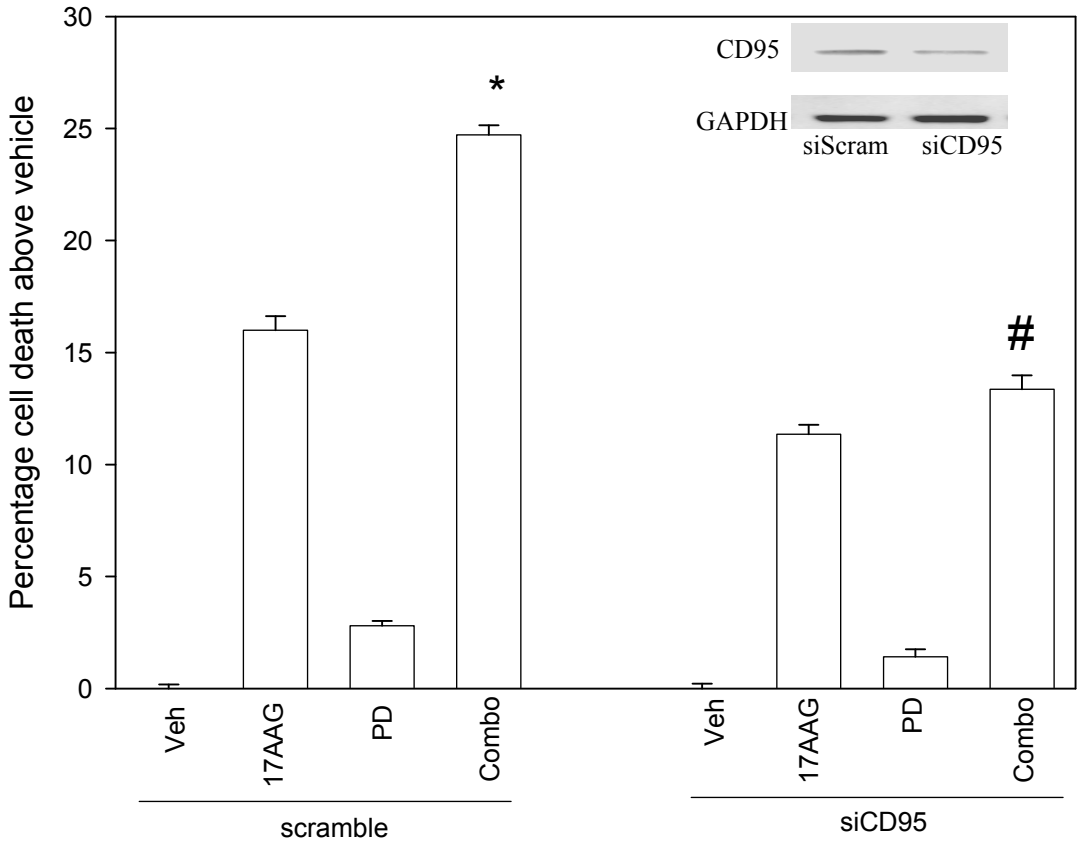

Figure 8.15. MiaPaca2 cells demonstrate a Fas-dependent mechanism. MiaPaca2 cells were transfected with siRNA molecules to knock down CD95 or scrambled siSCR control (20 nM). Twenty four h after infection or transfection, cells were treated with vehicle (DMSO), 0.1 μM 17AAG, 0.5 μM PD184352, or both drugs together. Forty eight hours after exposure, cells were isolated and the trypan blue exclusion assay was performed. Values represent the means for three separate experiments ± SD. * $p \leq 0.05$, greater cell killing than compared with any other treatment condition. # $p \leq 0.05$, less cell killing than compared with any parallel condition in vehicle-treated cells.

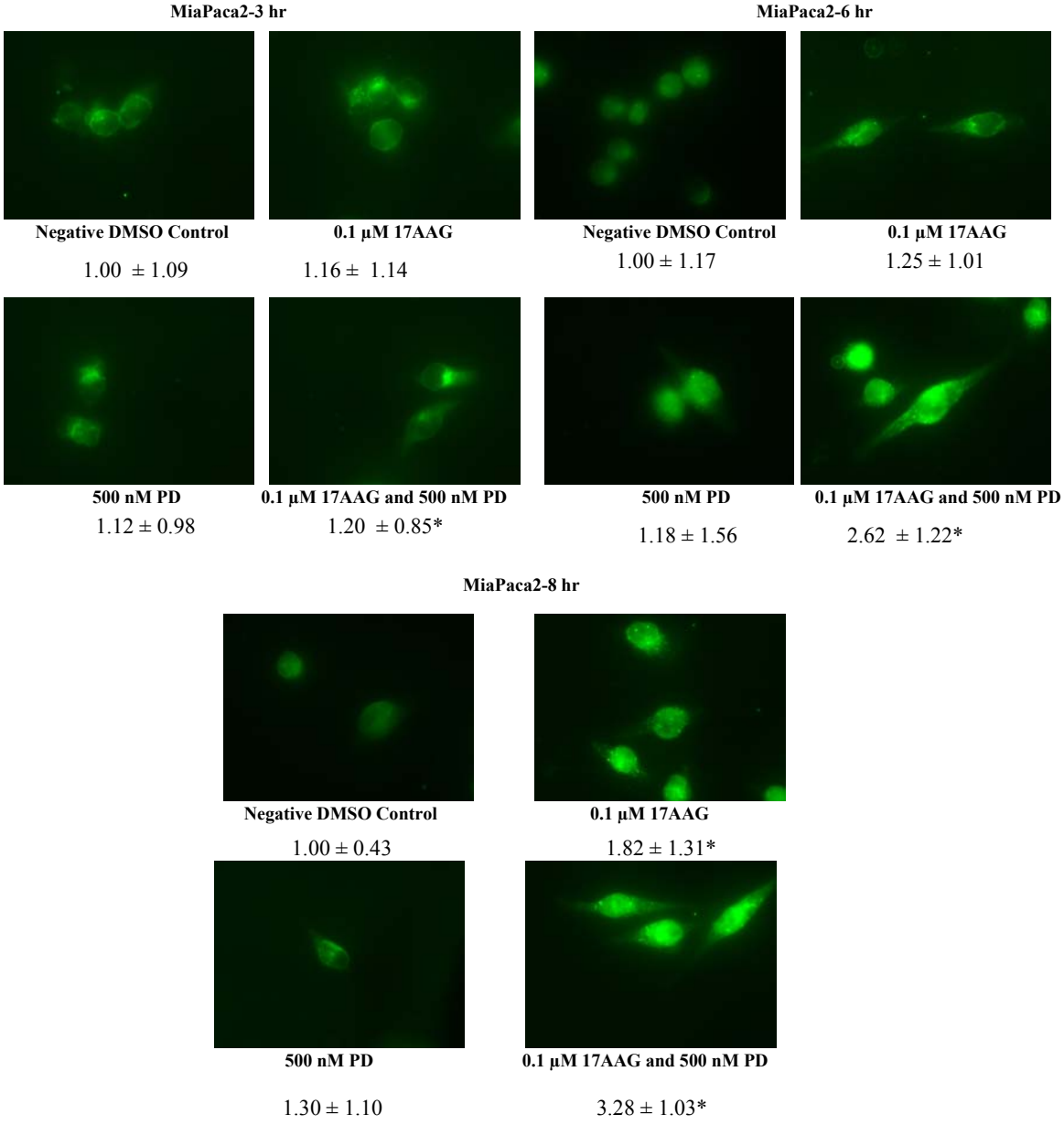

Figure 8.16. 17AAG and PD184352 induced CD95 activation in MiaPaca 2 cells. MiaPaca2 24h after plating in 4 well chamber slides, cells were exposed to vehicle (DMSO), 0.1 µM 17AAG, 500 nM PD184352 or the combination of both drugs. Cells were fixed and not permeabilized 0-8h after drug exposure. Fixed cells were immuno-stained for plasma membrane associated CD95 and visualized using an FITC conjugated secondary antibody. Images are representatives from two separate studies. * $p \leq 0.05$, value greater amount of cell surface CD95 compared to vehicle-treated conditions.

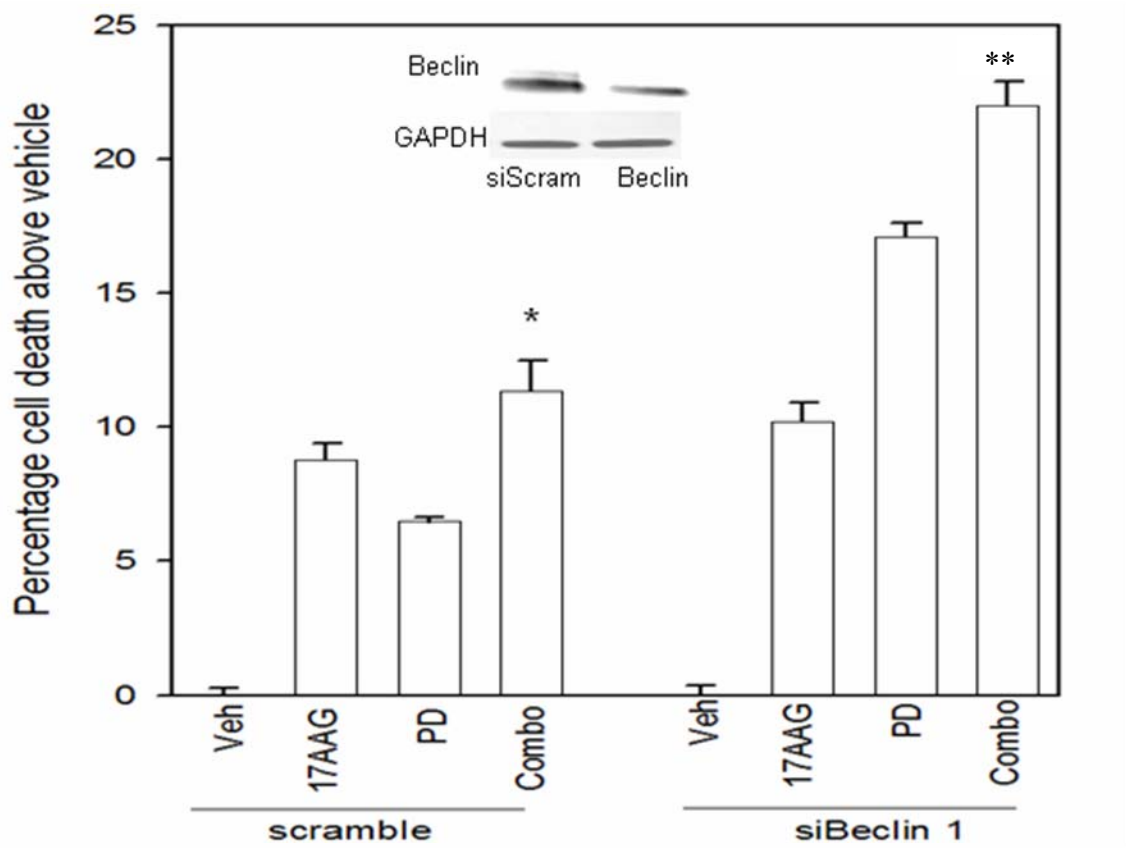

Figure 8.17. Knockdown of Beclin 1 expression enhanced 17AAG and PD184352 toxicity in HepG2 cells. HepG2 cells 24h after plating were transfected with siRNA molecules to knock down expression of Beclin1, or with a siScramble control (20 nM). Twenty four h after infection or transfection, cells were treated with vehicle (DMSO), 0.1 μM 17AAG, 0.5 μM PD184352, or both drugs together. Forty eight hours after exposure, cells were isolated and trypan blue exclusion assay was performed. Values represent the means for three separate experiments ± SD. * $p \leq 0.05$, greater cell killing than compared with any other treatment condition. **, greater cell killing than si-scramble parallel condition.

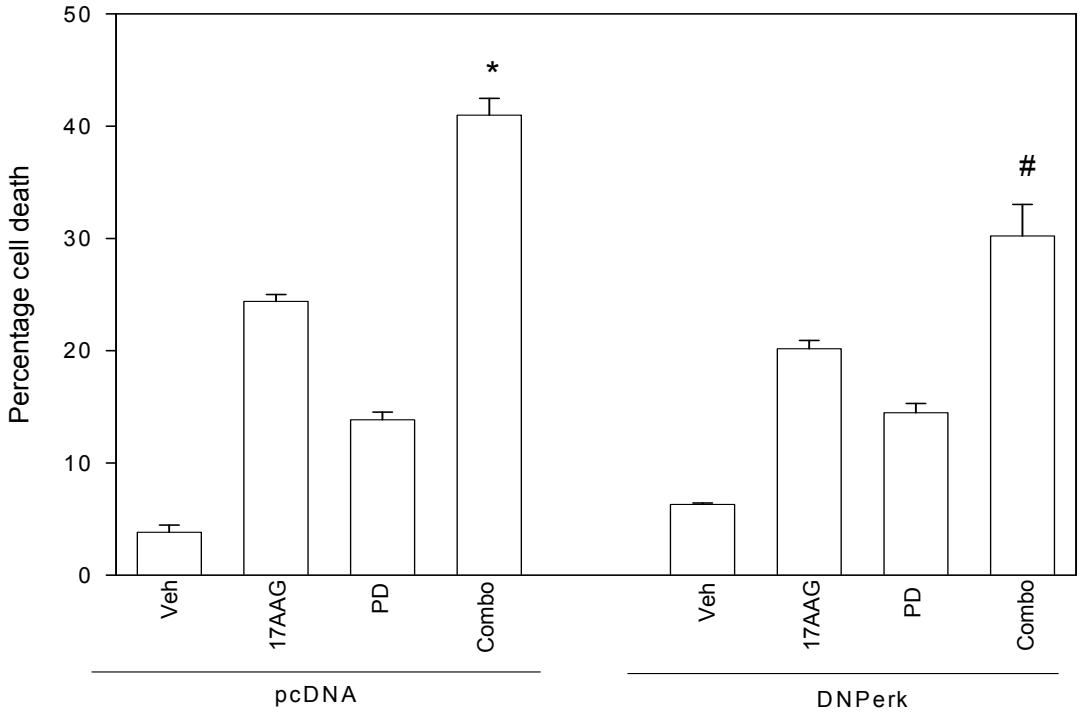

Figure 8.18. DnPERK protected HepG2 cells from 17AAG and PD18435 toxicity. HepG2 cells 24h after plating were transfected with either a vector control plasmid (CMV) or a plasmid to express dominant negative PERK. Twenty four h after infection or transfection, cells were treated with vehicle (DMSO), 0.1 μM 17AAG, 0.5 μM PD184352, or both drugs together. Forty eight hours after exposure, cells were isolated and trypan blue exclusion assay was performed. Values represent the means for two separate experiments ± SD. * $p \leq 0.05$, greater cell killing than compared with any other treatment condition. # $p \leq 0.05$, less cell killing than compared with any parallel condition in vehicle-treated cells.

CHAPTER 9 DISCUSSION: 17AAG and PD184352

Previous studies in our laboratory have shown that 17AAG and PD184352 interact to kill hepatocellular cancer cells via a CD95 dependent mechanism [122, 145]. The present studies were designed to examine whether 17AAG and PD184352 interact in a synergistic manner to cause cell death in colon and pancreatic cancer cells.

In short term cell viability assays, 17AAG and PD184352 caused an additive to greater than additive increase in colon cancer cell death. However, colony formation assays is deemed as the best in vitro measurements of the impact of tumor cell growth in vivo. In long-term colony formation assays, 17AAG and PD184352 treatment synergized to kill colon cancer cells. This data is in agreement with previous data in hepatoma and pancreatic cancer cell lines [122].

We then used the HCT transfectants to better understand the pathways leading to 17AAG and PD184352 toxicity. RAL guanine nucleotide dissociation stimulator (RALGDS) is one of several known Ras-regulated guanine-nucleotide exchange factors, or GEFs, that function by activating RAL A and B GTPases. RALGDS is a RAL-guanine-nucleotide exchange factor (GEF) that converts inactive RAL GTPase (both A and B isoforms) to its active GTP-bound state. RALGDS can directly interact with activated Ras, linking the RAL and Ras pathways. RALGDS was shown to bind to the same domain of the Ras-Raf interaction domain, and as such it acts as a sequestering inhibitor for the activation of Raf by Ras [146]. Thus, the HCT116-HRAS-V12-RAL effector mutant

significantly stimulated 17AAG and PD184352 cell death. Since RAL is known to interact with Raf and subsequently inhibit the Raf/MEK/ERK MAP kinase pathway, we infected these cells with an adenovirus to express constitutively active MEK (caMEKEE) and treated the cells with 17AAG and PD184352. Cell death was partially blocked by caMEKEE in HCT116-HRAS-V12-RAL cells. RAL is also known to activate the JNK pathway; however the JNK inhibitory peptide only partially blocked 17AAG and PD184352 cell death. HCT116-HRAS-V12-RAL cells have higher basal levels of JNK. There is also more ERK1/2 activation in HCT116-HRAS-V12-RAL cells. Additional studies beyond the scope of this dissertation would be required to identify the mechanism of cell killing in the HCT116-HRAS-V12-RAL cells.

As hepatoma cells have previously been identified to show that 17AAG and PD184352 kill by activation of CD95 and suppression of c-FLIP-s, we investigated whether this occurs in pancreatic cells. Overexpression of c-FLIP-s protected MiaPaca2 cells from 17AAG and PD184352 cells death. This indicates that treatment of these cancer cells by this drug combination is via the extrinsic pathway involving caspase 8. Overexpression of the mitochondrial protective protein BCL-xL or inhibition of caspase 9 also suppressed cell killing. This argues that while caspase 8 is needed to induce cell death, the intrinsic pathway and release of cytochrome c is crucial to the toxicity of this drug combination treatment.

As we have established in hepatoma cells the role of CD95 in 17AAG and PD184352 lethality, we investigated the role of ER stress. PERK can sense an increase of improper folded proteins within the ER [46]. Indeed, loss of PERK suppressed the cell death

response in hepatoma cells. This result further implicates ER stress as a mechanism by which 17AAG and PD184352 induces cell killing.

In conclusion, 17AAG and PD184352 interact to kill multiple cancer cell types. An active RAL mutant plays a significant role in the toxicity of this drug combination in colon cancer cells. Though in all cell types examined thus far, the activation of CD95 play a central role in drug lethality.

CHAPTER 10 DISCUSSION: GENERAL

Pre-cancerous cells can be eliminated from the body by programmed cell death. Unfortunately, a hallmark of most cancers is a defect in the normal programmed cell death that enables pre-cancerous cells to survive, proliferate, and become malignant. Because most traditional chemotherapeutics act by triggering programmed cell death, such agents are frequently ineffective against tumors that lack a functional programmed cell death mechanism. Such tumors are said to be chemotherapy-resistant. Resistance to traditional drugs has been a major impediment to successful therapeutic outcomes for human cancers [1].

Combination therapy (using two different drugs simultaneously to treat cancer) has proven to be a useful new tool for cancer patients who are refractory to traditional therapies. The new approach is based on the theory that one drug can be used to restore the ability of cells to commit suicide and the second can actually trigger the process. In projects, sorafenib+vorinostat or 17AAG+PD184352 we used a more specific inhibitor (i.e. sorafenib and PD184352) plus a very broad targeted drug (i.e. vorinostat, 17AAG).

Sorafenib alone has been approved for the use in renal cell carcinoma [88]. Vorinostat has been approved for the treatment of cutaneuous T cell lymphoma (CTCL) [106]. Sorafenib and HDACIs target multiple overlapping pathways. Sorafenib and vorinostat is now in Phase I clinical trials. This combination has been shown to be effective against CML cell lines in the laboratory [96]. In our drug combinations, sorafenib inhibits RAF, inhibiting the RAK/MEK/ERK MAP kinase pathway which promotes cell

survival [5, 6]. As stated previously, many cancer patients have active RAS mutations which induce constitutive activation of the RAF/MEK/ERK MAP kinase pathway [147]. Sorafenib thus can inhibit this pathway (even in cancers that have RAS mutations) [15]. Vorinostat can be used in combination to actually trigger the apoptotic process. A large number of cellular proteins are modified post-translationally by acetylation, leading to altered structure or function. Thus, vorinostat can induce oxidative injury as well as increase the expression of death receptors [105, 112]. It is likely that in different tumor types, inhibition of specific HDACs will alter distinct biological processes contributing to anti-cancer effects. This concept is analogous to the use of protein kinase inhibitors as anti-cancer therapeutics. Specific protein kinase inhibitors may directly affect specific types of human cancer.

17AAG alters hsp90 function, thereby promoting the proteosomal degradation of hsp90 client proteins such as AKT and Raf-1 [67]. PD184352 as a single agent does not alter tumor cell growth in phase II trials [148]. In vitro studies in our laboratory have shown that in chronic myelogenous leukemia cells, inhibitors of MEK1/2 enhanced 17AAG lethality by promoting mitochondrial dysfunction leading to apoptosis [149].

Our in vitro studies conclude that the combination of sorafenib+vorinostat or 17AAG+PD184352 induces a significant amount of cell death in colon, hepatoma, and pancreatic cancers, respectively. Future studies in animal models will provide further implications for these drug combinations in vivo.

Literature Cited

Literature Cited

References

1. Hanahan D, Weinberg RA. The hallmarks of cancer. Cell 2000;100(1):57.

2. Jemal A, Siegel R, Ward E, Hao Y, Xu J, Murray T, et al. Cancer statistics, 2008. CA 2008;58(2):71.

3. Dent P, Yacoub A, Fisher PB, Hagan MP, Grant S. MAPK pathways in radiation responses. Oncogene 2003;22(37):5885.

4. Grant S, Dent P. Kinase inhibitors and cytotoxic drug resistance. Clinical cancer research 2004;10(7):2205.

5. Dent P. MAP kinase pathways in the control of hepatocyte growth, metabolism, and survival. In: Signaling Pathways in Liver Diseases. Dufour, J.F.; Clavien, Pierre-Alain; Trautwein, C.; Graf, R. ed. Springer Press; 2005. p.223.

6. Dhillon AS. MAP kinase signalling pathways in cancer. Oncogene 2007;26(22):3279.

7. McCubrey JA, Steelman LS, Chappell WH, Abrams SL, Wong EW, Chang F, et al. Roles of the Raf/MEK/ERK pathway in cell growth, malignant transformation and drug resistance. Biochim Biophys Acta 2007 Aug;1773(8):1263-84.

8. Allan LA, Morrice N, Brady S, Magee G, Pathak S, Clarke PR. Inhibition of caspase-9 through phosphorylation at Thr 125 by ERK MAPK. Nature cell biology 2003;5(7):647.

9. Mori M, Uchida M, Watanabe T, Kirito K, Hatake K, Ozawa K, et al. Activation of extracellular signal-regulated kinases ERK1 and ERK2 induces Bcl-xL up-regulation via inhibition of caspase activities in erythropoietin signaling. Journal of cellular physiology 2003;195(2):290.

10. Ley R, Balmanno K, Hadfield K, Weston C, Cook SJ. Activation of the ERK1/2 signaling pathway promotes phosphorylation and proteasome-dependent degradation of the BH3-only protein, Bim. The Journal of biological chemistry 2003;278(21):18811.

11. Wang YF, Jiang CC, Kiejda KA, Gillespie S, Zhang XD, Hersey P. Apoptosis induction in human melanoma cells by inhibition of MEK is caspase-independent and mediated by the Bcl-2 family members PUMA, Bim, and Mcl-1. Clinical cancer research 2007;13(16):4934.

12. Qiao L, Han SI, Fang Y, Park JS, Gupta S, Gilfor D, et al. Bile acid regulation of C/EBPbeta, CREB, and c-Jun function, via the extracellular signal-regulated kinase and c-Jun NH2-terminal kinase pathways, modulates the apoptotic response of hepatocytes. Molecular and cellular biology 2003;23(9):3052.

13. Kolch W. Meaningful relationships: the regulation of the Ras/Raf/MEK/ERK pathway by protein interactions. Biochem J 2000 Oct 15;351 Pt 2:289-305.

14. Kolch W. The role of Raf kinases in malignant transformation. Expert reviews in molecular medicine 2002;4(8):1.

15. Roberts PJ, Der CJ. Targeting the Raf-MEK-ERK mitogen-activated protein kinase cascade for the treatment of cancer. Oncogene 2007 May 14;26(22):3291-310.

16. Wan PTC, Garnett MJ, Roe SM, Lee S, Niculescu-Duvaz D, Good VM, et al. Mechanism of activation of the RAF-ERK signaling pathway by oncogenic mutations of B-RAF. Cell 2004;116(6):855.

17. Kyriakis JM, Avruch J. Mammalian mitogen-activated protein kinase signal transduction pathways activated by stress and inflammation. Physiological reviews 2001;81(2):807.

18. Lei K, Davis RJ. JNK phosphorylation of Bim-related members of the Bcl2 family induces Bax-dependent apoptosis. Proceedings of the National Academy of Sciences of the United States of America 2003;100(5):2432.

19. Roux PP, Blenis J. ERK and p38 MAPK-activated protein kinases: a family of protein kinases with diverse biological functions. Microbiology and molecular biology reviews 2004;68(2):320.

20. Han J, Sun P. The pathways to tumor suppression via route p38. Trends in biochemical sciences 2007;32(8):364.

21. Engelman JA, Luo J, Cantley LC. The evolution of phosphatidylinositol 3-kinases as regulators of growth and metabolism. Nature reviews. Genetics 2006;7(8):606.

22. Gaidarov I, Smith ME, Domin J, Keen JH. The class II phosphoinositide 3-kinase C2alpha is activated by clathrin and regulates clathrin-mediated membrane trafficking. Molecular cell 2001;7(2):443.

23. Nobukuni T, Joaquin M, Roccio M, Dann SG, Kim SY, Gulati P, et al. Amino acids mediate mTOR/raptor signaling through activation of class 3 phosphatidylinositol 3OH-kinase. Proceedings of the National Academy of Sciences of the United States of America 2005;102(40):14238.

24. Cully M, You H, Levine AJ, Mak TW. Beyond PTEN mutations: the PI3K pathway as an integrator of multiple inputs during tumorigenesis. Nature reviews. Cancer 2006;6(3):184.

25. Manning BD, Cantley LC. AKT/PKB signaling: navigating downstream. Cell 2007;129(7):1261.

26. Elmore S. Apoptosis: a review of programmed cell death. Toxicologic pathology 2007;35(4):495.

27. Sharma K. Death the Fas way: regulation and pathophysiology of CD95 and its ligand. Pharmacology therapeutics 2000;88(3):333.

28. Schmitz I, Kirchhoff S, Krammer PH. Regulation of death receptor-mediated apoptosis pathways. Int J Biochem Cell Biol 2000 Nov-Dec;32(11-12):1123-36.

29. Adams JM, Cory S. The Bcl-2 apoptotic switch in cancer development and therapy. Oncogene 2007 Feb 26;26(9):1324-37.

30. Li H. Cleavage of BID by caspase 8 mediates the mitochondrial damage in the Fas pathway of apoptosis. Cell 1998;94(4):491.

31. Youle RJ. The BCL-2 protein family: opposing activities that mediate cell death. Nature reviews. Molecular cell biology 2008;9(1):47.

32. Dean EJ. Novel therapeutic targets in lung cancer: Inhibitor of apoptosis proteins from laboratory to clinic. Cancer Treatment Reviews 2007;33(2):203.

33. Levine B, Kroemer G. Autophagy in the Pathogenesis of Disease. Cell 2008 Jan 11;132(1):27-42.

34. Amaravadi RK, Thompson CB. The roles of therapy-induced autophagy and necrosis in cancer treatment. Clin Cancer Res 2007 Dec 15;13(24):7271-9.

35. Kundu M. Autophagy: basic principles and relevance to disease. Annual review of pathology 2008;3:427.

36. Mariño G. Autophagy: molecular mechanisms, physiological functions and relevance in human pathology. Cellular and molecular life sciences 2004;61(12):1439.

37. Mizushima N. Mouse Apg16L, a novel WD-repeat protein, targets to the autophagic isolation membrane with the Apg12-Apg5 conjugate. Journal of cell science 2003;116(Pt 9):1679.

38. Uchiyama Y. Autophagy-physiology and pathophysiology. Histochemistry and Cell Biology 2008;129(4):407.

39. Ding W, Yin X. Sorting, recognition and activation of the misfolded protein degradation pathways through macroautophagy and the proteasome. Autophagy 2008;4(2):141.

40. Mizushima N. Autophagy: process and function. Genes development 2007;21(22):2861.

41. Seglen PO. 3-Methyladenine: specific inhibitor of autophagic/lysosomal protein degradation in isolated rat hepatocytes. Proceedings of the National Academy of Sciences of the United States of America 1982;79(6):1889.

42. Petiot A. Distinct classes of phosphatidylinositol 3'-kinases are involved in signaling pathways that control macroautophagy in HT-29 cells. The Journal of biological chemistry 2000;275(2):992.

43. Mizushima N. Autophagy fights disease through cellular self-digestion. Nature 2008;451(7182):1069.

44. Saeki K. Bcl-2 down-regulation causes autophagy in a caspase-independent manner in human leukemic HL60 cells. Cell death and differentiation 2000;7(12):1263.

45. Liang C. Autophagic and tumour suppressor activity of a novel Beclin1-binding protein UVRAG. Nature cell biology 2006;8(7):688.

46. Schröder M. Endoplasmic reticulum stress responses. Cellular and molecular life sciences 2008;65(6):862.

47. Wek RC, Cavener DR. Translational Control and the Unfolded Protein Response. Antioxid Redox Signal 2007 Aug 30.

48. Hitomi J. Involvement of caspase-4 in endoplasmic reticulum stress-induced apoptosis and Abeta-induced cell death. The Journal of cell biology 2004;165(3):347.

49. Lin CF, Chen CL, Lin YS. Ceramide in apoptotic signaling and anticancer therapy. Current medicinal chemistry 2006;13(14):1609.

50. Zheng W, Kollmeyer J, Symolon H, Momin A, Munter E, Wang E, et al. Ceramides and other bioactive sphingolipid backbones in health and disease: lipidomic analysis, metabolism and roles in membrane structure, dynamics, signaling and autophagy. Biochimica et biophysica acta 2006;1758(12):1864.

51. Kitatani K, Idkowiak-Baldys J, Hannun YA. The sphingolipid salvage pathway in ceramide metabolism and signaling. Cellular signalling 2008;20(6):1010.

52. Marchesini N, Hannun YA. Acid and neutral sphingomyelinases: roles and mechanisms of regulation. Biochemistry and cell biology 2004;82(1):27.

53. Hannun YA, Obeid LM. Principles of bioactive lipid signalling: lessons from sphingolipids. Nature reviews. Molecular cell biology 2008;9(2):139.

54. Shida D, Takabe K, Kapitonov D, Milstien S, Spiegel S. Targeting SphK1 as a new strategy against cancer. Current drug targets 2008;9(8):662.

55. Cuvillier O, Pirianov G, Kleuser B, Vanek PG, Coso OA, Gutkind S, et al. Suppression of ceramide-mediated programmed cell death by sphingosine-1-phosphate. Nature 1996;381(6585):800.

56. Hartl FU. Molecular chaperones in cellular protein folding. Nature 1996 Jun 13;381(6583):571-9.

57. Morimoto RI. Regulation of the heat shock transcriptional response: cross talk between a family of heat shock factors, molecular chaperones, and negative regulators. Genes Dev 1998 Dec 15;12(24):3788-96.

58. Cullinan SB, Whitesell L. Heat shock protein 90: a unique chemotherapeutic target. Semin Oncol 2006 Aug;33(4):457-65.

59. Nakamoto H, Vigh L. The small heat shock proteins and their clients. Cell Mol Life Sci 2007 Feb;64(3):294-306.

60. Sun Y, MacRae TH. Small heat shock proteins: molecular structure and chaperone function. Cell Mol Life Sci 2005 Nov;62(21):2460-76.

61. Nollen EA, Morimoto RI. Chaperoning signaling pathways: molecular chaperones as stress-sensing 'heat shock' proteins. J Cell Sci 2002 Jul 15;115(Pt 14):2809-16.

62. Maurizi MR, Xia D. Protein binding and disruption by Clp/Hsp100 chaperones. Structure 2004 Feb;12(2):175-83.

63. Nathan DF, Vos MH, Lindquist S. In vivo functions of the Saccharomyces cerevisiae Hsp90 chaperone. Proc Natl Acad Sci U S A 1997 Nov 25;94(24):12949-56.

64. Wegele H, Muller L, Buchner J. Hsp70 and Hsp90--a relay team for protein folding. Rev Physiol Biochem Pharmacol 2004;151:1-44.

65. Picard D, Khursheed B, Garabedian MJ, Fortin MG, Lindquist S, Yamamoto KR. Reduced levels of hsp90 compromise steroid receptor action in vivo. Nature 1990 Nov 8;348(6297):166-8.

66. Xu Y, Lindquist S. Heat-shock protein hsp90 governs the activity of pp60v-src kinase. Proc Natl Acad Sci U S A 1993 Aug 1;90(15):7074-8.

67. Isaacs JS, Xu W, Neckers L. Heat shock protein 90 as a molecular target for cancer therapeutics. Cancer cell 2003;3(3):213.

68. Prodromou C, Roe SM, O'Brien R, Ladbury JE, Piper PW, Pearl LH. Identification and structural characterization of the ATP/ADP-binding site in the Hsp90 molecular chaperone. Cell 1997 Jul 11;90(1):65-75.

69. Minami Y, Kimura Y, Kawasaki H, Suzuki K, Yahara I. The carboxy-terminal region of mammalian HSP90 is required for its dimerization and function in vivo. Mol Cell Biol 1994 Feb;14(2):1459-64.

70. Compton SA, Elmore LW, Haydu K, Jackson-Cook CK, Holt SE. Induction of nitric oxide synthase-dependent telomere shortening after functional inhibition of Hsp90 in human tumor cells. Mol Cell Biol 2006 Feb;26(4):1452-62.

71. Ozawa K, Murakami Y, Eki T, Soeda E, Yokoyama K. Mapping of the gene family for human heat-shock protein 90 alpha to chromosomes 1, 4, 11, and 14. Genomics 1992 Feb;12(2):214-20.

72. Eustace BK, Sakurai T, Stewart JK, Yimlamai D, Unger C, Zehetmeier C, et al. Functional proteomic screens reveal an essential extracellular role for hsp90 alpha in cancer cell invasiveness. Nat Cell Biol 2004 Jun;6(6):507-14.

73. Moore SK, Kozak C, Robinson EA, Ullrich SJ, Appella E. Murine 86- and 84-kDa heat shock proteins, cDNA sequences, chromosome assignments, and evolutionary origins. J Biol Chem 1989 Apr 5;264(10):5343-51.

74. Voss AK, Thomas T, Gruss P. Mice lacking HSP90beta fail to develop a placental labyrinth. Development 2000 Jan;127(1):1-11.

75. Picard D.

76. Pratt WB, Toft DO. Regulation of signaling protein function and trafficking by the hsp90/hsp70-based chaperone machinery. Exp Biol Med (Maywood) 2003 Feb;228(2):111-33.

77. Russell LC, Whitt SR, Chen MS, Chinkers M. Identification of conserved residues required for the binding of a tetratricopeptide repeat domain to heat shock protein 90. J Biol Chem 1999 Jul 16;274(29):20060-3.

78. Prodromou C, Panaretou B, Chohan S, Siligardi G, O'Brien R, Ladbury JE, et al. The ATPase cycle of Hsp90 drives a molecular 'clamp' via transient dimerization of the N-terminal domains. EMBO J 2000 Aug 15;19(16):4383-92.

79. Connell P, Ballinger CA, Jiang J, Wu Y, Thompson LJ, Hohfeld J, et al. The co-chaperone CHIP regulates protein triage decisions mediated by heat-shock proteins. Nat Cell Biol 2001 Jan;3(1):93-6.

80. Rabindran SK, Giorgi G, Clos J, Wu C. Molecular cloning and expression of a human heat shock factor, HSF1. Proc Natl Acad Sci U S A 1991 Aug 15;88(16):6906-10.

81. McMillan DR, Xiao X, Shao L, Graves K, Benjamin IJ. Targeted disruption of heat shock transcription factor 1 abolishes thermotolerance and protection against heat-inducible apoptosis. J Biol Chem 1998 Mar 27;273(13):7523-8.

82. Liu PC, Thiele DJ. Modulation of human heat shock factor trimerization by the linker domain. J Biol Chem 1999 Jun 11;274(24):17219-25.

83. Baler R, Dahl G, Voellmy R. Activation of human heat shock genes is accompanied by oligomerization, modification, and rapid translocation of heat shock transcription factor HSF1. Mol Cell Biol 1993 Apr;13(4):2486-96.

84. Shi Y, Mosser DD, Morimoto RI. Molecular chaperones as HSF1-specific transcriptional repressors. Genes Dev 1998 Mar 1;12(5):654-66.

85. Zou J, Guo Y, Guettouche T, Smith DF, Voellmy R. Repression of heat shock transcription factor HSF1 activation by HSP90 (HSP90 complex) that forms a stress-sensitive complex with HSF1. Cell 1998 Aug 21;94(4):471-80.

86. Schatzkin A, Freedman LS, Dawsey SM, Lanza E. Interpreting precursor studies: what polyp trials tell us about large-bowel cancer. Journal of the National Cancer Institute 1994;86(14):1053.

87. Van Geelen CM, de Vries EG, de Jong S. Lessons from TRAIL-resistance mechanisms in colorectal cancer cells: paving the road to patient-tailored therapy. Drug Resist Updat 2004 Dec;7(6):345-58.

88. Flaherty KT. Sorafenib: delivering a targeted drug to the right targets. Expert Review of Anticancer Therapy 2007;7(5):617.

89. Strumberg D, Clark JW, Awada A, Moore MJ, Richly H, Hendlisz A, et al. Safety, pharmacokinetics, and preliminary antitumor activity of sorafenib: a review of four phase I trials in patients with advanced refractory solid tumors. Oncologist 2007 Apr;12(4):426-37.

90. Rini BI. Sorafenib. Expert Opinion on Pharmacotherapy 2006;7(4):453.

91. Strumberg D. Preclinical and clinical development of the oral multikinase inhibitor sorafenib in cancer treatment. Medicamentos de actualidad 2005;41(12):773.

92. Gollob JA. Sorafenib: scientific rationales for single-agent and combination therapy in clear-cell renal cell carcinoma. Clinical genitourinary cancer 2005;4(3):167.

93. Rahmani M, Davis EM, Bauer C, Dent P, Grant S. Apoptosis induced by the kinase inhibitor BAY 43-9006 in human leukemia cells involves down-regulation of Mcl-1 through inhibition of translation. J Biol Chem 2005 Oct 21;280(42):35217-27.

94. Rahmani M, Nguyen TK, Dent P, Grant S. The multikinase inhibitor sorafenib induces apoptosis in highly imatinib mesylate-resistant bcr/abl+ human leukemia cells in association with signal transducer and activator of transcription 5 inhibition and myeloid cell leukemia-1 down-regulation. Mol Pharmacol 2007 Sep;72(3):788-95.

95. Rahmani M, Davis EM, Crabtree TR, Habibi JR, Nguyen TK, Dent P, et al. The kinase inhibitor sorafenib induces cell death through a process involving induction of endoplasmic reticulum stress. Mol Cell Biol 2007 Aug;27(15):5499-513.

96. Dasmahapatra G, Yerram N, Dai Y, Dent P, Grant S. Synergistic interactions between vorinostat and sorafenib in chronic myelogenous leukemia cells involve Mcl-1 and p21CIP1 down-regulation. Clinical cancer research 2007;13(14):4280.

97. Gregory PD, Wagner K, Hörz W. Histone acetylation and chromatin remodeling. Experimental cell research 2001;265(2):195.

98. Marks PA, Miller T, Richon VM. Histone deacetylases. Current opinion in pharmacology 2003;3(4):344.

99. Bali P, Pranpat M, Swaby R, Fiskus W, Yamaguchi H, Balasis M, et al. Activity of suberoylanilide hydroxamic Acid against human breast cancer cells with amplification of her-2. Clinical cancer research 2005;11(17):6382.

100. Kwon SH, Ahn SH, Kim YK, Bae G, Yoon JW, Hong S, et al. Apicidin, a histone deacetylase inhibitor, induces apoptosis and Fas/Fas ligand expression in human acute promyelocytic leukemia cells. The Journal of biological chemistry 2002;277(3):2073.

101. Marks PA. Discovery and development of SAHA as an anticancer agent. Oncogene 2007;26(9):1351.

102. Pang RWC, Poon RTP. From molecular biology to targeted therapies for hepatocellular carcinoma: the future is now. Oncology 2007;72 Suppl 1:30.

103. Venturelli S, Armeanu S, Pathil A, Hsieh C, Weiss TS, Vonthein R, et al. Epigenetic combination therapy as a tumor-selective treatment approach for hepatocellular carcinoma. Cancer 2007;109(10):2132.

104. Wise LD, Turner KJ, Kerr JS. Assessment of developmental toxicity of vorinostat, a histone deacetylase inhibitor, in Sprague-Dawley rats and Dutch Belted rabbits. Birth defects research. Part B, Developmental and reproductive toxicology 2007;80(1):57.

105. Dokmanovic M. Histone deacetylase inhibitors: overview and perspectives. Molecular cancer research 2007;5(10):981.

106. Rubin EH, Agrawal NG, Friedman EJ, Scott P, Mazina KE, Sun L, et al. A study to determine the effects of food and multiple dosing on the pharmacokinetics of vorinostat given orally to patients with advanced cancer. Clin Cancer Res 2006 Dec 1;12(23):7039-45.

107. Zhang G, Park MA, Mitchell C, Hamed H, Rahmani M, Martin AP, et al. Vorinostat and sorafenib synergistically kill tumor cells via FLIP suppression and CD95 activation. Clinical cancer research 2008;14(17):5385.

108. Park MA, Zhang G, Martin AP, Hamed H, Mitchell C, Hylemon PB, et al. Vorinostat and sorafenib increase ER stress, autophagy and apoptosis via ceramide-dependent CD95 and PERK activation. Cancer biology therapy 2008;7(10).

109. Beeram M, Patnaik A, Rowinsky EK. Raf: a strategic target for therapeutic development against cancer. Journal of clinical oncology 2005;23(27):6771.

110. Wilhelm SM, Carter C, Tang L, Wilkie D, McNabola A, Rong H, et al. BAY 43-9006 exhibits broad spectrum oral antitumor activity and targets the RAF/MEK/ERK pathway and receptor tyrosine kinases involved in tumor progression and angiogenesis. Cancer research 2004;64(19):7099.

111. Grant S, Easley C, Kirkpatrick P. Vorinostat. Nature reviews. Drug discovery 2007;6(1):21.

112. Xu WS, Parmigiani RB, Marks PA. Histone deacetylase inhibitors: molecular mechanisms of action. Oncogene 2007 Aug 13;26(37):5541-52.

113. Yan Z, Chen M, Perucho M, Friedman E. Oncogenic Ki-ras but not oncogenic Ha-ras blocks integrin beta1-chain maturation in colon epithelial cells. J Biol Chem 1997 Dec 5;272(49):30928-36.

114. Dobó J. Cytokine response modifier a inhibition of initiator caspases results in covalent complex formation and dissociation of the caspase tetramer. The Journal of biological chemistry 2006;281(50):38781.

115. Voelkel-Johnson C, Hannun YA, El-Zawahry A. Resistance to TRAIL is associated with defects in ceramide signaling that can be overcome by exogenous C6-ceramide without requiring down-regulation of cellular FLICE inhibitory protein. Molecular cancer therapeutics 2005;4(9):1320.

116. White-Gilbertson S, Mullen T, Senkal C, Lu P, Ogretmen B, Obeid L, et al. Ceramide synthase 6 modulates TRAIL sensitivity and nuclear translocation of active caspase-3 in colon cancer cells. Oncogene 2009;28(8):1132.

117. Göttlicher M, Minucci S, Zhu P, Krämer OH, Schimpf A, Giavara S, et al. Valproic acid defines a novel class of HDAC inhibitors inducing differentiation of transformed cells. The EMBO journal 2001;20(24):6969.

118. Yu C, Dasmahapatra G, Dent P, Grant S. Synergistic interactions between MEK1/2 and histone deacetylase inhibitors in BCR/ABL human leukemia cells. Leukemia 2005;19(9):1579.

119. Ozaki K, Minoda A, Kishikawa F, Kohno M. Blockade of the ERK pathway markedly sensitizes tumor cells to HDAC inhibitor-induced cell death. Biochemical and biophysical research communications 2006;339(4):1171.

120. Yu C, Subler M, Rahmani M, Reese E, Krystal G, Conrad D, et al. Induction of apoptosis in BCR/ABL cells by histone deacetylase inhibitors involves reciprocal effects on the RAF/MEK/ERK and JNK pathways. Cancer biology therapy 2003;2(5):544.

121. Portanova P, Russo T, Pellerito O, Calvaruso G, Giuliano M, Vento R, et al. The role of oxidative stress in apoptosis induced by the histone deacetylase inhibitor suberoylanilide hydroxamic acid in human colon adenocarcinoma HT-29 cells. International journal of oncology 2008;33(2):325.

122. Park MA, Zhang G, Mitchell C, Rahmani M, Hamed H, Hagan MP, et al. Mitogen-activated protein kinase kinase 1/2 inhibitors and 17-allylamino-17-demethoxygeldanamycin synergize to kill human gastrointestinal tumor cells in vitro via suppression of c-FLIP-s levels and activation of CD95. Molecular cancer therapeutics 2008;7(9):2633.

123. Qiao L, Yacoub A, Studer E, Gupta S, Pei XY, Grant S, et al. Inhibition of the MAPK and PI3K pathways enhances UDCA-induced apoptosis in primary rodent hepatocytes. Hepatology 2002;35(4):779.

124. Wang Y, Singh R, Lefkowitch JH, Rigoli RM, Czaja MJ. Tumor necrosis factor-induced toxic liver injury results from JNK2-dependent activation of caspase-8 and the mitochondrial death pathway. The Journal of biological chemistry 2006;281(22):15258.

125. Hochedlinger K, Wagner EF, Sabapathy K. Differential effects of JNK1 and JNK2 on signal specific induction of apoptosis. Oncogene 2002;21(15):2441.

126. Barnhart BC. The CD95 type I/type II model. Seminars in immunology 2003;15(3):185.

127. Kolesnick R, Fuks Z. Radiation and ceramide-induced apoptosis. Oncogene 2003;22(37):5897.

128. Ogretmen B, Hannun YA. Biologically active sphingolipids in cancer pathogenesis and treatment. Nature reviews. Cancer 2004;4(8):604.

129. Futerman AH, Riezman H. The ins and outs of sphingolipid synthesis. Trends in cell biology 2005;15(6):312.

130. Detailed Guide: Pancreatic Cancer. ;February, 2009.

131. Cancer Facts and Figures. ;Febuary, 2009.

132. Yeo CJ, Abrams RA, Grochow LB, Sohn TA, Ord SE, Hruban RH, et al. Pancreaticoduodenectomy for pancreatic adenocarcinoma: postoperative adjuvant chemoradiation improves survival. A prospective, single-institution experience. Annals of surgery 1997;225(5):621.

133. Parkin DM, Whelan SL, Ferlay J, et al. Cancer incidence in five continents. Volume VII. IARC Sci Publ 1997(143):i.

134. Ross RK, Yuan JM, Yu MC, Wogan GN, Qian GS, Tu JT, et al. Urinary aflatoxin biomarkers and risk of hepatocellular carcinoma. The Lancet 1992;339(8799):943.

135. El-Serag HB, Marrero JA, Rudolph L, Reddy KR. Diagnosis and treatment of hepatocellular carcinoma. Gastroenterology 2008;134(6):1752.

136. Whitesell L, Mimnaugh EG, De Costa B, Myers CE, Neckers LM. Inhibition of heat shock protein HSP90-pp60v-src heteroprotein complex formation by benzoquinone ansamycins: essential role for stress proteins in oncogenic transformation. Proc Natl Acad Sci U S A 1994 Aug 30;91(18):8324-8.

137. Schulte TW, Akinaga S, Soga S, Sullivan W, Stensgard B, Toft D, et al. Antibiotic radicicol binds to the N-terminal domain of Hsp90 and shares important biologic activities with geldanamycin. Cell Stress Chaperones 1998 Jun;3(2):100-8.

138. Roe SM, Prodromou C, O'Brien R, Ladbury JE, Piper PW, Pearl LH. Structural basis for inhibition of the Hsp90 molecular chaperone by the antitumor antibiotics radicicol and geldanamycin. J Med Chem 1999 Jan 28;42(2):260-6.

139. Kamal A, Thao L, Sensintaffar J, Zhang L, Boehm MF, Fritz LC, et al. A high-affinity conformation of Hsp90 confers tumour selectivity on Hsp90 inhibitors. Nature 2003 Sep 25;425(6956):407-10.

140. Supko JG, Hickman RL, Grever MR, Malspeis L. Preclinical pharmacologic evaluation of geldanamycin as an antitumor agent. Cancer Chemother Pharmacol 1995;36(4):305-15.

141. Egorin MJ, Rosen DM, Wolff JH, Callery PS, Musser SM, Eiseman JL. Metabolism of 17-(allylamino)-17-demethoxygeldanamycin (NSC 330507) by murine and human hepatic preparations. Cancer Res 1998 Jun 1;58(11):2385-96.

142. Lorusso PM, Adjei AA, Varterasian M, Gadgeel S, Reid J, Mitchell DY, et al. Phase I and pharmacodynamic study of the oral MEK inhibitor CI-1040 in patients with advanced malignancies. Journal of clinical oncology 2005;23(23):5281.

143. Sydor JR, Normant E, Pien CS, Porter JR, Ge J, Grenier L, et al. Development of 17-allylamino-17-demethoxygeldanamycin hydroquinone hydrochloride (IPI-504), an anti-cancer agent directed against Hsp90. Proceedings of the National Academy of Sciences of the United States of America 2006;103(46):17408.

144. Georgakis GV, Li Y, Rassidakis GZ, Martinez-Valdez H, Medeiros LJ, Younes A. Inhibition of heat shock protein 90 function by 17-allylamino-17-demethoxy-geldanamycin in Hodgkin's lymphoma cells down-regulates Akt kinase, dephosphorylates

extracellular signal-regulated kinase, and induces cell cycle arrest and cell death. Clinical cancer research 2006;12(2):584.

145. Mitchell C, Park MA, Zhang G, Han SI, Harada H, Franklin RA, et al. 17-Allylamino-17-demethoxygeldanamycin enhances the lethality of deoxycholic acid in primary rodent hepatocytes and established cell lines. Mol Cancer Ther 2007 Feb;6(2):618-32.

146. Wolthuis RM, Bos JL. Ras caught in another affair: the exchange factors for Ral. Current opinion in genetics development 1999;9(1):112.

147. Bos JL, Fearon ER, Hamilton SR, Verlaan-de Vries M, van Boom JH, van der Eb AJ, et al. Prevalence of ras gene mutations in human colorectal cancers. Nature 1987 May 28-Jun 3;327(6120):293-7.

148. Rinehart J, Adjei AA, Lorusso PM, Waterhouse D, Hecht JR, Natale RB, et al. Multicenter phase II study of the oral MEK inhibitor, CI-1040, in patients with advanced non-small-cell lung, breast, colon, and pancreatic cancer. Journal of clinical oncology 2004;22(22):4456.

149. Nguyen TK, Rahmani M, Gao N, Kramer L, Corbin AS, Druker BJ, et al. Synergistic interactions between DMAG and mitogen-activated protein kinase kinase 1/2 inhibitors in Bcr/abl+ leukemia cells sensitive and resistant to imatinib mesylate. Clin Cancer Res 2006 Apr 1;12(7 Pt 1):2239-47.